Physical Modeling and Control of Low Temperature Combustion in Engines

Widd, Anders

2012

Document Version:
Publisher's PDF, also known as Version of record

[Link to publication](#)

Total number of authors:
1

Physical Modeling and Control of
Low Temperature Combustion in Engines

Physical Modeling and Control of
Low Temperature Combustion in Engines

Anders Widd

Department of Automatic Control
Lund University
Lund, 2012

Abstract

The topic of this thesis is model-based control of two combustion engine concepts, Homogeneous Charge Compression Ignition (HCCI) and Partially Premixed Combustion (PPC), using physics-based models. The studied combustion concepts hold promise of reducing the emission levels and fuel consumption of internal combustion engines.

A cycle-to-cycle model of HCCI, including heat losses to the cylinder wall, was derived. The continuous heat transfer between the cylinder wall and the gas in the cylinder was approximated by three heat transfer events during each cycle. This allowed the model to capture the main dynamics of the cylinder wall temperature while keeping the complexity of the resulting model at a tractable level.

The model was used to derive model predictive controllers for the combustion phasing using the inlet air temperature and inlet valve closing timing as control signals. The resulting controllers were evaluated experimentally and achieved promising results in terms of set-point tracking and disturbance rejection.

Additionally, the differences in performance between using a switched state feedback controller and a hybrid model predictive controller for controlling exhaust recompression HCCI were investigated. The dynamics of exhaust recompression HCCI vary significantly between certain operating points, and the model predictive controller produced smoother transients in both simulations and experiments.

A continuous-time model of PPC was derived and implemented in the Modelica language. The model structure, a single-zone model, and implementation platform, JModelica.org, were chosen in order to allow for numerical optimization based on the model equations. The resulting framework allowed the calibration of the model parameters to be formulated as an optimization problem penalizing deviations between a measured pressure trace and that of the model. The calibrated model predicted the effects of variations in the injection timing with satisfactory accuracy.

5

Acknowledgements

First of all, I would like to thank my supervisor, Rolf Johansson, for his guidance over the years. It has been very inspiring to work with someone with such deep knowledge within several fields as Rolf, and he has been very supportive both of my work and of me as a person throughout my time as a Ph.D. student.

I would like to thank my co-supervisor, Per Tunestål, for making time for many enlightening discussions and providing useful suggestions and ideas on matters related to both combustion engines and control.

Johan Åkesson joined as co-supervisor during the last year of this work and I am grateful for his commitment and generous sharing of time.

I would also like to thank Per Hagander for being my co-supervisor during my first years at the department, and Bengt Johansson for being the director of KCFP, the research project I have been a part of during my time as a Ph.D. student.

I have had several collaborations with fellow Ph.D. students at the Department of Energy Sciences in Lund and I would like to thank Carl Wilhelmsson, Kent Ekholm, Patrick Borgqvist, and Magnus Lewander. I would also like to thank the technicians in the Engine Lab for keeping the engines and other equipment operational and making modifications when necessary.

I am very grateful to Prof. J. Christian Gerdes for allowing me to visit his research group at Stanford University during the fall of 2009. I would like to acknowledge everyone at the Dynamic Design Lab for being such extraordinary hosts, and Dr. Hsien-Hsin Liao for a very rewarding collaboration.

I would like to thank Daniel Adén, Magnus Lewander, and Per-Ola Larsson for their helpful comments on this thesis, and Leif Andersson for his help with the typesetting and various other computer-related issues. I would also like to thank Dr. Lars Eriksson for reviewing my licentiate thesis.

Acknowledgements

The Department of Automatic Control in Lund is an excellent place to work and I am happy to be a part of it. I am grateful to the technical and the administrative staff for keeping the equipment and the people in the department running smoothly. I would also like to acknowledge Maria Henningsson for sharing the interest in combustion engine control. There are several people at the department I would like to thank for being nice persons to talk to but instead of attempting to list everyone, I will just make a special mention of the people responsible for all the entertaining lunch discussions.

Last, but not least, I would like to thank my friends and family. I am sure I have some of the best friends you could hope for, and I truly appreciate the support and encouragement my family has provided me with my entire life.

<div align="right">

Anders

</div>

Contents

Contents

Preface

This chapter outlines the structure and contributions of the thesis. Parts of the work were carried out in collaboration with co-authors and colleagues from the Division of Combustion Engines, Department of Energy Sciences at Lund University (Sweden) and the Department of Mechanical Engineering at Stanford University, California (USA).

The experimental data used for model validation in Ch. 4 were obtained from Carl Wilhelmsson, and the experimental work presented in Ch. 5 was performed together with Kent Ekholm at Lund University. During the fall 2009, I visited Prof. J. Christian Gerdes lab at Stanford University and the work described in Ch. 6 was performed in collaboration with Dr. Hsien-Hsin Liao and Prof. Gerdes during that time. The experimental data on partially premixed combustion used in Ch. 7 were obtained from Patrick Borgqvist, Lund University.

Two of my supervisors, Rolf Johansson and Per Tunestål, are listed as co-authors on all publications and contributed through extensive discussions during the work and provided feedback on the papers. Johan Åkesson joined as supervisor during the last year of this work and has made a significant contribution through assistance with the JModelica.org platform and numerical optimization.

The contributions of other co-authors are specified in conjunction with each publication.

Outline and Contributions

Chapter 1: Introduction to Internal Combustion Engines

This chapter contains a brief introduction to internal combustion engines and the defining characteristics of Homogeneous Charge Compression Ignition (HCCI) and Partially Premixed Combustion (PPC), along with a

description of how pressure sensors were utilized and the available control signals.

Chapter 2: Introduction to Physical Modeling and Control

This chapter gives an overview of the types of physics-based engine models discussed in Chs. 4 and 7, as well as the control methods used in Chs. 5 and 6, and the optimization method used in Ch. 7.

Chapter 3: Experimental Setup

This chapter contains technical specifications on the different test engines used in later chapters.

Chapter 4: Cycle-to-Cycle Modeling of HCCI

A cycle-to-cycle, physics-based model of HCCI is presented in this chapter. The model was of second order and had the crank angle of 50 percent burned and the indicated mean effective pressure as outputs. The cylinder wall temperature has a considerable effect on the combustion phasing when the engine is run with small amounts of trapped residuals. A simple model of the dynamic interaction between the gas charge and cylinder wall temperatures was therefore included. The continuous heat transfer between the cylinder wall and the gas charge was approximated by three heat transfer events during each cycle. This allowed the model to capture the time constant of the wall temperature while keeping the complexity of the resulting model at a tractable level.

Related Publications

Anders Widd, Per Tunestål, and Rolf Johansson, "*Physical Modeling and Control of Homogeneous Charge Compression Ignition (HCCI) Engines*," in *47th IEEE Conference on Decision and Control (CDC2008)*, Cancun, Mexico, pp. 5615-5620, December 2008.

A. Widd performed the analysis and the simulations. The experimental results were obtained in collaboration with Kent Ekholm.

Anders Widd, Per Tunestål, Carl Wilhelmsson, and Rolf Johansson, "*Control-Oriented Modeling of Homogeneous Charge Compression Ignition incorporating Cylinder Wall Temperature Dynamics*," in *Proc. 9th International Symposium on Advanced Vehicle Control (AVEC2008)*, Kobe, Japan, pp. 146-151, October 2008.

A. Widd derived the model. The experimental data were obtained from Carl Wilhelmsson.

Chapter 5: HCCI Control using FTM and VVA

Linearizations of the model described in Ch. 4 were used to design Model Predictive Controllers (MPC) for controlling the combustion phasing using Variable Valve Actuation (VVA) and the temperature of the inlet air as control signals. A Fast Thermal Management (FTM) system was implemented and controlled in order to obtain fast actuation of the intake temperature. The performance of the controllers was experimentally investigated in terms of response time and output variance. The resulting closed-loop system followed step changes in the desired combustion phasing within at most 20 engine cycles. Multi-cylinder experiments were also carried out.

Related Publications

Anders Widd, Kent Ekholm, Per Tunestål, and Rolf Johansson, "*Physics-Based Model Predictive Control of HCCI Combustion Phasing Using Fast Thermal Management and VVA*," in *IEEE Transactions on Control Systems Technology*, vol. PP, no. 99, pp. 1-12, April 2011.

This is a journal version of the following conference publication.

Anders Widd, Kent Ekholm, Per Tunestål, and Rolf Johansson, "*Experimental Evaluation of Predictive Combustion Phasing Control in an HCCI Engine using Fast Thermal Management and VVA*," in *Proc. 2009 IEEE Multi-Conference on Systems and Control*, Saint Petersburg, Russia, pp. 334-339, July 2009.

The experiments were performed in collaboration with K. Ekholm, who also designed the FTM system. The FTM control system was designed and implemented in collaboration with K. Ekholm. A. Widd performed the analysis.

Chapter 6: Hybrid Control of Exhaust Recompression HCCI

Using multiple linearization of the model of exhaust recompression HCCI presented in [Ravi *et al.*, 2010], a hybrid model predictive controller was designed for controlling the combustion phasing. The control performance was evaluated in simulations and experiments and compared to that of a switching state feedback controller. The predictive controller had the advantage of producing smoother transients when large changes in the desired combustion phasing were made.

Related Publications

Anders Widd, Hsien-Hsin Liao, J. Christian Gerdes, Per Tunestål, and Rolf Johansson, "*Hybrid Model Predictive Control of Exhaust Recompression HCCI*," submitted to *Asian Journal of Control*.

This is a journal version of the following publication.

Anders Widd, Hsien-Hsin Liao, J. Christian Gerdes, Per Tunestål, and Rolf Johansson, "*Control of Exhaust Recompression HCCI using Hybrid Model Predictive Control*," in *Proc. 2011 American Control Conference (ACC2011)*, San Francisco, CA, USA, pp. 420-425, June 2011.

The model predictive controller was designed by A. Widd. The experiments and analysis were carried out in collaboration with H.H. Liao.

Chapter 7: Modeling of PPC for Optimization

The model presented in this chapter aims to describe the main features of PPC combustion within the closed part of an engine cycle. The model was given on Differential Algebraic Equation (DAE) form and was a single-zone model, meaning that spatial variations within the cylinder were not considered. The model included heat losses to the cylinder walls as well as vaporization losses. The aim of the modeling was to be able to use the resulting model for optimization, and the model complexity and simulation framework were chosen with this in mind. The single-zone approach reduces the complexity of the resulting model compared to multi-zone models, and the chosen framework allows for formulation of optimization problems based on the model equations.

The model calibration was formulated as an optimization problem penalizing deviations between an experimental pressure trace and that of the model. It was demonstrated that parts of the calibration can be done automatically by means of optimization.

Related Publications

Anders Widd, Per Tunestål, Johan Åkesson, and Rolf Johansson, "*Single-Zone Modeling of Diesel PPC for Control*," accepted for publication in *Proc. 2012 American Control Conference (ACC2012)*, Montréal, Canada, June 2012.

A. Widd derived the model and did the numerical implementation. The experimental data were obtained from Patrick Borgqvist.

Anders Widd, Johan Åkesson, Per Tunestål, and Rolf Johansson, "*Modeling of Partially Premixed Combustion for Optimization*," Manuscript in preparation, 2012.

The optimization was performed by A. Widd.

Other Related Publications

The following publications on engine modeling and control were also completed during the Ph.D. studies, but not included in the thesis.

Nikhil Ravi, Hsien-Hsin Liao, Adam F. Jungkunz, Anders Widd, J. Christian Gerdes, "*Model predictive control of HCCI using variable valve actuation and fuel injection*," in *Control Engineering Practice*, vol. 20, issue 4, pp. 421-430, April 2012.

Magnus Lewander, Anders Widd, Bengt Johansson, and Per Tunestål, "*Steady State Fuel Consumption Optimization through Feedback Control of Estimated Cylinder Individual Efficiency*," accepted for publication in *Proc. 2012 American Control Conference (ACC2012)*, Montréal, Canada, June 2012.

Anders Widd, Patrick Borgqvist, Per Tunestål, Rolf Johansson, and Bengt Johansson, "*Investigating Mode Switch from SI to HCCI using Early Intake Valve Closing and Negative Valve Overlap*," in *2011 JSAE/SAE International Powertrains, Fuel & Lubricants*, Kyoto, Japan, August 2011.

Hsien-Hsin Liao, Nikhil Ravi, Adam Jungkunz, Anders Widd, and J. Christian Gerdes, "*Controlling Combustion Phasing of Recompression HCCI with a Switching Controller*," in *Proc. Sixth IFAC Symposium on Advances in Automotive Control*, Munich, Germany, July 2010.

Rolf Johansson, Per Tunestål, and Anders Widd, "*Modeling and Model-based Control of Homogeneous Charge Compression Ignition (HCCI) Engine Dynamics*," in L. del Re, F. Allgöwer, L. Glielmo, C. Guardiola, I. Kolmanovsky (Eds.): *Automotive Model Predictive Control—Models, Methods and Applications*, Springer-Verlag, Berlin-Heidelberg, May 2010.

Carl Wilhelmsson, Per Tunestål, Anders Widd, and Rolf Johansson, "*A Fast Physical NOx Model Implemented on an Embedded System*," in *Proc. IFAC Workshop on Engine and Powertrain Control, Simulation and Modeling (ECoSM 2009)*, Rueil-Malmaison, France, November 2009.

Anders Widd, "*Predictive Control of HCCI Engines using Physical Models*," *Licentiate Thesis TFRT–3246–SE,* Department of Automatic Control, Lund University, Sweden, May 2009.

Carl Wilhelmsson, Per Tunestål, Anders Widd, Rolf Johansson, and Bengt Johansson, "*A Physical Two-Zone NOx Model Intended for Embedded Implementation*," in *SAE Technical Papers 2009-01-1509, SAE World Congress & Exhibition*, Detroit, MI, USA, April 2009. (Also in Modeling of SI and Diesel Engines, Vol. SP-2244, 2009, ISBN 978-0-7680-2140-0, April 2009).

Preface

1

Introduction to Internal Combustion Engines

The predecessors of the modern internal combustion engines have been used as a means to convert chemically bound energy to work since the late 19th century when the Otto and Diesel engines were invented [Heywood, 1988]. The engines of today, however, share only the fundamental principles with the original inventions. This chapter outlines the basics of internal combustion engines and the two traditional combustion modes, spark ignition and compression ignition, to help understand the two modes that are modeled and controlled in later chapters: Homogeneous Charge Compression Ignition (HCCI) and Partially Premixed Combustion (PPC).

1.1 Geometry and Conventional Operating Modes

Figure 1.1 shows the basic geometry of an engine cylinder. The linear movement of the piston is translated to rotation of the crank shaft. The rotation is usually measured in crank angles, denoted θ in this text. The crank angles corresponding to the top and bottom positions of the piston are denoted θ_{TDC} and θ_{BDC}, respectively, after the acronyms TDC and BDC for Top Dead Center and Bottom Dead Center. The minimum volume attained when the piston is in the top position is called the *clearance volume*, and denoted V_c. The volume that is swept by the piston is called the *displacement volume*, and denoted V_d. The instantaneous cylinder volume corresponding to a certain crank angle can be calculated as

$$V = V_c + \frac{V_d}{2}\left(R_v + 1 - \cos(\theta) - \sqrt{R_v^2 - \sin^2(\theta)}\right) \qquad (1.1)$$
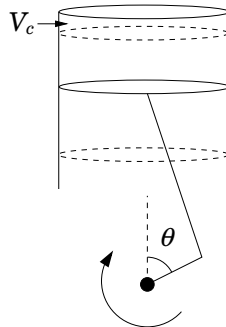
Figure 1.1 Basic geometry of an engine cylinder showing the definition of the crank angle, θ, and the clearance volume, V_c.

where R_v is the ratio between the connecting rod length and the crank radius.

In a four stroke engine, every other revolution of the crank shaft is devoted to combustion and every other revolution to scavenging of the resulting combustion products and introduction of fresh gases. The combustion results in an increase in the thermal energy in the cylinder which increases the pressure and thus forces the piston downwards so that work can be extracted.

Conventional internal combustion engines include Otto and Diesel engines, named after their inventors Nikolaus Otto (1832-1891) and Rudolf Diesel (1858-1913). These modes are also referred to, after their respective principle of ignition, as Spark Ignition (SI) or Compression Ignition (CI) engines. The following brief overview is based mainly on [Heywood, 1988].

Spark Ignition Engines

In spark ignition engines, a mixture of fuel and air is ignited by a spark plug. This means that the timing of the spark has a pronounced influence on the combustion timing and, in turn, the overall behavior of the engine cycle [Heywood, 1988]. Once combustion has been initiated, the combustion proceeds as a turbulent flame front from the spark plug through the combustion chamber. The Otto engines of today with modern aftertreatment systems produce very small amounts of nitrogen oxides and soot emissions. However, SI engines typically have lower efficiency at part load than CI engines, which results in a higher fuel consumption and thereby higher emissions of CO_2.

Compression Ignition Engines

In compression ignition engines, fuel is injected into the cylinder when the temperature inside the cylinder is sufficiently high from compression for auto-ignition to occur. Following a period of time, denoted *ignition delay*, when the fuel and air are mixed into a burnable charge, part of the fuel burns in a pre-mixed manner. The rest of the fuel burns in and around the spray while the injected fuel is continuously mixed with the surrounding air [Dec, 1997]. The tail pipe emissions of NO_x and soot are typically higher than those from SI engines. The efficiency is, however, also higher, yielding a lower fuel consumption and thereby less CO_2 per unit of produced work.

1.2 Emissions and Low Temperature Combustion

The aim of most engine research is to reduce the emissions and the fuel consumption of transportation. The main emissions generated by internal combustion engines are water (H_2O), carbon monoxide (CO), carbon dioxide (CO_2), nitrogen oxides (NO_x), hydrocarbons, and particulate matter [Heywood, 1988]. Of these emissions, only CO_2 and water are currently not regulated. While some emissions, such as nitrogen oxides and soot, are immediately harmful to humans and the local environment, carbon dioxide emissions are receiving increased attention due to the ongoing discussions about climate change. Various after-treatment systems for reducing the harmful emissions are available, such as particulate filters and Selective Catalytic Reduction (SCR) [Majewski, 2005] for diesel engines. However, in order to reduce the emissions of carbon dioxide, the engine efficiency must be increased so that less fuel is consumed per unit of produced work. By altering the combustion mode, the emissions can be reduced compared to CI engines, while simultaneously increasing the engine efficiency compared to SI engines.

Low Temperature Combustion

The production of NO_x is mainly influenced by the temperature of the gases in the cylinder. A class of combustion concepts aimed at exploiting this property is usually referred to as Low Temperature Combustion (LTC) [Jääskeläinen, 2008]. Among the LTC concepts, Homogeneous Charge Compression Ignition and Partially Premixed Combustion are studied in this thesis. In HCCI, the fuel-air mixture is designed to be diluted and completely homogeneous before combustion starts through auto-ignition. This results in a lower gas temperature and the diluted homogeneous charge has the additional benefit of reducing soot production,

which is mainly driven by locally fuel-rich zones in the cylinder [Heywood, 1988; Zhao and Asmus, 2003]. PPC has similarities to both HCCI and traditional Diesel combustion since part of the fuel burns in a premixed manner while the remaining fuel burns in mixing controlled combustion.

1.3 HCCI

This section outlines the development of the Homogeneous Charge Compression Ignition engine, the operating principle, and the need for closed-loop control.

HCCI Background

Early studies of HCCI were made on two-stroke engines and include [Onishi *et al.*, 1979; Ishibashi and Asai, 1979]. In the eighties, [Najt and Foster, 1983] showed HCCI operation in a four-stroke engine. During the nineties HCCI research increased, largely due to the possibility of decreased emissions. Publications from the late nineties include [Aoyama *et al.*, 1996; Christensen *et al.*, 1999]. This work has continued and the last ten years has seen much research aimed at making HCCI feasible for the market.

HCCI Operation

HCCI is characterized by auto-ignition of a diluted homogeneous mixture of fuel and air. There is no spark or injection event that triggers combustion. Instead, the auto-ignition is determined by the properties of the charge, the temperature, and the pressure [Chiang and Stefanopoulou, 2009; Bengtsson *et al.*, 2007]. HCCI has the advantage of a combustion without hot zones which reduces NO_x-emissions, and, since the charge is homogeneous, no locally rich zones occur, reducing soot formation [Heywood, 1988]. The efficiency in part load is fairly high, which reduces the fuel consumption, and thereby the CO_2-emissions, compared to spark ignition engines.

A somewhat simplified four stroke HCCI engine cycle can be described by the following five stages where *(up)* and *(down)* indicate whether the piston is moving upwards or downwards. This partitioning of the engine cycle will be used in the model derivation in Ch. 4. Four of the stages are also illustrated in Fig. 1.2, which also shows the opening of the inlet and exhaust valves.

1. Intake: The intake valve opens and a homogeneous mixture of fuel and air enters the cylinder *(down)*;
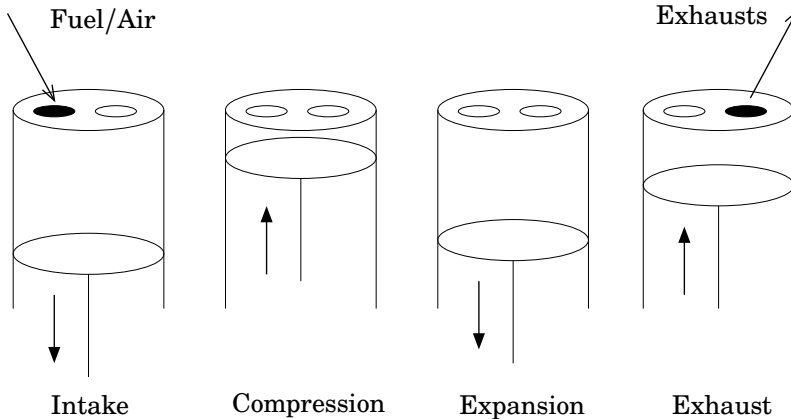
Figure 1.2   Principle of HCCI combustion. Black indicates an open valve.

2. Compression: The intake valve closes and the in-cylinder charge is compressed *(up)*;

3. The charge auto-ignites;

4. Expansion: The pressure increase from the combustion forces the piston downwards and work is extracted *(down)*;

5. Exhaust: The exhaust valve opens and the residual gases leave the cylinder *(up)*.

To achieve HCCI, a fairly high initial temperature is required. One way of accomplishing such a temperature is to utilize the exhausts of the previous cycle. This can be done either by *trapping*, where the exhaust valve is closed before the cylinder has been entirely scavenged [Shaver *et al.*, 2006b], or by introducing an additional opening of the exhaust valve, called *re-breathing* [Chiang *et al.*, 2007]. Another option is to raise the initial temperature using an electric heater on the intake air [Christensen and Johansson, 2000]. However, the presence of inert (non-reactive) exhaust gases still affects the combustion. A long-route Exhaust Gas Recirculation (EGR) system can be used to dilute the charge. This increases the specific heat capacity of the charge, yielding a lower peak temperature.

HCCI Control

An inherent difficulty with HCCI is to control the point of auto-ignition. Since there is a wide range of factors that influence the combustion phasing, there are several possible control signals, but also many possible disturbances that the control system must account for or be robust against.

Possible control signals that have been tested in experiments include variable valve timing [Bengtsson, 2004], the intake temperature [Christensen and Johansson, 2000], the amount of residuals trapped in the cylinder [Shaver *et al.*, 2006b; Chiang *et al.*, 2007], as well as mixing fuels with different octane number [Olsson *et al.*, 2001; Strandh *et al.*, 2004]. A survey on HCCI modeling and control was presented in [Bengtsson *et al.*, 2007].

A possible categorization of control efforts for HCCI is a top layer aiming to minimize emissions, fuel consumption, and combustion noise, producing set points for a combustion phasing controller, which in turn governs actuator controllers on the valves, injection system, etc. For HCCI to be a viable option for vehicles, an additional control layer is necessary as the driver must be able to give set-points in terms of the desired engine torque. The work in this thesis is focused on achieving model-based control of the combustion phasing. A few topics related to actuator control are discussed in Ch. 5.

1.4 PPC

Partially Premixed Combustion is achieved by injecting the fuel early enough for substantial mixing to occur before combustion starts, but not so early that the mixture is homogeneous. This results in a combustion mode with better controllability than HCCI without increasing the emissions of NO_x and soot to the levels of traditional Diesel engines [Lewander, 2011]. Recent studies of PPC include [Manente *et al.*, 2010b; Manente *et al.*, 2010a]. The definition of PPC chosen in [Lewander, 2011] is that combustion is initiated only after the fuel has been completely injected, i.e., that the ignition delay is longer than the injection duration.

1.5 Pressure Sensors and Heat Release

The pressure in the cylinder is usually measured in laboratory settings using a pressure transducer. The sensor outputs a signal proportional to the pressure that affects it. The measured pressure, p, can be used to calculate relevant engine variables such as the heat release from combustion. Using the first law of thermodynamics, the rate of change in the total thermal energy in the cylinder, Q_{tot}, can be computed as [Heywood, 1988]

$$\frac{dQ_{\text{tot}}}{d\theta} = \frac{\gamma}{\gamma - 1}p\frac{dV}{d\theta} + \frac{1}{\gamma - 1}V\frac{dp}{d\theta} \tag{1.2}$$

where γ is the ratio of specific heats

$$\gamma = \frac{c_p}{c_v} \tag{1.3}$$

where c_p and c_v are the specific heat capacities of the gas at constant pressure and constant volume, respectively [Heywood, 1988].

The term *heat release* usually refers to the heat that is released from the combustion of fuel. The total change in thermal energy in the cylinder is, however, also affected by several other variables, such as heat transfer to the cylinder walls, fuel vaporization and heating, etc. The change in thermal energy computed in Eq. (1.2) is usually referred to as the *apparent heat release*, and indicates the total change in thermal energy in the cylinder as indicated from the pressure trace. In the model framework used in Ch. 7, Q_{tot} corresponds to the apparent heat release and the actual heat release corresponding to fuel combustion is denoted Q_{c}.

To obtain Q_{c} from experimental data, the additional effects that influence Q_{tot} must be accounted for. Two possible approaches are to model the heat losses, blow-by (fuel mass losses to crevices), and other effect [Gatowski *et al.*, 1984], or to let the changes in thermal energy not related to combustion be described as a change in the polytropic exponent [Tunestål, 2009]. The polytropic exponent, usually denoted κ, fulfills

$$pV^\kappa = C_{\text{poly}} \tag{1.4}$$

where C_{poly} is a constant. The polytropic exponent will in general differ from the ratio of specific heats, γ, in Eq. (1.2).

Based on the heat release profile, the crank angle corresponding to a certain percentage x of released energy, θ_x, can be calculated. It is defined by

$$x = 100 \frac{Q_{\text{c}}(\theta_x)}{\max_\theta Q_{\text{c}}(\theta)} \tag{1.5}$$

Crank angles such as θ_{10}, θ_{50}, and θ_{90} are often used to characterize the combustion and θ_{50} in particular is a popular proxy for combustion timing in HCCI control [Bengtsson *et al.*, 2007].

The net Indicated Mean Effective Pressure (IMEP$_n$) can also be determined from the pressure trace [Kiencke and Nielsen, 2005]

$$\text{IMEP}_n = \frac{1}{V_d} \int_{\text{cycle}} p\,dV \tag{1.6}$$

where V_d is the displacement volume. This produces a measure of the work output, normalized by the displacement volume of the engine.

Currently, pressure sensors are rarely implemented in production engines. It is possible that this might change in the future, if the benefits of including the sensors outweigh the economical and implementational difficulties associated with them. Additionally, there is research aimed at removing the need for pressure sensors by instead using ion-current sensors in the combustion chamber [Strandh *et al.*, 2003] or knock sensors mounted on the engine block [Chauvin *et al.*, 2008] to estimate the relevant combustion parameters.

1.6 Engine Control Signals

As previously mentioned, the combustion process is affected by several adjustable variables that can be used as control signals. This section gives a brief overview of a few of these.

Variable Valve Actuation

Variable Valve Actuation (VVA) can be used to alter the timing of the exhaust and inlet valves opening and closing, and have a direct effect on the thermodynamic process inside the cylinder. In the model structures used in this thesis, the main effects are related to the effective compression ratio and the composition and temperature of the charge. The following discussion therefore excludes a few more subtle effects.

Inlet Valve Closing The crank angle of inlet valve closing, θ_{IVC}, determines the effective compression ratio. Only values between bottom dead center and top dead center are considered, so that a greater value of θ_{IVC} means a smaller initial volume which results in less compression and lower temperatures. This introduces a magnitude limitation on the control signal, but it can be changed freely between cycles using certain variable valve actuation systems. The inlet valve closing timing was used as a control signal in the experiments presented in Ch. 5.

Exhaust Valve Opening The crank angle of exhaust valve closing, θ_{EVC}, can influence the temperature and composition of the subsequent cycle. Closing the valve earlier will increase the amount of residuals in the charge of the subsequent cycle. Depending on the temperatures of the residuals and the fresh charge, it also increases or decreases the initial temperature. The exhaust valve closing timing was used as a control signal in the experiments presented in Ch. 6.

Negative Valve Overlap and Rebreathing Negative Valve Overlap (NVO) indicates that the exhaust valve is closed before the inlet valve

is opened. The residuals are then compressed and expanded by piston motion passing the top dead center. *Rebreathing* is achieved through an additional opening of the exhaust valve while the inlet valve is open, so that residuals are re-inducted into the cylinder.

Intake Temperature

A more direct way of altering the pre-compression temperature is to vary the temperature of the intake gases. This can be achieved either through the use of an electric heater or through utilization of the increased temperature of the exhausts. In the experiments presented in Ch. 5, the inlet air temperature was modified by mixing a heated and a cooled air flow. This technique is known as Fast Thermal Management (FTM) [Haraldsson, 2005].

Exhaust Gas Recirculation

Exhaust gas recirculation is achieved by feeding the exhaust gases back to the intake. This affects the composition of the charge in the same way as internal residuals achieved through valve actuation. However, the external residuals can be cooled or heated so that the initial temperature and the composition can be altered independently.

Fuel Injection

The amount of injected fuel affects the maximum achievable work output from the cycle. The injection timing also affects the start of combustion, particularly for PPC operation as it changes the time available for vaporization and mixing of the injected fuel.

Additional fueling strategies include the use of multiple fuels with different auto-ignition properties or multiple injections. One such example is *fumigation* where a portion of the fuel is port injected and mixes substantially before a direct injection occurs closer to combustion initiation.

2

Introduction to Physical Modeling and Control

This chapter gives an overview of the control methods used in the thesis, and engine modeling for control purposes.

2.1 Control-Oriented Modeling of Engines

Modeling for purposes of control, like most other forms of modeling, has its own unique requirements, and what constitutes a suitable model depends heavily on the application. In many cases, a seemingly very simple model can describe the main dynamics of a system with sufficient accuracy to be used for control design. The increased complexity associated with simulation and analysis needs to be weighed against the possible increase in the resulting control performance when considering a more detailed model.

Engine modeling involves several disciplines such as thermodynamics, chemical kinetics, and mechanics, and describing all of these aspects in detail typically results in large models of high complexity. To allow for fast simulation and analysis, models of lower complexity are of interest.

Among the physics-based models aimed at engine control, a distinction can be made between cycle-to-cycle models and continuous-time models. The cycle-to-cycle models update once per cycle to describe the dynamic evolution of the engine state. The model presented in Ch. 4 is of this type. Continuous-time models are used for several purposes, for instance modeling the dynamics within a particular cycle, which was the aim of the model presented in Ch. 7, or the dynamics of the entire engine system. One particular category of continuous-time models is *Mean-value models* [Hendricks, 1986], usually aimed at modeling the dynamics of the engine intake system, gas composition, etc. [Guzzella and Onder, 2004]. The continuous-time models often take the form of Ordinary Differen-

tial Equations (ODEs), or Differential Algebraic Equations (DAEs) when they include discrete events, such as the valves opening or closing and the start of combustion. They allow for a natural formulation of certain physical phenomena such as mass flow while the cycle-to-cycle models take a form suitable for cycle-to-cycle control design, which is often performed by linearizing the models around an operating point to obtain a linear system representation. The continuous-time models are mainly used for validation and evaluation of controllers as an intermediate step between control design and lab experiments.

Cycle-to-Cycle Modeling

To facilitate model-based control design, both statistical and physical cycle-to-cycle models have been considered [Bengtsson *et al.*, 2007]. Statistical models can often provide a more accurate fit to experiments when using sufficient data to obtain them. A drawback with statistical models, however, is that the models, and the resulting controllers, can be difficult to migrate to a different engine or operating point. Calibration and re-calibration of the parameters in a physical model is not always a trivial task, but it may require less calibration data to yield a model which is valid in a fairly large operating range. An additional benefit of physical models is that they offer some understanding of the engine behavior.

Recent examples of cycle-to-cycle models of HCCI for control design include [Chiang *et al.*, 2007; Shaver *et al.*, 2009; Rausen and Stefanopoulou, 2005], where [Shaver *et al.*, 2009] also presented experimental results of closed-loop control. A cycle-to-cycle model including heat transfer effects was presented in [Canova *et al.*, 2005] where the wall surface temperature was determined by averaging the gas and coolant temperatures. A cycle-to-cycle model tracking species concentration was presented in [Ravi *et al.*, 2010].

The resulting model typically takes the form of a nonlinear discrete-time system

$$x(k+1) = F(x(k), u(k)) \tag{2.1a}$$
$$y(k) = G(x(k), u(k)) \tag{2.1b}$$

where $F(x(k), u(k))$ and $G(x(k), u(k))$ are nonlinear functions of the states, x, and the inputs, u. The outputs are denoted y, and k corresponds to the cycle index. To enable the use of linear control methods, the resulting model can be linearized around a steady-state operating point (x^0, u^0) of interest, yielding a linear model on the form

$$\Delta x(k+1) = A \Delta x(k) + B \Delta u(k) \tag{2.2a}$$
$$\Delta y(k) = C \Delta x(k) + D \Delta u(k) \tag{2.2b}$$

where

$$A = \frac{\partial F(x(k), u(k))}{\partial x(k)}(x^0, u^0), \quad B = \frac{\partial F(x(k), u(k))}{\partial u(k)}(x^0, u^0)$$
$$C = \frac{\partial G(x(k), u(k))}{\partial x(k)}(x^0, u^0), \quad D = \frac{\partial G(x(k), u(k))}{\partial u(k)}(x^0, u^0)$$

(2.3)

and Δx, Δu, and Δy correspond to deviations from the linearization point.

$$\Delta x = x - x^0, \quad \Delta u = u - u^0 \quad \Delta y = y - (Cx^0 + Du^0)$$

(2.4)

The controllers in Chs. 5 and 6 were based on such linearizations.

Continuous-Time Modeling

There are several continuous-time Diesel models at different levels of complexity presented in the literature. In [Chmela *et al.*, 2007], a generic heat release model of diesel combustion was presented including both chemical and turbulence induced effects on the burn rate as well as a simple model of the geometry of the fuel spray. Models of lower complexity were presented in [Tauzia *et al.*, 2006; Gogoi and Baruah, 2010]. The former considered a division of the injected fuel into unprepared, prepared, and burned fuel. The heat release rate was expressed as a piecewise linear function of the crank angle. The latter calculated the ignition delay using an empirical expression similar to the Arrhenius rate of radical formation [Chiang and Stefanopoulou, 2009], and used a Wiebe function [Heywood, 1988] to compute the subsequent heat release. A study on different models of HCCI combustion was presented in [Wang *et al.*, 2006], and [Friedrich *et al.*, 2006] also proposed a method for calibrating models of this type. A mean value model implemented in Simulink was presented in [Gambarotta and Lucchetti, 2011]. Continuous-time models of HCCI used for simulation and validation of control strategies include [Shaver *et al.*, 2006a; Bengtsson *et al.*, 2004]. A highly detailed model of compression ignition operation was optimized using genetic algorithms to minimize emissions, fuel consumption, and combustion noise in [Dempsey and Reitz, 2011].

The DAE form of a continuous time models can be written as

$$F(\dot{x}(t), x(t), w(t), u(t), \mathbf{p}) = 0$$

(2.5)

where x, w, u, and $\mathbf{p}$ correspond to the continuous states (such as pressure and fuel mass), the algebraic variables (such as start of combustion), the control signals (such as the fuel injection), and the model parameters, respectively.

2.2 Model-Based Control

There are several well developed methods for model-based control design. Most of the methods used in this thesis are based on a linear system description of the control object, such as the innovation form

$$x(k+1) = Ax(k) + Bu(k) + K_w w(k) \qquad (2.6a)$$
$$y(k) = Cx(k) + w(k) \qquad (2.6b)$$

where x, y, and u are the states, outputs, and inputs of the system, respectively. The matrices A, B, and C define the system dynamics and K_w is a gain on the uncorrelated stochastic process w.

State Estimation

When the states are not measurable, a state estimator may be used to obtain estimates, $\hat{x}$, of the states. The state estimate can then be used instead of a state measurement in the controllers. The estimation can be performed in two steps

$$\hat{x}(k|k) = \hat{x}(k|k-1) + L\left(y(k) - C\hat{x}(k|k-1)\right) \qquad (2.7a)$$
$$\hat{x}(k+1|k) = A\hat{x}(k|k) + Bu(k) \qquad (2.7b)$$

where Eq. (2.7a) is known as the *measurement update* or *error update*, Eq. (2.7b) is known as the *time update*, $\hat{x}(j|k)$ denotes the estimate of x at sample j given a measurement at sample k, and L is a gain matrix [Anderson and Moore, 1990]. State estimators were used in the control experiments presented in Ch. 5 and Ch. 6.

Linear Quadratic Control

A Linear Quadratic (LQ) state feedback controller of the form

$$u(k) = -Kx(k) \qquad (2.8)$$

is obtained by minimizing the following infinite horizon cost function

$$J_{\text{LQ}}(u) = \sum_{j=0}^{\infty} ||Q_y y(j)||_2 + ||Q_u u(j)||_2 \qquad (2.9)$$

where the matrices Q_y and Q_u define the penalties on output deviations and control usage, respectively, and $||\cdot||_2$ indicates the 2-norm [Anderson and Moore, 1990]. Reference tracking can be introduced by means of feedforward, so that the full control law takes the form

$$u(k) = N_u y^r(k) + K\left(N_x y^r(k) - x(k)\right) \qquad (2.10)$$
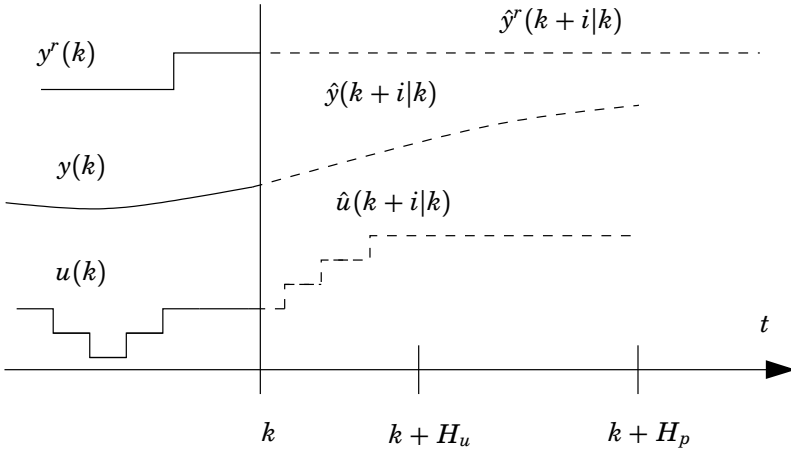
Figure 2.1   The reference signal, $y^r(k)$, the output, $y(k)$, and the control signal, $u(k)$ are shown up to sample k. After that, the predicted reference signal, $\hat{y}^r(k+i|k)$, the predicted output, $\hat{y}(k+i|k)$, and the predicted control signal $\hat{u}(k+i|k)$ are shown. The prediction horizon, H_p, and control horizon, H_u, are indicated on the horizontal axis. Figure reproduced from [Åkesson, 2006].

where the gains N_u and N_x assure that the steady-state output equals the reference value y^r. LQ control was compared to model predictive control of the combustion phasing in an HCCI engine in Ch. 6.

Model Predictive Control

Model predictive control (MPC) is a control strategy composed of solving a finite horizon optimal control problem at each sample and applying the first step of the optimal control sequence. The current state measurement, or state estimate, is used as initial condition in the optimization. When a new measurement is available, the optimization is repeated, yielding a new optimal sequence [Maciejowski, 2002]. The output predictions are done up to a *prediction horizon* H_p and the predicted control signal is allowed to vary up to a *control horizon* H_u. These horizons are visualized in Fig. 2.1.

Model predictive control was shown to be a suitable control strategy for HCCI [Bengtsson *et al.*, 2006] due to its MIMO capabilities and its ability to handle explicit constraints on control signals and outputs.

A typical cost function is given on the form

$$J_{\mathrm{MPC}}(k) = \sum_{j=k+1}^{k+H_p} \mathcal{Y}(j|k) + \sum_{j=k}^{k+H_u-1} \mathcal{U}(j|k) \qquad (2.11)$$

where $\mathcal{Y}$ and $\mathcal{U}$ are quadratic penalties on reference tracking and control signal usage, respectively,

$$\mathcal{Y}(j|k) = ||Q_y(\hat{y}(j|k) - y^r(j))||_2, \tag{2.12a}$$

$$\mathcal{U}(j|k) = ||Q_{\Delta u}(\Delta \hat{u}(j|k))||_2 + ||Q_u(\hat{u}(j|k) - u^r(j))||_2 \tag{2.12b}$$

where $\hat{y}(j|k)$ is the predicted output at sample j given a measurement at sample k, y^r is the reference values for y, $\hat{u}(j|k)$ is the predicted control signal at sample j, and Q_y, $Q_{\Delta u}$, and Q_u are weight matrices, respectively. This formulation penalizes both the control signal value and the predicted changes $\Delta \hat{u}$ depending on the choice of weight matrices. It can be convenient to avoid penalizing $\hat{u}$ directly since a non-zero steady-state control signal might be necessary in order to track a non-zero reference value. The reference signal for the control signals, u^r, can be used when there is more than one control signal combination that results in the same output. When there is no knowledge about future reference values, y^r and u^r, they are usually assumed constant over the prediction horizon.

Typically, the optimization is done subject to constraints on the form

$$
\begin{aligned}
y_{\min} &\leq y(k) \leq y_{\max} \\
x_{\min} &\leq x(k) \leq x_{\max} \\
u_{\min} &\leq u(k) \leq u_{\max} \\
\Delta u_{\min} &\leq \Delta u(k) \leq \Delta u_{\max}
\end{aligned}
\tag{2.13}
$$

for all k. This enforces minimum and maximum value constraints on the outputs, states, and control signals as well as a rate of change constraint on the control signals.

The predictions can be made using a linear plant model, like the one in Eq. (2.6), or based on nonlinear or hybrid model descriptions. The MPC in Ch. 5 was based on a linear model while the experiments presented in Ch. 6 were obtained using a controller based on a hybrid model formulation.

PID Control

The PID (Proportional-Integral-Derivative) controller is widely used in many different applications. There are several tuning methods for PID controllers, covering model-based methods as well as methods based on experiments, such as step responses, see [Åström and Hägglund, 2005].

A standard form is given by

$$u(t) = K\left(e(t) + \frac{1}{T_i}\int_{-\infty}^{t} e(\tau)d\tau + T_d\frac{de(t)}{dt}\right) \tag{2.14}$$

where the error $e(t)$ is given by

$$e(t) = y^r(t) - y(t) \qquad (2.15)$$

and K, T_i, and T_d denote the proportional gain, the integral time, and derivative time, respectively. A special case is when $T_d = 0$, which is referred to as a PI controller. PI controllers were used in the FTM control system in Ch. 5.

2.3 Dynamic Optimization

Dynamic optimization aims to solve problems based on general model descriptions such as the DAE form in Eq. (2.5). An optimal control problem based on a DAE representation of the system can be written as

$$
\begin{aligned}
\min_{u,\mathbf{p}} \ & J(x,w,u,\mathbf{p}) \\
\text{s.t. } & F(\dot{x}(t), x(t), w(t), u(t), \mathbf{p}) = 0 \\
& C_{\text{eq}}(\dot{x}(t), x(t), w(t), u(t), \mathbf{p}) = 0 \\
& C_{\text{ineq}}(\dot{x}(t), x(t), w(t), u(t), \mathbf{p}) \leq 0 \\
& C_{\text{end}}(\dot{x}(t_f), x(t_f), w(t_f), u(t_f), \mathbf{p}) = 0 \\
& x(t_0) = x_0
\end{aligned}
\qquad (2.16)
$$

where $J(x, u, w, \mathbf{p})$ is a scalar cost function and x_0 is the initial state. The functions C_{eq}, C_{ineq}, C_{end} specify the equality, inequality, and terminal constraints, respectively, and the optimization is done on the interval $[t_0, t_f]$, where t_f may be fixed or subject to optimization.

This section outlines the basics of collocation, the method used for solving the optimization problems in Ch. 7. It also describes the software used.

Collocation

Collocation is a *simultaneous* method for solving optimization problems of the type in Eq. (2.16), meaning that the entire system trajectory is obtained simultaneously from the optimizer rather than found through iterative integration over the time interval. The system trajectories are approximated by polynomials and the system equations are evaluated at specific time points denoted *collocation points*. The collocation points also act as *interpolation points* for the polynomials. The discretized optimization problem is formulated as a nonlinear program (NLP) [Biegler, 2010].

Collocation Points   The collocation points are obtained by dividing the time interval into N_e *elements* which in turn contain N_c collocation points each. The normalized length of element i is denoted h_i such that [Biegler, 2010]

$$\sum_{i=0}^{N_e-1} h_i = 1 \tag{2.17}$$

The time point t_i corresponding to the beginning of element i, denoted *mesh point*, can be written as

$$t_i = t_0 + (t_f - t_0) \sum_{k=0}^{i-1} h_k \tag{2.18}$$

There are several ways of choosing the locations of the collocation points, τ_j, within each element [Biegler, 2010]. In the platform used in Ch. 7, one of the collocation points is placed at the end of each element, and the remaining points are chosen using Radau collocation, i.e, chosen as the roots of a shifted Gauss-Legendre polynomial [Biegler, 2010].

To enforce continuity of the state variable trajectories, an extra interpolation point $\tau_0 = 0$ can be added at the start of each element. This is done so that continuity is enforced by requiring that the value of the discretized state at the last collocation point of each element must be equal to the value at the interpolation point τ_0 of the consecutive element.

The time point of a specific collocation point, $t_{i,j}$, where the first index denotes the element, and the second index denotes the collocation point within that element, is given by

$$t_{i,j} = t_0 + (t_f - t_0) \left(\sum_{k=0}^{i-1} h_k + \tau_j h_i \right) \tag{2.19}$$

Collocation Polynomials   The collocation points and the additional interpolation points for the states are used to define interpolation polynomials. While the DAE is only enforced at the collocation points, the extra interpolation point increases the order of the polynomials corresponding to the state trajectory within each element since the order of the polynomial must match the number of interpolation points. Thus, the state trajectories are approximated by Lagrange polynomials $\tilde{L}_j$ of order N_c

$$\tilde{L}_j(\tau) = \begin{cases} 1 & \text{if} \quad N_c = 1 \\ \prod_{k=0,k\neq j}^{N_c} \dfrac{\tau - \tau_k}{\tau_j - \tau_k} & \text{if} \quad N_c \geq 2 \end{cases} \tag{2.20}$$

while the trajectories without continuity requirements are approximated by Lagrange polynomials L_j of order $N_c - 1$

$$L_j(\tau) = \begin{cases} 1 & \text{if} \quad N_c = 1 \\ \prod_{k=1, k \neq j}^{N_c} \dfrac{\tau - \tau_k}{\tau_j - \tau_k} & \text{if} \quad N_c \geq 2 \end{cases} \tag{2.21}$$

The trajectories at time t within element i, corresponding to $t \in [t_i, t_{i+1}]$, can then be approximated by

$$x(t) = \sum_{j=0}^{N_c} x_{i,j} \tilde{L}_j \left(\frac{t - t_i}{h_i(t_f - t_0)} \right) \tag{2.22}$$

$$w(t) = \sum_{j=1}^{N_c} w_{i,j} L_j \left(\frac{t - t_i}{h_i(t_f - t_0)} \right) \tag{2.23}$$

$$u(t) = \sum_{j=1}^{N_c} u_{i,j} L_j \left(\frac{t - t_i}{h_i(t_f - t_0)} \right) \tag{2.24}$$

where $x_{i,j}$, $w_{i,j}$, and $u_{i,j}$ denote the values of the states, algebraic variables, and control signals at collocation point j in element i, respectively.

Since $L_j(\tau_k) = \tilde{L}_j(\tau_k) = 1$ for $j = k$ and $L_j(\tau_k) = \tilde{L}_j(\tau_k) = 0$ for $j \neq k$, the trajectory values at the interpolation points are

$$x(t_{i,j}) = \sum_{j=0}^{N_c} x_{i,j} \tilde{L}_j(\tau_j) = x_{i,j} \tag{2.25}$$

$$w(t_{i,j}) = \sum_{j=1}^{N_c} x_{i,j} L_j(\tau_j) = w_{i,j} \tag{2.26}$$

$$u(t_{i,j}) = \sum_{j=1}^{N_c} u_{i,j} L_j(\tau_j) = u_{i,j} \tag{2.27}$$

Approximate state derivatives in element i are obtained by differentiating Eq. (2.22), yielding

$$\dot{x}(t) = \frac{1}{h_i(t_f - t_0)} \sum_{j=0}^{N_c} x_{i,j} \dot{\tilde{L}}_j \left(\frac{t - t_i}{h_i(t_f - t_0)} \right) \tag{2.28}$$

and correspondingly

$$\dot{x}(t_{i,j}) = \frac{1}{h_i(t_f - t_0)} \sum_{j}^{N_c} x_{i,j} \dot{\tilde{L}}_j(\tau_j) = \dot{x}_{i,j} \tag{2.29}$$

NLP Formulation   The initial values of the states, algebraic variables, and control signals can be represented by the variables $x_{0,0}$, $w_{0,0}$, and $u_{0,0}$, respectively, and must fulfill the initial condition in Eq. (2.16)

$$x_{0,0} = x_0 \tag{2.30}$$

Additionally, the terminal constraint in Eq. (2.16) must be fulfilled for collocation point N_c in element $N_e - 1$

$$C_{\text{end}}(\dot{x}_{N_e-1,N_c}, x_{N_e-1,N_c}, w_{N_e-1,N_c}, u_{N_e-1,N_c}) = 0 \tag{2.31}$$

The DAE and the inequality and equality constraints in Eq. (2.16) are evaluated at the collocation points

$$F(\dot{x}_{i,j}, x_{i,j}, w_{i,j}, u_{i,j}) = 0 \tag{2.32}$$
$$C_{\text{eq}}(\dot{x}_{i,j}, x_{i,j}, w_{i,j}, u_{i,j}) = 0 \tag{2.33}$$
$$C_{\text{ineq}}(\dot{x}_{i,j}, x_{i,j}, w_{i,j}, u_{i,j}) \leq 0 \tag{2.34}$$

for $i \in [0, N_e - 1]$, $j \in [1, N_c]$.

The continuity condition on the state trajectory can be written as

$$x_{i,N_c} = x_{i+1,0}, \quad i \in [1, N_e - 1] \tag{2.35}$$

By collecting all the variables in a vector $\bar{x}$, the equality constraints in Eqs. (2.29)-(2.33) and Eq. (2.35) in a function $h(\bar{x}) = 0$, and the inequality constraint in Eq. (2.34) in a function $g(\bar{x}) \leq 0$, the optimization problem in Eq. (2.16) can be written as as an NLP

$$
\begin{aligned}
\min_{\bar{x}} \;\; & f(\bar{x}) \\
\text{s.t. } & h(\bar{x}) = 0 \\
& g(\bar{x}) \leq 0
\end{aligned}
\tag{2.36}
$$

where $f(\bar{x})$ represents an approximate discretized version of the cost function $J(x, w, u, \mathbf{p})$ in Eq.(2.16). Most of the optimization problems in Ch. 7 are on the form of parameter estimation problems, where the cost functions penalize the squared error between a measured signal y^m and some function of the system variables, y. The cost function, $J(y)$, can then be

approximated as described in [Magnusson, 2012]

$$J(y) = \int_{t_0}^{t_f} (y(t) - y^m(t))^T Q(y(t) - y^m(t))dt$$

$$= \sum_{i=1}^{N_e} \left(h_i \int_0^1 (y_i(\tau) - y^m(t_{i-1} + h_i\tau))^T Q(y_i(\tau) - y^m(t_{i-1} + h_i\tau))d\tau \right)$$

$$\approx \sum_{i=1}^{N_e} \left(h_i \sum_{j=1}^{N_c} \omega_j(y_i(\tau_j) - y^m(t_{i-1} + h_i\tau))^T Q(y_i(\tau_j) - y^m(t_{i-1} + h_i\tau)) \right)$$

$$= \sum_{i=1}^{N_e} \left(h_i \sum_{j=1}^{N_c} \omega_j (y_{i,k} - y^m(\tau_j))^T Q (y_{i,k} - y^m(\tau_j)) \right) \quad (2.37)$$

where ω_j are quadrature weights [Biegler, 2010]

$$\omega_j = \int_0^1 L_j^{N_c}(\tau)d\tau \quad (2.38)$$

When sampled measurement data is used, $y(\tau_j)$ may be obtained by interpolation of the available measurement points. In the platform used in Ch. 7, linear interpolation was used [Magnusson, 2012].

Modelica

Modelica [The Modelica Association, 2009] is an object-oriented, equation-based modeling language aimed at modeling of complex physical systems. It supports modeling of a variety of physical domains, such as mechanical, thermodynamical, and chemical systems. Being equation-based, the model equations may be entered without specifying the causality of the equations by, for instance, solving for the derivatives or entering the equations in a specific order. This is one of the main benefits of Modelica in the context of engine models, since they typically have fairly complex interdependences between the variables. The object-oriented nature of Modelica also allows reusable sub-models to be defined in a straightforward fashion. Both differential and algebraic equations are supported, making it a suitable language for models of DAE type.

Optimica

Optimica [Åkesson, 2007] extends the Modelica language with support for the formulation of optimization problems in terms of cost functions, constraints, and free optimization variables. This is done through a new optimization class as well as optimization attributes, such as the `free` attribute used to indicate optimization variables and the `initialGuess` attribute used to initialize them [Åkesson, 2008].

JModelica.org

JModelica.org [Åkesson *et al.*, 2010] is an open source platform for simulation and optimization based on Modelica models. It incorporates compilers for Modelica models and the optimization support introduced by Optimica to allow for high-level declaration of optimal control problems as well as parameter estimation problems. The collocation algorithm used in Ch. 7 was implemented in Python and based on the same formulation as the one presented in this chapter [Magnusson, 2012]. It translates the Modelica model and Optimica code to XML form and the resulting NLP problem is solved using the interior point solver IPOPT (Interior Point OPTimizer) [Wächter and Biegler, 2006]. JModelica.org features a Python [Python Software Foundation, 2012] interface for scripting, simulation and optimization, as well as visualizing or analyzing the results.

CasADi

To calculate the derivatives, CasADi (Computer algebra system with Automatic Differentiation) [Andersson *et al.*, 2010] was used in the optimization algorithm. CasADi calculates all the relevant derivatives needed for solving the resulting NLP.

3

Experimental Setup

Four different engines were used to obtain the experimental results presented in this thesis. Data from an optical single-cylinder engine was used for validating the model presented in Ch. 4. A six-cylinder engine was used for the control experiments in Ch. 5, and a single-cylinder engine was used for those in Ch. 6. The fourth engine was also a single-cylinder engine and was used for the PPC results in Ch. 7. All engines were equipped with cylinder pressure sensors.

3.1 Optical Engine

The optical engine was a Scania heavy-duty diesel engine converted to single-cylinder operation. The engine was equipped with a quartz piston allowing measurements of the wall temperature to be made using thermographic phosphors. For further details on the measurement technique and the experimental conditions, see [Wilhelmsson *et al.*, 2005]. Table 3.1 contains geometric data and relevant valve timings for the engine. During the experiments presented in Ch. 4, the engine was operated manually and only the injected fuel amount was varied in the experiments. The fuel used was iso-octane.

3.2 Six-Cylinder Engine

The six-cylinder engine shown in Fig. 3.1 was a Volvo heavy-duty diesel engine. The engine and the control system were described in detail in [Karlsson, 2008] and was based on the system used in [Strandh, 2006; Bengtsson, 2004]. The engine specifications are presented in Table 3.2.

The control system was run in Linux on a PC-computer with a 2.4 GHz Intel Pentium 4 CPU. Controllers were designed in Matlab/Simulink

Table 3.1   Optical Engine Specifications

Quantity	Value
Displacement volume	1966 cm^3
Bore	127.5 mm
Stroke	154 mm
Connecting rod length	255 mm
Compression ratio	16:1
Exhaust valve open	146° ATDC
Exhaust valve close	354° ATDC
Inlet valve open	358° ATDC
Inlet valve close	564° ATDC

and converted to C-code using Real-Time Workshop [Mathworks, 2006]. A graphical user interface allowed for enabling/disabling controllers as well as manual control of all variables. A wide selection of possible control signals were available. The control signals used in the experiments presented in Ch. 5 were the crank angle of inlet valve closing (θ_{IVC}) and the intake temperature (T_{in}). To investigate the robustness of the control system, the engine speed, the amount of injected fuel, and the amount of recycled exhausts were varied. The engine was equipped with a long-route Exhaust Gas Recirculation system.
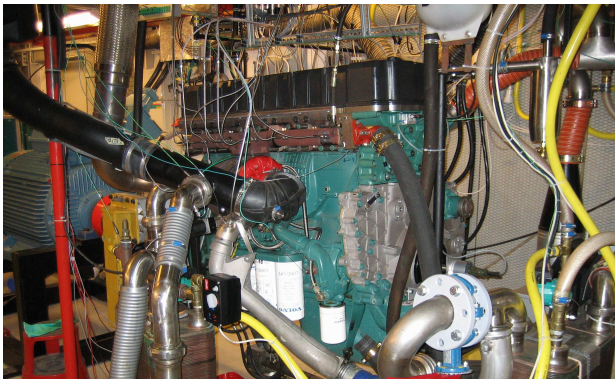
Figure 3.1   The six-cylinder engine used for the control experiments in Ch. 5.

Table 3.2 Six-Cylinder Engine Specifications

Quantity	Value
Displacement volume	2000 cm^3
Bore	131 mm
Stroke	150 mm
Connecting rod length	260 mm
Compression ratio	18.5:1
Exhaust valve open	101° ATDC
Exhaust valve close	381° ATDC
Inlet valve open	340° ATDC
Inlet valve close	variable

Table 3.3 Single-Cylinder Engine 1 Specifications

Quantity	Value
Displacement Volume	550 cm^3
Bore	81 mm
Stroke	93.2 mm
Connecting rod length	147 mm
Compression Ratio	13:1
Valves	variable

3.3 Single-Cylinder Engine 1

The hybrid control results in Ch. 6 were obtained on a 2.2-liter 4-cylinder General Motors Ecotech gasoline engine with direct fuel injection. The engine was equipped with a variable valve actuation (VVA) system, as described in [Liao *et al.*, 2011]. The system allowed for independent cycle-to-cycle control of both intake and exhaust valve timings. In the experiments presented in Ch. 6, the possibility of varying the exhaust valve closing timing on a cycle-to-cycle basis was utilized.
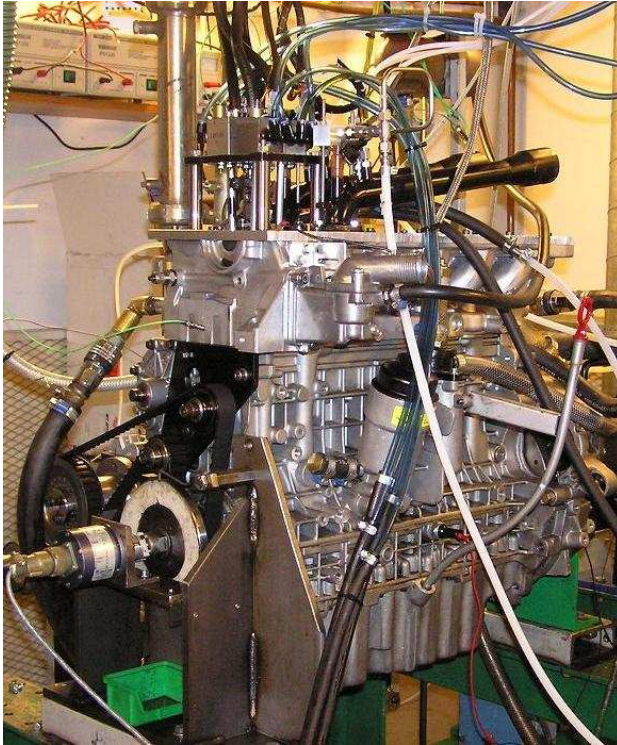
Figure 3.2   The single-cylinder engine used to generate the experimental data used in Ch. 7.

3.4 Single-Cylinder Engine 2

Experimental data for the PPC model presented in Ch. 7 were obtained from a Volvo D5 light duty engine operated on a single cylinder, shown in Fig. 3.2. The engine was equipped with a fully flexible pneumatic valve train system and direct injection of fuel. The engine was run naturally aspirated without cooled external exhaust gas recirculation. Additional engine specifications are listed in Table 3.2. The engine and the control and data acquisition system were described in more detail in [Borgqvist *et al.*, 2011].

Table 3.4   Single-Cylinder Engine 2 Specifications

Quantity	Value
Displacement Volume	480 cm^3
Bore	81 mm
Stroke	93.2 mm
Connecting rod length	152 mm
Compression Ratio	16.5:1
Valves	variable

4

Cycle-to-Cycle Modeling of HCCI

This chapter presents a cycle-to-cycle model of HCCI combustion including heat transfer effects between the gas charge and the cylinder walls. Most of the models referenced in Sec. 2.1 contain a cycle-to-cycle coupling through the residual gas temperature, also included in this model. However, when there is only a small amount of residuals present in the cylinder it is likely that the cylinder wall temperature plays a larger role in the dynamic coupling between the current cycle and subsequent ones. A simple model of the interaction between the wall temperature and the gas in the cylinder was therefore included.

The resulting model takes the form of a nonlinear discrete time dynamical system. The experimental control results presented in Ch. 5 were obtained using controllers based on linearizations of the model.

4.1 Heat Transfer

Heat transfer between the gas charge inside the cylinder and the cylinder walls is an important effect for explaining HCCI cycle-to-cycle behavior under certain operating conditions [Blom *et al.*, 2008]. Also, experimental data show considerable variations in wall temperature with varying operating conditions [Wilhelmsson *et al.*, 2005]. However, many modeling approaches for control only consider heat transfer from the gases to the walls during combustion, and assume a constant cylinder wall temperature [Bengtsson *et al.*, 2007]. Continuous-time models including cylinder wall temperature models were presented in [Roelle *et al.*, 2006; Blom *et al.*, 2008]. The latter synthesized an LQ controller using a cycle-to-cycle statistical version of the model and presented experimental results. A GT-power based engine model augmented with a heat transfer model
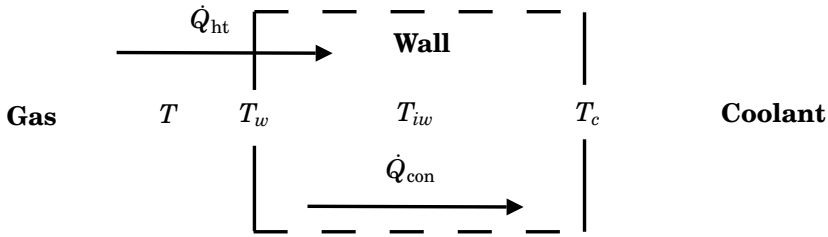
Figure 4.1   Principle of the cylinder wall model.

was used in a simulation study in [Chang *et al.*, 2007]. A more detailed study of the cylinder wall temperature was done in [Rakopoulos *et al.*, 2004], where Fourier analysis was applied to capture spatial variations. An experimental study of the cylinder wall temperature variations within a single engine cycle was presented in [Särner *et al.*, 2005]. Experimental studies of the heat transfer correlation for HCCI engines were presented in [Chang *et al.*, 2004; Soyhan *et al.*, 2009].

Single-Zone Cylinder Wall Model

The cylinder wall and piston head were modeled as a single mass with a slowly varying outer surface temperature, T_c, a heat flow between the in-cylinder gases and the cylinder wall, $\dot{Q}_{ht}$, and a conductive heat flow through the wall, $\dot{Q}_{con}$, see Fig. 4.1. The temperature of the gas inside the cylinder was denoted T and the wall surface temperature was denoted T_w.

The heat flow $\dot{Q}_{ht}$ is mainly due to convection and radiation [Heywood, 1988]. Radiation can be modeled as proportional to $(T - T_w)^4$ and typically becomes more pronounced at higher loads [Heywood, 1988]. For modeling of low temperature combustion, particularly at low load, the heat flow can be approximated by modeling convection as the only mode of heat transfer between the in-cylinder charge and the cylinder wall [Roelle *et al.*, 2006; Blom *et al.*, 2008].

Modeling of Convective Heat Flow   The convective heat flow was modeled using the Newton law

$$\dot{Q}_{ht} = h_c A_c (T - T_w) \tag{4.1}$$

where h_c is the convection coefficient, A_c is the wall surface area and T_w is the wall surface temperature. The convection coefficient is often modeled as some variation on the Woschni expression [Woschni, 1967; Bengtsson *et al.*, 2007]

$$h_c = \alpha_s B^{-0.2} p^{0.8} T^{-0.55} v^{0.8} \tag{4.2}$$

where α_s is a scaling factor, B is the cylinder bore, and v is the characteristic velocity of the gas defined as

$$v = C_1 S_p + C_2 \frac{V_d T_r}{p_r V_r}(p - p_{\text{motored}}) \tag{4.3}$$

where C_1 and C_2 are constants, S_p is the mean piston speed, T_r, p_r, and V_r are the temperature, pressure, and volume at some reference crank angle, and p_{motored} is the motored pressure. A modified version of the Woschni expression was presented in [Chang *et al.*, 2004]

$$h_c = \alpha_s L^{-0.2} p^{0.8} T^{-0.73} v_{\text{Chang}}^{0.8} \tag{4.4}$$

where

$$v_{\text{Chang}} = C_1 S_p + \frac{C_2}{6} \frac{V_d T_r}{p_r V_r}(p - p_{\text{motored}}) \tag{4.5}$$

A comparison of different models of h_c for HCCI heat transfer was presented in [Soyhan *et al.*, 2009], where it was found that the Hohenberg expression

$$h_c = \alpha_s V^{-0.06} p^{0.8} T^{-0.4} (S_p + b)^{0.8} \tag{4.6}$$

where b is a constant, [Hohenberg, 1979], was advantageous in terms of agreement with experimental data and ease of parameter adjustment.

Cylinder Wall Temperature Dynamics   The first law of thermodynamics applied to the gas when no work is performed yields the expression

$$\dot{T} = -\frac{\dot{Q}_{\text{ht}}}{mc_v} \tag{4.7}$$

for the time derivative of the temperature of the gas inside the cylinder, where m and c_v are the mass and specific heat of the gas, respectively. The time derivative of the inner wall temperature, T_{iw}, is given by

$$\dot{T}_{iw} = \frac{\dot{Q}_{\text{ht}} - \dot{Q}_{\text{con}}}{m_c C_p} \tag{4.8}$$

where C_p is the specific heat of the cylinder wall, m_c is the cylinder wall mass, and $\dot{Q}_{\text{con}}$ is the conductive heat flow through the wall, given by

$$\dot{Q}_{\text{con}} = \frac{(T_w - T_c)k_c A_c}{L_c} \tag{4.9}$$

where k_c is the conduction coefficient and L_c is the wall thickness.

Assuming that the steady-state temperature condition

$$T_{iw} = \frac{T_w + T_c}{2} \tag{4.10}$$

holds, the temperature equations, (4.1), (4.7), (4.8), and (4.9), may be written as

$$\dot{\mathcal{T}} = A_{ht}\mathcal{T} + B_{ht}T_c \tag{4.11}$$

where

$$A_{ht} = \begin{pmatrix} -\dfrac{h_c A_c}{m c_v} & \dfrac{h_c A_c}{m c_v} \\ 2\dfrac{h_c A_c}{m_c C_p} & -2\dfrac{h_c A_c + k_c A_c / L_c}{m_c C_p} \end{pmatrix}, \tag{4.12}$$

$$B_{ht} = \begin{pmatrix} 0 \\ 2\dfrac{k_c A_c}{L_c m_c C_p} \end{pmatrix}, \quad \mathcal{T} = \begin{pmatrix} T \\ T_w \end{pmatrix}$$

Equation (4.10) implies that the inner wall temperature is the average of the cylinder wall temperature and the coolant temperature. Similar assumptions were made in [Blom *et al.*, 2008; Roelle *et al.*, 2006]. The resulting model was used in a continuous-time formulation in the former while the latter updated the wall temperature once per cycle combined with continuous-time gas temperature dynamics. A more detailed model, such as the one in [Rakopoulos *et al.*, 2004], could be used to calculate the spatial dependence on the temperature profile within the wall.

Sampled Version for Cycle-to-Cycle Modeling   To be able to include a model of the heat transfer effects in a cycle-to-cycle model, some form of discretization is necessary. Since T_c is assumed to be slowly varying, it can be assumed constant over a short time interval of length t_i. The temperature state at time t_i, given an initial state $\mathcal{T}(0)$, can be calculated using a zero-order-hold approach

$$\mathcal{T}(t_i) = \Phi_i \mathcal{T}(0) + \Gamma_i T_c \tag{4.13}$$

where

$$\Phi_i = e^{A_{ht}t_i}, \quad \Gamma_i = \int_0^{t_i} e^{A_{ht}(t_i-\tau)} B_{ht} d\tau \tag{4.14}$$

In the model, Eq. (4.13) was used to update the gas temperature and the wall temperature after mixing, after combustion, and after expansion. Since the integration times, t_i, need to be adapted to each instant, and some of the parameters depend on operating conditions, three sets of matrices $\{\Phi_i, \Gamma_i\}$, $i = 1, 3, 5$ were used, where $i = 1$ corresponded to mixing,

$i = 3$ corresponded to combustion, and $i = 5$ corresponded to expansion. These heat transfer events modeled the lumped heat transfer during the corresponding stages of the cycle, while the compression and expansion were modeled as isentropic processes.

4.2 Chemistry

The chemical reaction describing complete, stoichiometric, combustion of a general hydrocarbon with x carbon atoms and y hydrogen atoms, C_xH_y, in air can be written [Heywood, 1988]

$$C_xH_y + \left(x + \frac{y}{4}\right) O_2 + 3.773 \left(x + \frac{y}{4}\right) N_2 \rightarrow$$
$$xCO_2 + \frac{y}{2}H_2O + 3.773 \left(x + \frac{y}{4}\right) N_2 \quad (4.15)$$
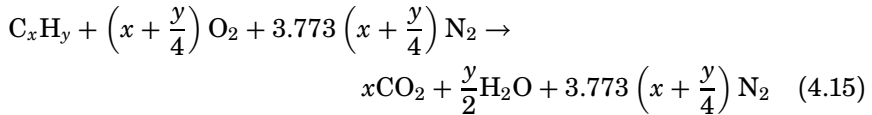
In some cases, it is desirable to re-induct, or retain, a portion of the exhaust gases in the cylinder either through a long route EGR system or by means of variable valve actuation as described in Ch. 1. A possible measure of the fraction of residuals in the cylinder is the ratio x_r

$$x_r = \frac{n_p}{n_r + n_p} \qquad (4.16)$$

where n_p and n_r correspond to the number of moles of combustion products and reactants, respectively. When no residuals are trapped or re-breathed, this measure can also be expressed as

$$\alpha = \frac{n_p}{n_r} = \frac{x_r}{1 - x_r} \qquad (4.17)$$

The measure α of the proportion of combustion products in the cylinder was used in [Shaver *et al.*, 2006b] among others.

The present residuals in the current cycle were assumed to correspond to the residuals produced in the same cycle. The motivation for this assumption is that the residual concentration typically does not vary much in steady state, and that transients are expected to be fast due to the large air excess in both HCCI and PPC. The cylinder contents following

injection of a hydrocarbon $C_x H_y$ can then be described as

$$\alpha \left(x CO_2 + \frac{y}{2} H_2 O + 3.773 (x + \frac{y}{4}) \frac{1}{\phi} N_2 + (x + \frac{y}{4}) \frac{1-\phi}{\phi} O_2 \right)$$

$$+ \left(C_x H_y + (x + \frac{y}{4}) \frac{1}{\phi} O_2 + 3.773 (x + \frac{y}{4}) \frac{1}{\phi} N_2 \right) \rightarrow$$

$$C_x H_y + \alpha x CO_2 + \alpha \frac{y}{2} H_2 O$$

$$+ 3.773 (1 + \alpha)(x + \frac{y}{4}) \frac{1}{\phi} N_2 + (\alpha(1 - \phi) + 1)(x + \frac{y}{4}) \frac{1}{\phi} O_2 \quad (4.18)$$

where the first term describes the residuals and the second term describes the fresh reactants and ϕ is the equivalence ratio, defined through the fuel to oxidizer ratio required for stoichiometric combustion, $\left(n_{C_x H_y} / n_{O_2} \right)_s$, where $n_{C_x H_y}$ and n_{O_2} denote the number of fuel and O_2 molecules, respectively

$$\phi = \frac{n_{C_x H_y}}{n_{O_2}} \Big/ \left(\frac{n_{C_x H_y}}{n_{O_2}} \right)_s \quad (4.19)$$

4.3 Temperature Trace

Compression and expansion were modeled as isentropic processes. The following relationships can be found in, e.g., [Heywood, 1988] and are derived from the first law of thermodynamics.

The temperature, T_B, and pressure, p_B, after isentropic compression or expansion from a volume V_A to a volume V_B with initial temperature and pressure T_A and p_A, are given by

$$T_B = T_A \left(\frac{V_A}{V_B} \right)^{\gamma-1}, \quad p_B = p_A \left(\frac{V_A}{V_B} \right)^{\gamma} \quad (4.20)$$

T_B after isentropic compression or expansion from a pressure p_A to a pressure p_B is given by

$$T_B = T_A \left(\frac{p_B}{p_A} \right)^{(\gamma-1)/\gamma} \quad (4.21)$$

Intake/Mixing

The gas temperature at the start of cycle k, $T_1(k)$, was modeled as the weighted average of the intake temperature and the temperature of the

trapped residuals, cf. [Shaver *et al.*, 2009]

$$T_1(k) = \frac{c_{v,in} T_{in}(k) + c_{v,EGR} \chi \alpha T_{5+}(k-1)}{c_{v,in} + \alpha c_{v,EGR}} \qquad (4.22)$$

where $c_{v,in}$ and $c_{v,EGR}$ are the specific heats of the fresh reactants and the residual gases, respectively, and α is the molar ratio between trapped residuals and inducted gases. It should be noted that this expression models trapped residuals. If a long-route, cooled, EGR system is used, only $c_{v,in}$ is affected. To model this, a second parameter, denoting the ratio between reinducted exhaust and fresh charge, would be required.

The final gas temperature of cycle $k-1$ is denoted $T_{5+}(k-1)$, and χ is a measure of how much the residual temperature has decreased. The initial wall temperature of cycle k was set equal to the final wall temperature of cycle $k-1$

$$T_{w1}(k) = T_{w5+}(k-1) \qquad (4.23)$$

Eq. (4.13), with $i = 1$, was applied to yield new temperatures $T_{1+}(k)$ and $T_{w1+}(k)$

$$\begin{pmatrix} T_{1+}(k) \\ T_{w1+}(k) \end{pmatrix} = \Phi_1 \begin{pmatrix} T_1(k) \\ T_{w1}(k) \end{pmatrix} + \Gamma_1 T_c \qquad (4.24)$$

Compression

Isentropic compression from the intake pressure, p_{in}, at the volume at inlet valve closing, $V_1(k)$, to the volume at auto-ignition, $V_2(k)$, was assumed, yielding the temperature $T_2(k)$ and the pressure $p_2(k)$

$$T_2(k) = T_{1+}(k) \left(\frac{V_1(k)}{V_2(k)} \right)^{\gamma-1}, \quad p_2(k) = p_{in} \left(\frac{V_1(k)}{V_2(k)} \right)^{\gamma} \qquad (4.25)$$

Combustion

Assuming complete isochoric combustion, without heat losses to the cylinder walls, the increase in mean gas temperature due to combustion can be computed using the fuel mass, $m_f(k)$, and the lower heating value, ξ_{LHV}, of the fuel [Heywood, 1988]

$$T_3(k) = T_2(k) + \frac{m_f(k)}{m(k)} \frac{\xi_{LHV}}{c_v} \qquad (4.26)$$

The total gas mass can be decomposed as

$$m(k) = m_a(k) + m_f(k) + m_p(k) \qquad (4.27)$$

where $m_p(k)$ is the mass of the residuals from the previous cycle. Using Eqs. (4.19), (4.17), and (4.27) the ratio $m_f(k)/m(k)$ in Eq. (4.26) can be estimated as

$$\frac{m_f(k)}{m(k)} = \frac{1}{(\phi^{-1}(m_a/m_f)_s + 1)(1 + f_\alpha(\phi))} \tag{4.28}$$

where

$$f_\alpha(\phi) = \frac{\alpha M_p}{\phi^{-1}(m_a/m_f)_s + 1}\left(\frac{\phi^{-1}(m_a/m_f)_s}{M_a} + \frac{1}{M_f}\right) \tag{4.29}$$

with M_p, M_a, and M_f denoting the molar masses of the products, air, and fuel, respectively. However, the variation in $f_\alpha(\phi)$ for the values of ϕ investigated was less than one percent. For simplicity, the approximation

$$\frac{m_p(k)}{m_a(k) + m_f(k)} \approx \alpha \tag{4.30}$$

was used, replacing $f_\alpha(\phi)$ with α in Eq. (4.28) yielding an error of less than one percent in the mass ratio estimate. This yields the following expression for $T_3(k)$

$$T_3(k) = T_2(k) + \frac{\xi_{\text{LHV}}}{(1 + \alpha)(\phi^{-1}(m_a/m_f)_s + 1)c_v} \tag{4.31}$$

Equation (4.13) was then applied with $i = 3$ and $T_{w3}(k) = T_{w1+}(k)$ to find new temperatures, $T_{3+}(k)$ and $T_{w3+}(k)$

$$\begin{pmatrix} T_{3+}(k) \\ T_{w3+}(k) \end{pmatrix} = \Phi_3 \begin{pmatrix} T_3(k) \\ T_{w3}(k) \end{pmatrix} + \Gamma_3 T_c \tag{4.32}$$

The pressure after combustion is then

$$p_3(k) = \frac{T_{3+}(k)}{T_2(k)} p_2(k) \tag{4.33}$$

Expansion

The gas temperature and pressure after expansion, $T_4(k)$ and $P_4(k)$, were calculated assuming isentropic expansion from $V_2(k)$ to the volume at exhaust valve opening, $V_4(k)$

$$T_4(k) = T_{3+}(k)\left(\frac{V_2(k)}{V_4(k)}\right)^{\gamma-1}, \quad p_4(k) = p_3(k)\left(\frac{V_2(k)}{V_4(k)}\right)^{\gamma} \tag{4.34}$$

Isentropic expansion from the pressure inside the cylinder to atmospheric pressure was assumed at exhaust valve opening, yielding the temperature $T_5(k)$

$$T_5(k) = T_4(k) \left(\frac{p_{\text{in}}}{p_4(k)} \right)^{(\gamma-1)/\gamma} \tag{4.35}$$

Finally, Eq. (4.13) was applied with $i = 5$ and $T_{w5}(k) = T_{w3+}(k)$ to obtain the final gas temperature, $T_{5+}(k)$, and the final wall temperature, $T_{w5+}(k)$

$$\begin{pmatrix} T_{5+}(k) \\ T_{w5+}(k) \end{pmatrix} = \Phi_5 \begin{pmatrix} T_5(k) \\ T_{w5}(k) \end{pmatrix} + \Gamma_5 T_c \tag{4.36}$$

4.4 Prediction of Auto-Ignition

The combustion timing has a pronounced impact on how the subsequent combustion behaves, and several models of the auto-ignition of fuel have been suggested. The ignition delay can be modeled explicitly as a function of relevant engine variables [Assanis *et al.*, 2003; Gogoi and Baruah, 2010] or implicitly through an *Arrhenius integral* [Shaver *et al.*, 2006b; Friedrich *et al.*, 2006; Chmela *et al.*, 2007; Chiang and Stefanopoulou, 2009] or *knock integral* [Hillion *et al.*, 2008; Shahbakhti and Koch, 2007].

The Arrhenius Integral

The onset of combustion is triggered by the formation of a critical amount of radicals, molecules with an unpaired electron, $R\cdot$ [Chiang and Stefanopoulou, 2009]. The reaction rate of two species, A and B, is proportional to the concentrations of the reactants via a rate coefficient k_{bimolec} [Turns, 2006]

$$\frac{d[A]}{dt} = -k_{\text{bimolec}}[A][B] \tag{4.37}$$

Within a limited temperature range, the rate coefficient can be expressed on Arrhenius form as

$$k_{\text{bimolec}} = C_{\text{Arr}} \exp\left(-\frac{E_a}{RT} \right) \tag{4.38}$$

where E_a is the activation energy and C_{Arr} is a constant. While combustion of hydrocarbons proceeds in multiple steps, a global or quasi-global model can be a useful approximation. The combustion is then modeled as a single mechanism with an approximate reaction rate similar to that in Eq. (4.38) [Turns, 2006]

$$\frac{d[C_x H_y]}{dt} = -C_{\text{Arr}} \exp\left(-\frac{E_a}{RT} \right) [C_x H_y]^a [O_2]^b \tag{4.39}$$

where $[C_xH_y]$ and $[O_2]$ denote the concentrations of fuel and oxygen, and a, and b are sensitivity measures towards the concentrations of fuel and oxygen, respectively.

For prediction of auto-ignition, the reaction rate is sometimes augmented with a dependence on pressure, yielding the following expression for the formation rate of radicals [Chiang and Stefanopoulou, 2009]

$$\frac{d[R\cdot]}{dt} = C_{\text{Arr}} p^{n_{p,\text{Arr}}} \exp\left(-\frac{E_a}{RT}\right)[C_xH_y]^a[O_2]^b \tag{4.40}$$

where the parameter $n_{p,\text{Arr}}$ denotes the sensitivity towards pressure. By neglecting the small amount of radicals at inlet valve closing, i.e., setting $[R\cdot](\theta_{\text{IVC}}) = 0$, the critical amount of radicals needed to initiate combustion, $[R\cdot]_c$, can be expressed as

$$[R\cdot]_c = \int_{\theta_{\text{IVC}}}^{\theta_{\text{SOC}}} \frac{d[R\cdot]}{d\theta} d\theta \tag{4.41}$$

where θ_{SOC} denotes the crank angle corresponding to start of combustion. To simplify the notation, the function r_{Arr} and the constant K can be introduced according to

$$r_{\text{Arr}} = \frac{d[R\cdot]}{d\theta}, \quad K = [R\cdot]_c \tag{4.42}$$

The condition for auto-ignition can then be written as

$$\frac{1}{K} \int_{\theta_{\text{SOI}}}^{\theta_{\text{SOC}}} r_{\text{Arr}} d\theta = 1 \tag{4.43}$$

A sensitivity analysis presented in [Chiang and Stefanopoulou, 2009] suggested that the dependence on temperature was much greater than the dependence on fuel and air concentrations, and that the following expression could be suitable for purposes of control design for HCCI

$$1 = \int_{\theta_{\text{IVC}}}^{\theta_{\text{SOC}}} C_{\text{Arr}} p^{n_{p,\text{Arr}}} \exp\left(-\frac{E_a}{RT}\right) d\theta \tag{4.44}$$

Assuming isentropic compression the condition can be rewritten using the notation in Sec. 4.3 as

$$\int_{\theta_{\text{IVC}}(k)}^{\theta_{\text{SOC}}(k)} f_k(\theta) d\theta = 1 \tag{4.45}$$

where

$$f_k(\theta) = A_a p_{\text{in}}^{n_{p,\text{Arr}}} \mathcal{V}_k^{\gamma n_{p,\text{Arr}}}(\theta) \exp\left(-\frac{E_a \mathcal{V}_k^{1-\gamma}(\theta)}{RT_{1+}(k)}\right) \tag{4.46}$$

and

$$\mathcal{V}_k(\theta) = V_1(k)/V(\theta) \tag{4.47}$$

Approximate Version for Cycle-to-Cycle Modeling

To obtain an explicit expression for θ_{SOC}, an approach similar to that in [Shaver *et al.*, 2009] was adopted. The integrand was approximated with its maximum value, which is attained at top dead center, i.e.,

$$f_k(\theta) \approx f_k(\theta_{\text{TDC}}) \tag{4.48}$$

The lower integration limit was then shifted from θ_{IVC} to θ_{TDC} and the resulting integral equation was solved for $\theta_{\text{SOC}}(k)$

$$\theta_{\text{SOC}}(k) = \Delta\theta_A + \frac{1}{f_k(\theta_{\text{TDC}})} \tag{4.49}$$

where $\Delta\theta_A$ is an crank angle offset. This makes $\theta_{\text{SOC}}(k)$ an explicit function of $\theta_{\text{IVC}}(k)$, p_{in}, and $T_{1+}(k)$.

Another simplification was suggested in [Chiang *et al.*, 2007], where a linear approximation of the dependence on the temperature at inlet valve closing for a specific amount of injected fuel was used.

4.5 Model Summary and Outputs

The temperature trace, including the heat transfer events, can be described in algorithmic form, where the variables in each stage can be computed from those of the previous stages. The following five steps describe the evolution of the gas and wall temperature during each model stage, mapping the states from the previous cycle, $T_{5+}(k-1)$ and $T_{w5+}(k-1)$, and the inputs, $\theta_{\text{IVC}}(k)$ and $T_{\text{in}}(k)$, to the states at the current cycle, $T_{5+}(k)$ and $T_{w5+}(k)$.

1. Intake/Mixing with heat transfer

$$\begin{pmatrix} T_{1+}(k) \\ T_{w1+}(k) \end{pmatrix} = \Phi_1 \begin{pmatrix} \dfrac{c_{v,in}T_{\text{in}}(k) + c_{v,\text{EGR}}\chi\alpha T_{5+}(k-1)}{c_{v,\text{in}} + \alpha c_{v,\text{EGR}}} \\ T_{w5+}(k-1) \end{pmatrix} + \Gamma_1 T_c$$

2. Prediction of Auto-ignition and Compression

$$\theta_{\text{SOC}}(k) = \Delta\theta_A + \frac{1}{f_k(\theta_{\text{TDC}})}$$

$$T_2(k) = T_{1+}(k) \left(\frac{V_1(k)}{V_2(k)} \right)^{\gamma-1}$$

$$p_2(k) = p_{\text{in}} \left(\frac{V_1(k)}{V_2(k)} \right)^{\gamma}$$

3. Combustion with heat transfer

$$\begin{pmatrix} T_{3+}(k) \\ T_{w3+}(k) \end{pmatrix} = \Phi_3 \begin{pmatrix} T_2(k) + \dfrac{\xi_{\text{LHV}}}{(1+\alpha)(\phi^{-1}(m_a/m_f)_s + 1)c_v} \\ T_{w1+}(k) \end{pmatrix} + \Gamma_3 T_c$$

$$p_3(k) = \frac{T_{3+}(k)}{T_2(k)}$$

4. Expansion

$$T_4(k) = T_{3+}(k) \left(\frac{V_2(k)}{V_4(k)} \right)^{\gamma-1}$$

$$p_4(k) = p_3(k) \left(\frac{V_2(k)}{V_4(k)} \right)^{\gamma}$$

5. Exhaust with heat transfer

$$\begin{pmatrix} T_{5+}(k) \\ T_{w5+}(k) \end{pmatrix} = \Phi_5 \begin{pmatrix} T_4(k) \left(\dfrac{p_{\text{in}}}{p_4(k)} \right)^{(\gamma-1)/\gamma} \\ T_{w3+}(k) \end{pmatrix} + \Gamma_5 T_c$$

The combustion duration is a function of the charge temperature, composition, and θ_{SOC} [Chiang and Stefanopoulou, 2009]. Around an operating point, the combustion duration was assumed constant, yielding the following expression for θ_{50}, where $\Delta\theta$ is a crank angle offset

$$\theta_{50}(k) = \theta_{\text{SOC}}(k) + \Delta\theta \tag{4.50}$$

The indicated mean effective pressure was calculated from the gas temperatures [Heywood, 1988]

$$\text{IMEP}_n(k) = \frac{mc_v}{V_d} \left(T_{1+}(k) - T_2(k) + T_{3+}(k) - T_4(k) \right) \tag{4.51}$$

The resulting model takes the form

$$\begin{aligned}
x(k+1) &= \mathbf{F}(x(k), u(k)) \\
y(k) &= \mathbf{G}(x(k), u(k))
\end{aligned} \tag{4.52}$$

where

$$x(k) = \begin{pmatrix} T_{5+}(k) \\ T_{w5+}(k) \end{pmatrix} \tag{4.53}$$

and

$$y(k) = \begin{pmatrix} \mathrm{IMEP}_n(k) \\ \theta_{50}(k) \end{pmatrix}, \quad u(k) = \begin{pmatrix} \theta_{\mathrm{IVC}}(k) \\ T_{\mathrm{in}}(k) \end{pmatrix} \tag{4.54}$$

and the functions $\mathbf{F}(x(k), u(k))$ and $\mathbf{G}(x(k), u(k))$ are parametrized by the amount of injected fuel, the amount of recycled exhaust gases, the intake pressure, etc.

State Selection and Linearization

Using Eqs. (4.13), (4.46), (4.49), (4.31), (4.50), (4.51), and the assumption of isentropic compression and expansion, the temperature state can be calculated from the outputs:

$$T_{1+}(k) = \frac{E_a \mathcal{V}_k^{1-\gamma}(\theta_{\mathrm{TDC}})}{R \ln \left(A_a P_{\mathrm{in}}^{n_{p,\mathrm{Arr}}} \mathcal{V}_k^{\gamma n_{p,\mathrm{Arr}}}(\theta_{\mathrm{TDC}}) \theta_m(k) \right)} \tag{4.55}$$

where $\theta_m(k) = \theta_{50}(k) - \Delta\theta_A - \Delta\theta$, and

$$T_{w1+}(k) = \frac{\mathrm{IMEP}_n(k) - (mc_v/V_d)(c_1 T_{1+}(k) + c_2 c_3)}{c_3 (mc_v/V_d)\Phi_{3[1,2]}} \tag{4.56}$$

where

$$c_1 = 1 - \left(\frac{V_1(k)}{V_2(k)} \right)^{\gamma-1} + c_3 \Phi_{3[1,1]} \left(\frac{V_1(k)}{V_2(k)} \right)^{\gamma-1} \tag{4.57a}$$

$$c_2 = \frac{\Phi_{3[1,1]}\xi_{\mathrm{LHV}}}{(1+\alpha)\left(\phi^{-1}\left(\frac{m_a}{m_f} \right)_s + 1 \right) c_v} + \Gamma_{3[1,1]} T_c \tag{4.57b}$$

$$c_3 = 1 - \left(\frac{V_2(k)}{V_4(k)} \right)^{\gamma-1} \tag{4.57c}$$

and $\Phi_{3[i,j]}$ indicates element (i,j) of Φ_3.

This makes it possible to have IMEP_n and θ_{50} as states. Both quantities can be obtained from in-cylinder pressure measurements. The model then takes the following form.

$$y(k+1) = \hat{\mathbf{F}}(y(k), u(k)) \tag{4.58}$$

where $\hat{\mathbf{F}}(y(k), u(k))$ is obtained by going through the cycle from the previous set of output measurements.

To obtain linearizations for use in the control design in Ch. 5, the symbolic toolbox in MATLAB [Mathworks, 2008] was used to obtain linearizations according to

$$y(k+1) = Ay(k) + Bu(k) \tag{4.59}$$

where

$$A = \frac{\partial \hat{\mathbf{F}}(y(k), u(k))}{\partial y(k)}(y^0, u^0), \quad B = \frac{\partial \hat{\mathbf{F}}(y(k), u(k))}{\partial u(k)}(y^0, u^0) \tag{4.60}$$

and (y^0, u^0) is a stationary operating point.

4.6 Calibration

Initially, only the parameters connected to the heat transfer equations were optimized. A stationary operating point was used for the calibration and the model was then validated dynamically with data from step changes in the amount of fuel. Calibration of the prediction of autoignition was done once the temperature trace had been determined. Calibration data was obtained from the single-cylinder engine described in Sec. 3.1, equipped with a quartz piston, allowing measurements of the wall temperature to be made using thermographic phosphors [Wilhelmsson *et al.*, 2005]. The model was implemented in the Modelica language [The Modelica Association, 2009] and then translated into AMPL code (A Modeling Language for Mathematical Programming) [Fourer *et al.*, 2002] using Optimica [Åkesson, 2008]. This allowed the parameter calibration problem to be cast as an optimization problem minimizing the error between the model outputs and the measured outputs while respecting upper and lower bounds on the parameter values. The model was implemented using difference equations describing the temperature and pressure state in each stage of the cycle. The initial condition was the temperatures of the gas charge and cylinder wall at the end of the engine cycle.

Due to the structure of the matrices in Eq. (4.12), the parameters can be lumped into the following products in a parameter vector, $\mathbf{p}$,

$$\mathbf{p} = \left(\begin{array}{cccccc} (h_c A_c)_1 & (h_c A_c)_2 & (h_c A_c)_3 & k_c A_c/L_c & 1/m c_v & 1/m_c C_p \end{array} \right) \quad (4.61)$$

The calibration then consists of determining values for $\mathbf{p}$, the integration times t_1, t_3, and t_5, as well as initial values, x_0, of the states. With a quadratic cost function penalizing deviations between the IMEP_n and T_w obtained from experimental data and that of the model for a particular engine cycle, k, the resulting optimization problem can be written as

$$
\begin{aligned}
\min_{\mathbf{p}, t_1, t_3, t_5, x_0} \quad & \left(\text{IMEP}_n^m(k) - \text{IMEP}_n(k)\right)^2 + \delta \left(T_w^m(k) - T_w(k)\right)^2 \\
\text{s.t.} \quad & x(k+1) = \mathbf{F}\left(x(k), u(k)\right) \\
& y(k) = \mathbf{G}\left(x(k), u(k)\right) \\
& x(k+1) = x(k) = x_0 \\
& \mathbf{p}_{\min} \leq \mathbf{p} \leq \mathbf{p}_{\max} \\
& t_{\min} \leq t_i \leq t_{\max}, \quad i = 1, 2, 3 \\
& x_{0,\min} \leq x_0 \leq x_{0,\max}
\end{aligned}
\quad (4.62)
$$

where $\mathbf{p}_{\min}$, $\mathbf{p}_{\max}$, $t_{\min}$, $t_{\max}$, $x_{0,\min}$, and $x_{0,\max}$ specify lower and upper bounds on the parameter values, integration times, and initial state respectively. The constraint $x(k+1) = x(k) = x_0$ guarantees that the model is in steady state. In the cost function, IMEP_n^m and T_w^m denote the indicated mean effective pressure and wall temperature obtained from experimental data, and δ is a scalar weight.

Figure 4.2 shows the response of the nonlinear model run in open loop and θ_{50}, IMEP_n, and T_w from experimental data. Around cycle index 200, the amount of injected fuel was increased. The model captured the qualitative and quantitative behavior of the three outputs.

Figure 4.3 shows the model outputs and the wall temperature during a negative step in equivalence ratio from approximately $\phi = 0.27$ to approximately $\phi = 0.17$. The model somewhat overestimated the wall temperature and IMEP_n at the lower load.

Figure 4.4 shows a measured pressure trace with the estimated pressures superimposed. The peak pressure was underestimated slightly, but qualitatively the model captures the experimental results. Note that the point where the post combustion temperature $T_{3+}(k)$ is calculated does not correspond to a specific crank angle, since it is the temperature after modeling the lumped heat transfer during the combustion event, and this will influence the absolute value of the expansion pressure. The expansion
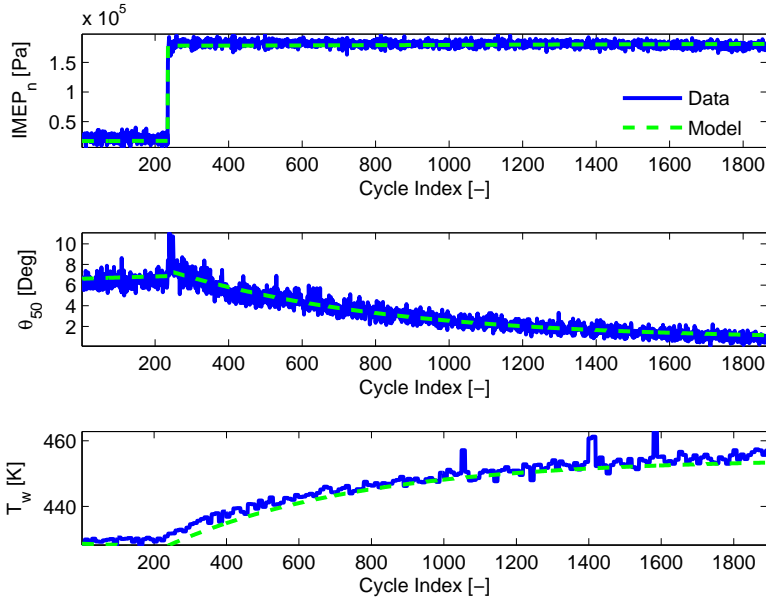
Figure 4.2 $IMEP_n$, θ_{50}, and T_w vs. cycle index. Data and model output as indicated. The amount of injected fuel was increased around cycle 200.

stroke could also be modeled as a polytropic process, obeying

$$pV^{\kappa} = C_{\text{poly}} \tag{4.63}$$

where κ is the polytropic index and C_{poly} is a constant. By taking the logarithm of both sides of the equation, an empirical value of κ for the expansion process may be found using linear regression. For the cycle shown in Fig. 4.4, it took the value $\kappa = 1.3$ whereas the specific heat ratio used in the model was $\gamma = 1.35$.

4.7 Discussion

The accuracy of model-based predictive control relies on predictions and to this purpose both physical models and statistical covariance properties could be exploited. The physical model presented in this chapter was of second order and captured the main effects on the combustion phasing due to the dynamic interaction between the gas charge and the cylinder wall
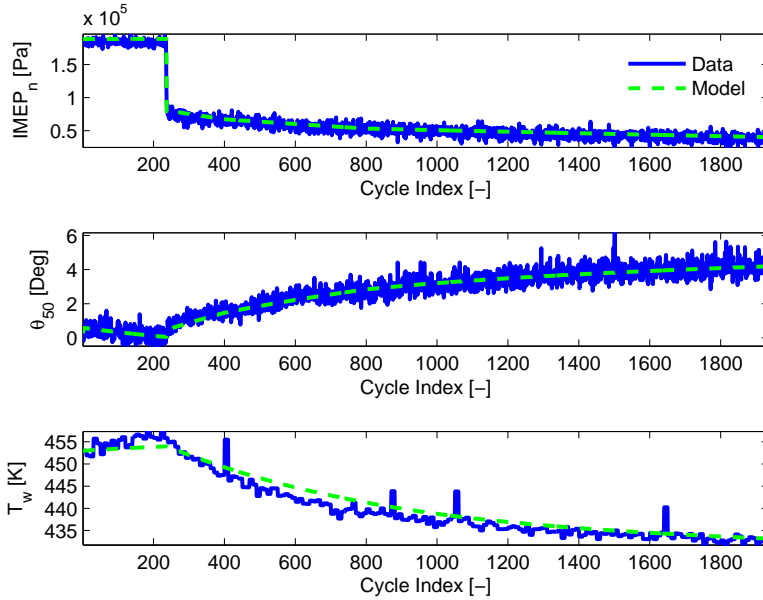
Figure 4.3   IMEP$_n$, θ_{50}, and T_w vs. cycle index. Data and model output as indicated. The amount of injected fuel was decreased around cycle 200.

temperatures. In order to see the interaction between gas temperature and wall temperature, the states, obtained from open-loop simulation, during the negative step in ϕ are shown in Fig. 4.5. There is an immediate decrease in gas temperature in response to the reduction in injected fuel. However, the dependence on the wall temperature is evident after this initial transient.

The model states were the mean gas temperature and the mean wall temperature after the exhaust valve has opened. These states are not measurable on an actual engine but the model formulation allows for using IMEP$_n$ and θ_{50} as states, enabling control design based on state feedback.

A benefit of including the slower dynamics of HCCI is that the resulting model is time-invariant. If the slower dynamics are omitted, they will act as calibration drift or time-varying dynamics or disturbances on the model and must be accounted for by integral action or other control outside the model-based control context. The cylinder wall temperature dynamics provide a reasonable explanation for the slower cycle-to-cycle dynamics in
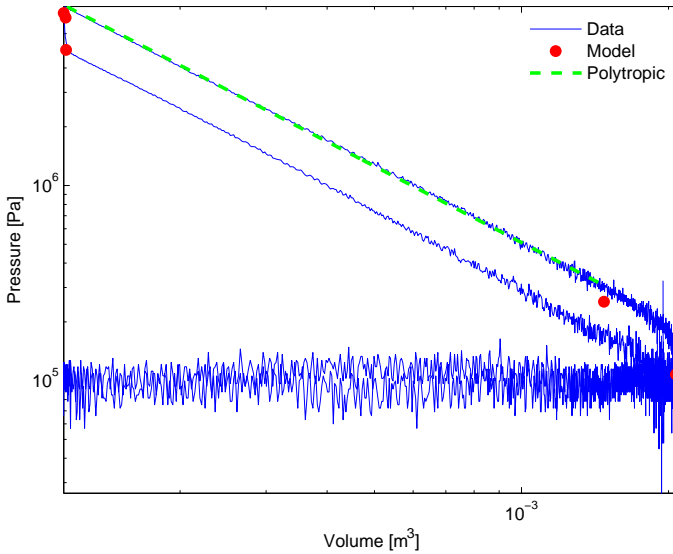
Figure 4.4 Pressure versus volume during an engine cycle. Data and model output as indicated. The '.' indicate the points where the temperatures $T_{1+}(k)$, $T_2(k)$, $T_3(k)$, $T_{3+}(k)$, and $T_4(k)$ were evaluated. The pressure obtained with an empirically determined polytropic index is superimposed during the expansion stroke.

HCCI when only small amounts of residuals are trapped in the cylinder. However, if the engine is operated with high levels of recycled, hot exhaust gases, it is disputable if this effect is of great importance.

In the calibration procedure, a number of parameters related to heat transfer were used as lumped coefficients and determined using optimization techniques. Another possibility would be to use average values for the heating values, the wall thickness and mass, and the heat transfer coefficients during each part of the cycle, leaving only the integration times as optimization parameters. The specific heat, and conduction coefficient, of the cylinder wall can be found in tables [Heywood, 1988] while a rough estimate of the wall mass and thickness could be obtained using geometric data on the engine. The wall area is a function of the crank angle and can be expressed in the cylinder volume as

$$A_c(\theta) = \frac{\pi B^2}{2} + 4\frac{V(\theta)}{B} \tag{4.64}$$

As seen in Fig. 4.4, the fit to an experimental pressure trace may be improved by adjusting the specific heat ratio, or modeling the expansion
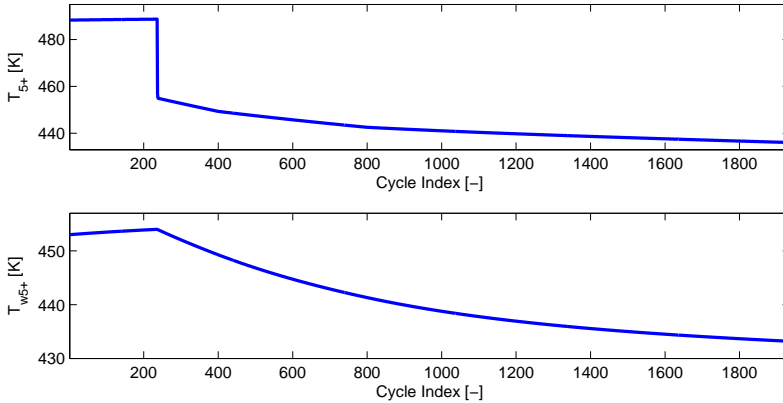
Figure 4.5   The simulated states, T_{5+} and T_{w5+} during the negative step in equivalence ratio.

as a polytropic process. The polytropic curve in Fig. 4.4 was, however, obtained using knowledge of the empirical pressure trace for the particular cycle, while the model output was predicted. The parameters related to the auto-ignition model in Eq. (4.49) can be determined through experiments [Chiang and Stefanopoulou, 2009] although some tuning may be required after the approximations made to obtain an explicit expression.

4.8 Conclusion

A physics-based, cycle-to-cycle model of HCCI including cylinder wall temperature dynamics was presented. The model was formulated with the gas charge and cylinder wall temperatures as states but manipulated to allow for state feedback. The compression and expansion were modeled as isentropic processes and three heat transfer events following mixing, combustion, and expansion were included. The model was validated against experimental data obtained from an optical engine allowing measurements of the wall temperature to be made using thermographic phosphors. The heat transfer parameters were calibrated using numerical optimization and the calibrated model captured the main characteristics of the studied outputs well.

5

HCCI Control using FTM and VVA

This chapter describes the design and experimental evaluation of a controller for θ_{50}, which was used as a proxy for combustion timing. The experimental results were obtained using the inlet air temperature and the crank angle of inlet valve closing as control signals, and the control design was based on linearizations of the model presented in Ch. 4. Note, however, that the model structure described in Ch. 4 not is limited to these two inputs but could also be used to describe, e.g., the effects of changes in the injected fuel quantity. The use of variable valve actuation allowed the inlet valve closing timing to be varied on a cycle-to-cycle basis while actuation of the inlet temperature is done on a considerably longer time-scale. The control system used for altering the inlet temperature, referred to as a Fast Thermal Management, is discussed in Sec. 5.2. In the lab environment, the intake temperature was modulated by a dedicated heater and cooler. This approach has some practical limitations for use in a vehicle, such as the heater consuming both energy and space. A possible, more practical, way of achieving the same result would be to use the hot exhaust gases to raise the inlet temperature.

Several methods have been evaluated for HCCI control. In [Bengtsson, 2004], a similar closed-loop performance in certain operating conditions was demonstrated using PID, linear quadratic, and model predictive controllers based on identified models. From a tuning perspective, however, the ability to enforce explicit constraints on the control signals using model predictive control is preferred [Maciejowski, 2002]. The majority of the actuators available for HCCI control have amplitude constraints, and rate constraints are not unusual for the control variables that include some form of mass flow.

5.1 Control Design

As only control of θ_{50} was the objective, there was no penalty on IMEP_n, but it was used as a measurement signal. The considered cost function was

$$J(k) = \sum_{i=1}^{H_p} \mathcal{Y}(i|k) + \sum_{i=0}^{H_u-1} \mathcal{U}(i|k) \tag{5.1}$$

where

$$\begin{aligned}
\mathcal{Y}(i|k) &= ||Q_{\theta_{50}}(\hat{\theta}_{50}(k+i|k) - \theta_{50}^r(k+i|k))||_2, \\
\mathcal{U}(i|k) &= ||Q_{\Delta u}(\Delta \hat{u}(k+i|k))||_2 + ||Q_u(\hat{\theta}_{\text{IVC}}(k+i|k) - \theta_{\text{IVC}}^r)||_2
\end{aligned} \tag{5.2}$$

where θ_{50}^r denotes the reference value for θ_{50}, θ_{IVC}^r denotes the reference signal for θ_{IVC}, $\Delta \hat{u}(k+i|k)$ denotes the predicted change in control signal at cycle $k+i$, and

$$u = \begin{pmatrix} \theta_{\text{IVC}} & T_{\text{in}} \end{pmatrix} \tag{5.3}$$

A small weight was added to penalize $\theta_{\text{IVC}} - \theta_{\text{IVC}}^r$ in order to obtain a slight mid-ranging effect, since there are several combinations of control signals that achieve the same θ_{50}. Including $\Delta \hat{u}(k+i|k)$ rather than $\hat{u}(k+i|k)$ in the cost function avoids penalizing non-zero control signals corresponding to a non-zero reference value for the output. The linear model in Eq. (4.59) was used to generate the predicted future outputs $\hat{\theta}_{50}(k+i)$. The parameters H_p and H_u define the length of the prediction horizon and the control horizon, respectively, and $Q_{\theta_{50}}$, $Q_{\Delta u}$, and Q_u are weights. The optimization was done subject to constraints of the form

$$\begin{aligned}
u_{\min} &\le u(k) \le u_{\max} \\
\Delta u_{\min} &\le \Delta u(k) \le \Delta u_{\max}
\end{aligned} \tag{5.4}$$

for all k. To avoid excitation effects related to the gas exchange, θ_{IVC} was restricted to $\theta_{\text{IVC}} \in [550, 620]$. The inlet temperature was restricted to $T_{\text{in}} \in [110, 135]$. To obtain error-free tracking, a disturbance observer [Åkesson and Hagander, 2003] was used. The prediction- and control horizons were set to 5 and 2 respectively.

Disturbance Modeling

With knowledge about the properties of the output measurement noise, an additional extension is possible [Bemporad *et al.*, 2004]. The state vector can be extended with a system driven by white noise and the output of this system can be added to the measured output. For prediction purposes, the noise input is assumed zero over the prediction horizon. This approach was applied in order to reduce the steady-state output variance as described in Sec. 5.3.

5.2 Experimental Setup

The six-cylinder engine described in Sec. 3.2 was used for the experimental evaluation. The experiments were performed at an engine speed of 1200 rotations per minute (rpm), yielding a sample period of 0.1 seconds per cycle, and ethanol was port injected. The injected fuel energy was 1400 [J] and no exhausts were recycled, yielding an IMEP_n of approximately 3.5 [bar] in all experiments. When evaluating the robustness towards disturbances, the engine speed, the fuel energy, and the amount of recycled exhaust gases were varied. Due to technical circumstances, four of the six cylinders (cylinder 1, 3, 5, and 6) were operated while the remaining two were motored.

Fast Thermal Management

The intake temperature was governed by two valves, a cooler, and a heater, see Fig. 5.1. A similar system was denoted Fast Thermal Management in [Haraldsson, 2005]. The heater power, q_h, could be set as well as the positions of the two valves, denoted α_{HV} and α_{CV}, for the heater valve and the cooler valve, respectively.

Assuming that the thermodynamic conditions before and after the throttles are approximately equal, the mass flow and pressure after the throttles can be maintained by requiring that the total projected flow area of the two throttles is kept constant. This assumption is not likely to hold for the individual throttles, but the experiments suggested that the impact on the resulting intake pressure was small. The projected flow areas, A_{HV} and A_{CV}, of the throttle plates in the heater path and cooler path, respectively, are given by

$$A_{\text{HV}} = (1 - \cos \alpha_{\text{HV}}) \, \bar{A}_{\text{th}}, \quad A_{\text{CV}} = (1 - \cos \alpha_{\text{CV}}) \, \bar{A}_{\text{th}} \tag{5.5}$$

where $\bar{A}_{\text{th}}$ denotes the area of each throttle plate. The condition of constant
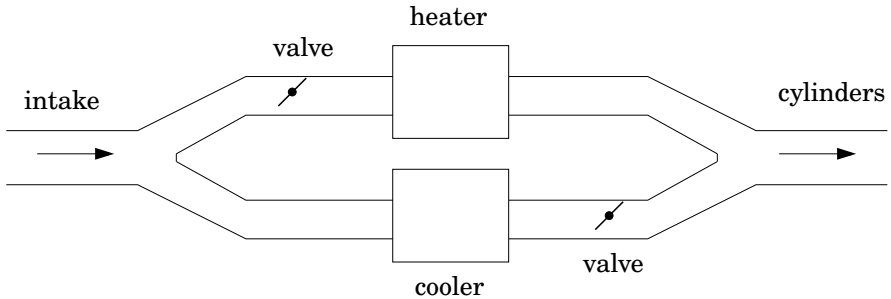

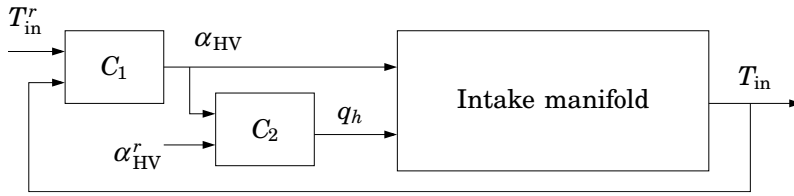**Figure 5.1**   Schematic of the fast thermal management control system.

Figure 5.2   Midranging intake temperature control strategy.

projected flow area can be written

$$\bar{A}_{\text{th}} = A_{\text{HV}} + A_{\text{CV}} \tag{5.6}$$

and solving for α_{CV} yields

$$\alpha_{\text{CV}} = \cos^{-1}(1 - \cos(\alpha_{\text{HV}})) \tag{5.7}$$

With this relation between α_{HV} and α_{CV} the intake temperature control system has two inputs (α_{HV} and q_h) and one output (T_{in}). The heater input is relatively slow while the valve has a faster response but a narrower operating range. This makes the system suitable for mid-ranging control [Allison and Isaksson, 1998]. An example of HCCI control using a mid-ranging strategy was presented in [Karlsson *et al.*, 2007]. A block diagram of the mid-ranging control strategy for control of the intake temperature is shown in Fig. 5.2. Controller C_1 governed α_{HV} to fulfill $T_{\text{in}} = T_{\text{in}}^r$ where T_{in}^r is the desired intake temperature. Controller C_2 governed q_h in order to keep α_{HV} at a desired value α_{HV}^r. Choosing α_{HV}^r slightly above the middle of the operating range gave a fairly fast response to changes in desired intake temperature.

The controllers were of PI-type and manually tuned. Figure 5.3 shows a typical step response for the closed-loop system. Completing the same step response using only the heater took approximately 700 engine cycles. Also shown in Fig. 5.3 is the intake pressure, which showed very small variations during the step. It should be noted that there was a noticeable delay in the temperature sensor. Anti-windup was implemented to handle power constraints on the heater and bounds on α_{HV}. A lower bound on α_{HV} greater than zero was introduced in order to always maintain a minimum hot flow to avoid damaging the heater.

Controller Implementation

The inlet valve closing of each operated cylinder was governed by identical controllers while the intake temperature was governed only by the controller corresponding to cylinder 5. The standard PC-computer, described
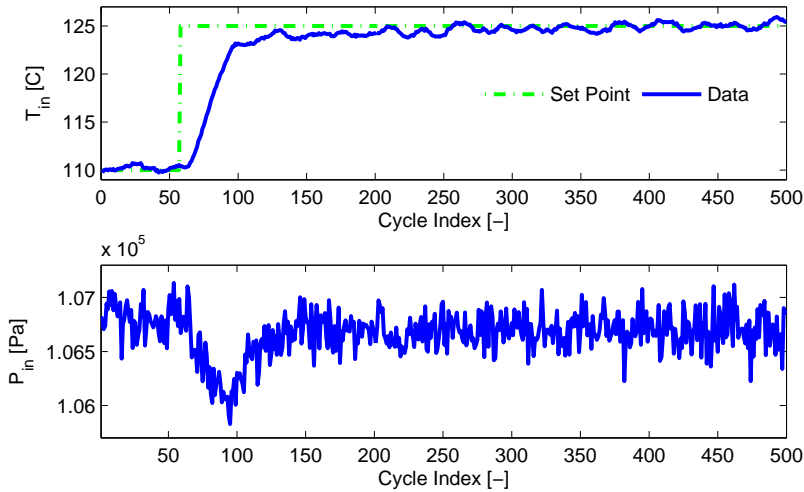
Figure 5.3 Intake temperature (top) and pressure (bottom) using the FTM controller. Set point and data as indicated. The reference value for the temperature was increased after cycle 50.

in Sec. 3.2, was sufficient in order to run the control system. The midranging control strategy for T_{in} was implemented in C++ while the predictive controllers were implemented in Simulink and compiled using Realtime Workshop [Mathworks, 2006].

5.3 Experimental Results

A typical response to a sequence of steps with increasing amplitude is shown in Fig. 5.4. The response time was less than 20 cycles for all steps. The intake temperature changed only slightly until the final step, where the inlet valve reached its constraint.

Statistical Properties

The output variance increased notably with later combustion phasing, see Fig. 5.5 which shows the steady-state output variance plotted against the reference value for θ_{50}.

Disturbance Modeling   In an attempt to reduce the steady-state output variance at the later combustion phasing, a disturbance model was
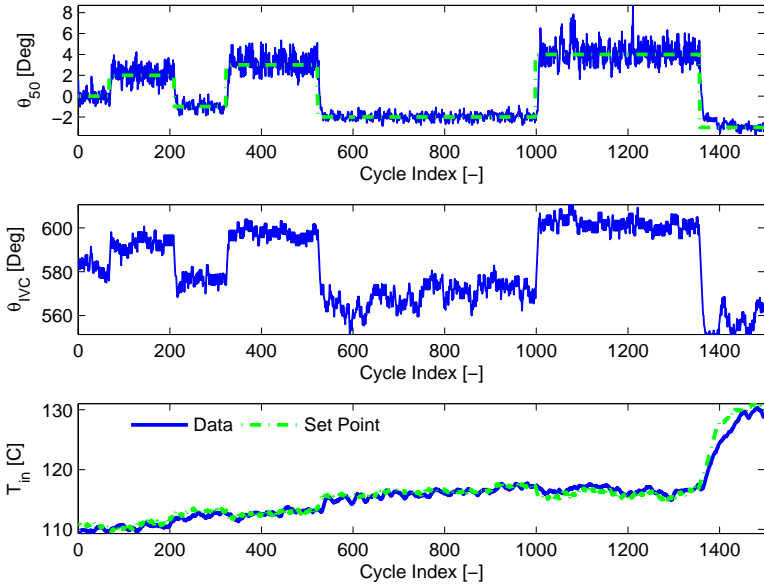
Figure 5.4   The controlled output, θ_{50}, and the control signals, θ_{IVC} and T_{in}. Set point and data as indicated. The reference signal for θ_{50} consisted of steps of increasing amplitude, and the reference for T_{in} was calculated by the MPC. All set-point changes were accomplished within 20 engine cycles.
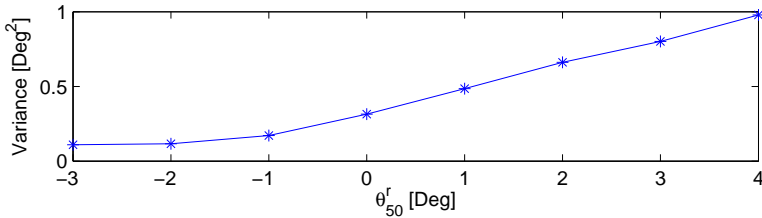
Figure 5.5   Output variance plotted against the set-point for θ_{50}.

identified. The model output residuals, $e_m(k)$, were defined as

$$e_m(k) = \theta_{50}(k) - \hat{\theta}_{50}(k) \tag{5.8}$$

where $\hat{\theta}_{50}(k)$ is the output of the linearized model in response to the input signals. Measurement data from steady-state operation were used. A stochastic realization was found using a subspace-based identification

algorithm [Johansson, 1993]. There was a distinct gap in magnitude after the first singular value of the identified subspace, indicating that a first-order model was sufficient. A model on the following form was obtained

$$e_x(k+1) = ae_x(k) + Kv(k)$$
$$e_m(k) = Ce_x(k) + v(k)$$

(5.9)

where e_x is the state and $v(k)$ is white noise.

Extended Controller The model in Eq. (4.59) was extended with the disturbance model in Eq. (5.9), yielding

$$x(k+1) = Ax(k) + Bu(k)$$
$$e_x(k+1) = ae_x(k) + Kv(k)$$
$$y(k+1) = x(k) + Ce_x(k) + v(k)$$

(5.10)

A controller was designed based on the extended model using the same design parameters as for the nominal controller. For set-points close to $\theta_{50}^r = 0$ there was no noticeable reduction in the output variance. However, for $\theta_{50}^r = 4$ the output variance was reduced slightly from approximately 1.15 $[\text{deg}^2]$ to just over 1 $[\text{deg}^2]$, corresponding to almost 10 percent of the original variance. A comparable reduction was achieved by replacing the nominal linear model with a new linearization performed around this set-point.

Robustness Towards Disturbances

The robustness towards disturbances in the amount of fuel, the engine speed, and the amount of recycled exhaust gases was investigated experimentally. Figure 5.6 shows the response as disturbances were added sequentially. At cycle 200, the engine speed was increased from 1200 [rpm] to 1400 [rpm]. The injected fuel energy was reduced from 1400 [J] to 1200 [J] at cycle 700. Finally, the amount of EGR was increased from approximately 0 percent to 30 percent at cycle 1350. The bottom plot shows IMEP_n which reflects the impact of the disturbances in engine speed and fuel energy. The combustion phasing was maintained relatively well through the whole sequence and the average output variance was 1 $[\text{deg}^2]$.

Multi-Cylinder Control

As previously mentioned, Cylinders 1, 3, 5, and 6 were operated in the experiments and the controller for Cylinder 5 governed the intake temperature. The response from all four cylinders to two consecutive step changes in the set point for θ_{50} is shown in Fig. 5.7. The θ_{50} of each cylinder followed the reference signal, while the θ_{IVC}-values requested by the
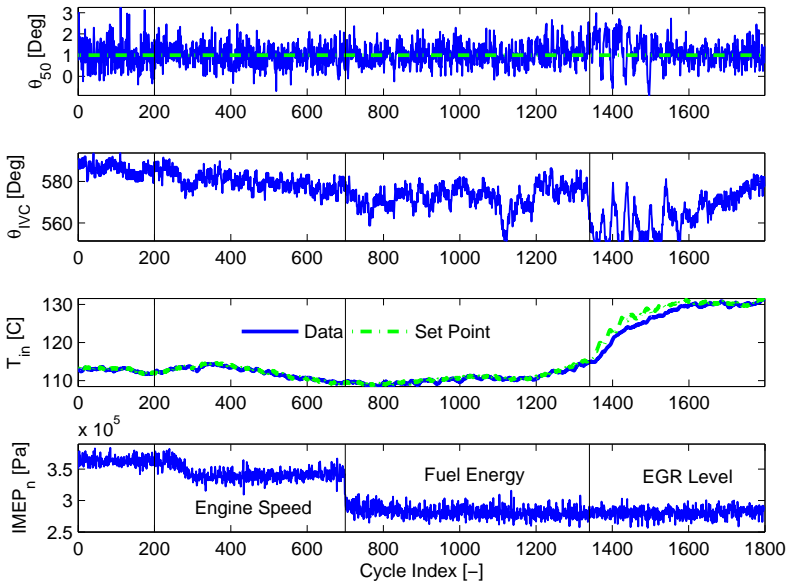
Figure 5.6 The controlled output, θ_{50}, the control signals, θ_{IVC} and T_{in}, and the additional output $IMEP_n$. Disturbances in the engine speed, the amount of injected fuel, and the amount of EGR were added successively. $IMEP_n$ is included to visualize the disturbances in engine speed and fuel energy.

controllers showed a large spread. The output variance of Cylinder 1 was around 0.8 crank angle degrees for the earlier phasing and 2.5 for the later reference value, whereas that of the other cylinders was around 0.3 for the earlier phasing and 0.8 for the later phasing. The response time was also slightly longer for Cylinder 1. There is a spike in the θ_{50} for Cylinder 1 before cycle 400, which indicates that it may have misfired.

Figure 5.8 shows the same set-point sequence but with a different initial state where the intake temperature was lower. In this case tracking is poor for Cylinder 1 and only the θ_{IVC} for Cylinder 5 stays within the allowed range throughout the entire experiment while the other three controllers exhibit saturation after the negative step change in the reference. Additionally, only the θ_{IVC} for Cylinder 5 is close to the middle of the allowed range before the step changes. Note that the controller for Cylinder 5 governed the intake temperature for all cylinders. The variance of the outputs was similar to the response in Fig. 5.7.
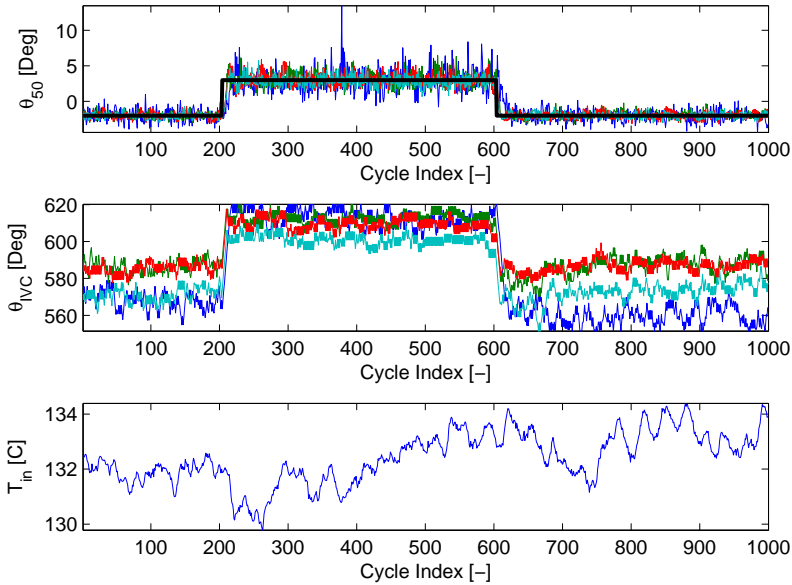
Figure 5.7   The controlled output, θ_{50}, the control signals, θ_{IVC} and T_{in}. θ_{50} and θ_{IVC} are shown for cylinders 1 (blue), 3 (green), 5 (red), and 6 (cyan). The set point for θ_{50} is shown in black. The controller for cylinder 5 governed the intake temperature.

5.4 Discussion

The closed-loop system showed a fairly short response time. For step changes of a few degrees around the linearization point in θ_{50} the response time was approximately ten cycles. Only the larger steps in the reference signal took around 15 cycles, which compares well with previously published results obtained using the same engine [Blom *et al.*, 2008; Bengtsson *et al.*, 2007]. The inlet valve closing was a sufficient control signal in many operating points. However, an additional control signal was needed to extend the range of the controller. This is apparent after cycle 1400 in Fig. 5.4, and during the EGR-disturbance in Fig. 5.6, where θ_{IVC} saturates.

The output variance under closed-loop control increased with later combustion phasing, as shown in Fig. 5.5. As the variance could be reduced slightly either by introducing a disturbance model or by using a linearization made closer to the operating point, the cause seems to be
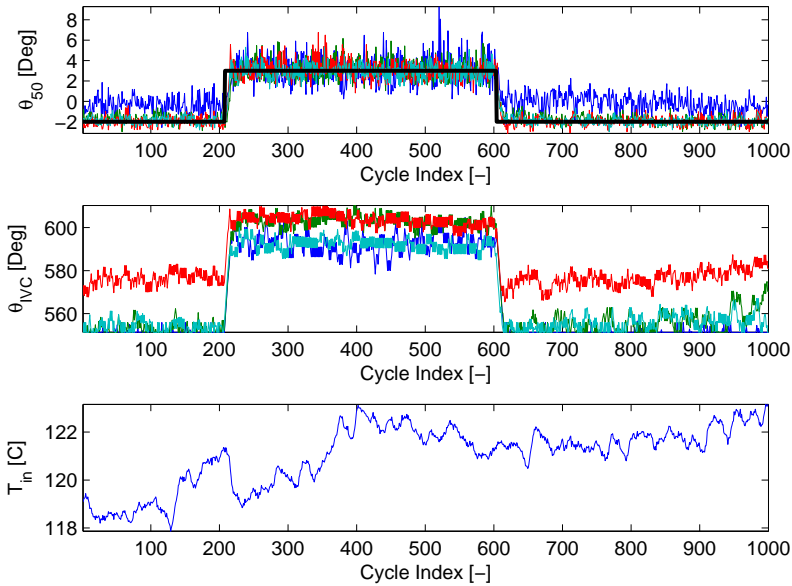
Figure 5.8 The controlled output, θ_{50}, the control signals, θ_{IVC} and T_{in}. θ_{50} and θ_{IVC} are shown for cylinders 1 (blue), 3 (green), 5 (red), and 6 (cyan). The set point for θ_{50} is shown in black. The controller for cylinder 5 governed the intake temperature.

a combination of physical effects and model errors. Note that the disturbance model was not intended to capture the actual disturbances acting on the model perfectly, but rather a combination of such disturbances and model aliasing. The important result is that changing the linearization point provided a performance improvement comparable to that achieved when using statistical methods. Around top dead center the output variance was relatively low in all cases. This could be partially explained by the operating procedure. As the engine is run with very small amounts of hot residuals, the dependence on the charge temperature of the previous cycle is weakened, giving the control signals greater impact.

The closed-loop system showed good robustness to disturbances in engine speed, fuel amount, and EGR level. The EGR seems to have the greatest impact on θ_{50}, and there was a clear transient occurring in response to the increase. A likely cause for this is that the thermal properties of the charge are altered by increasing the amount of combustion products. Also, as seen in Fig. 5.6, the change in EGR is not reflected in $IMEP_n$,

which was used as measurement in the controller. During the increase in EGR level, there is also notable oscillations in the inlet valve closing. The cause of this is not entirely clear at this point but could be investigated further in future work. A possible explanation for the oscillations is that the change in EGR level caused inhomogeneities in the intake.

No improvement in performance was noted by increasing the prediction and control horizons beyond 5 and 2, respectively. The response of the linear model to step changes in the inputs decayed within less than five engine cycles. Since the linear model excludes the dynamics of the fast thermal management system, experimental counterparts should reflect a slower response to changes in the inlet temperature. The linear model does, however, imply that the response to an actual change in the inlet temperature is sufficiently fast to be captured within the prediction horizon. This might not hold true for other model formulations or experimental settings, but does suggest that a relatively small computational effort is required in order to obtain satisfactory control performance.

The initial multi-cylinder control results seem promising. There was, however, a fairly wide distribution in the required θ_{IVC} for the cylinders. This is likely due to variations in the individual cylinders as well as their positions in the engine block. The controller for Cylinder 1 nearly saturated at the final set-point in Fig. 5.7, and all controllers except that for Cylinder 5 saturated in Fig. 5.8. The situation is similar to that in [Karlsson *et al.*, 2007] where a long-route EGR-system was used together with VVA. Both the long-route EGR level and the intake temperature are global variables shared by all cylinders. The solution adopted in [Karlsson *et al.*, 2007] was to use the mean value of the EGR levels requested by each controller, which should be suitable for the intake temperature in this setting. However, it is apparent in Fig. 5.8 that each cylinder may have very individual and different thermal characteristics. Also, these characteristics are not necessarily static, as seen by comparing Fig. 5.7 and Fig. 5.8. A possible improvement could be to attempt to model the flow dynamics in the intake to handle these variations.

5.5 Conclusion

Using a physical model, model predictive control of the combustion phasing in an HCCI engine was investigated. To obtain fast control of the intake temperature, Fast Thermal Management was implemented using mid-ranging control. The resulting closed-loop system followed step changes in the desired combustion phasing within at most 20 engine cycles. The robustness of the controller was investigated by introducing disturbances in the engine speed, the amount of fuel, and the amount

of recycled exhaust gases. The output variance was investigated and a disturbance model was included in the controller, yielding a decrease in the steady-state variance at certain operating points. A comparable decrease was, however, achieved when using a linearization of the physical model performed closer to the operating point, showing the advantage of physically motivated models. The experimental results also suggested that fairly short control- and prediction horizons are sufficient. Multi-cylinder experiments were also carried out where four of the six cylinders were operated.

6

Hybrid Control of Exhaust Recompression HCCI

This chapter describes work on exhaust recompression HCCI where only the exhaust valve timing was used as control signal. In [Liao *et al.*, 2010a], a switching model consisting of three linear sub-models that captures the qualitative changes in dynamics was proposed. Using this switching linear model as a basis, this chapter presents experimental results on control of the combustion phasing of recompression HCCI using a model predictive controller. MPC based on the switching linear model was particularly useful for large step changes from an early ignition phasing point to a late phasing point.

Previous publications on control design considering the qualitative changes in thermal HCCI dynamics include [Chiang *et al.*, 2007; Liao *et al.*, 2010b; Chiang and Stefanopoulou, 2007; Kang *et al.*, 2009]. In [Chiang and Stefanopoulou, 2007], a dynamic feed-forward controller aimed at load transitions was presented and [Kang *et al.*, 2009] developed a HCCI controller including mode switches to spark ignited operation, and was evaluated on single-cylinder and multi-cylinder engines. A nonlinear observer-based controller was presented in [Chiang *et al.*, 2007]. A previous publication on hybrid model predictive engine control is [Giorgetti *et al.*, 2006], where the authors modeled a spark-ignited engine using separate models for operation with homogeneous and stratified charge, respectively.

The experimental results in this chapter were evaluated in terms of the dynamic response to set-point changes in the desired combustion phasing. A fast response to set-point changes with little overshoot can be critical to avoid misfire or excessive peak pressures during transient operation. A switching linear quadratic controller was also implemented and compared to the MPC in simulation and experiments. Due to the limited computational capability of the experimental testbed, the explicit representation

of the model predictive controller was calculated and implemented. The two controller types performed similarly during smaller changes in set point and produced similar levels of output variance. However, during larger transients, when a change in combustion phasing from around top dead center to a later phasing point was desired, the linear quadratic controller produced a large overshoot and subsequent oscillations. A sufficiently large overshoot could possibly lead to misfire, and in the case of exhaust recompression HCCI it can be difficult to recover from a single misfire as the charge temperature of the subsequent cycle will be low.

6.1 Dynamics of Exhaust Recompression HCCI

The trapping of the exhaust gases of the previous cycle, in order to enable auto-ignition in the subsequent cycle, creates a cycle-to-cycle coupling in exhaust recompression HCCI affecting both the temperature and the composition of the charge. The dynamics of this coupling can vary dramatically at different operating points. Figure 6.1 shows open-loop data collected at early and late phasing, respectively. In the upper diagram, the exhaust valve was closed earlier which yielded a higher concentration of exhaust gases in the next cycle. The difference in variance between the operating points is evident. In [Liao *et al.*, 2010a], it was demonstrated that there were three qualitative types of temperature dynamics of exhaust recompression HCCI across a wide range of ignition phasing points: smooth decaying for early ignition phasing, oscillatory for late ignition phasing, and strongly converging for moderate phasing. Analysis of the cycle-to-cycle dynamics in HCCI engines with varying amounts of exhaust gases in the cylinder [Chiang and Stefanopoulou, 2007; Chiang and Stefanopoulou, 2004; Kang *et al.*, 2009] demonstrated similar characteristics.

6.2 Modeling

A physics-based nonlinear model on the form

$$[O_2](k+1) = f_1([O_2](k), T(k), V_{\text{EVC}}(k))$$
$$T(k+1) = f_2([O_2](k), T(k), V_{\text{EVC}}(k))$$
$$\theta_{50}(k) = g([O_2](k), T(k)) \tag{6.1}$$

where the functions $f_1([O_2](k), T(k), V_{\text{EVC}}(k))$, $f_2([O_2](k), T(k), V_{\text{EVC}}(k))$, and $g([O_2](k), T(k))$ are nonlinear, was presented in [Ravi *et al.*, 2010]. The system states, $[O_2]$ and T, denote the oxygen concentration in the
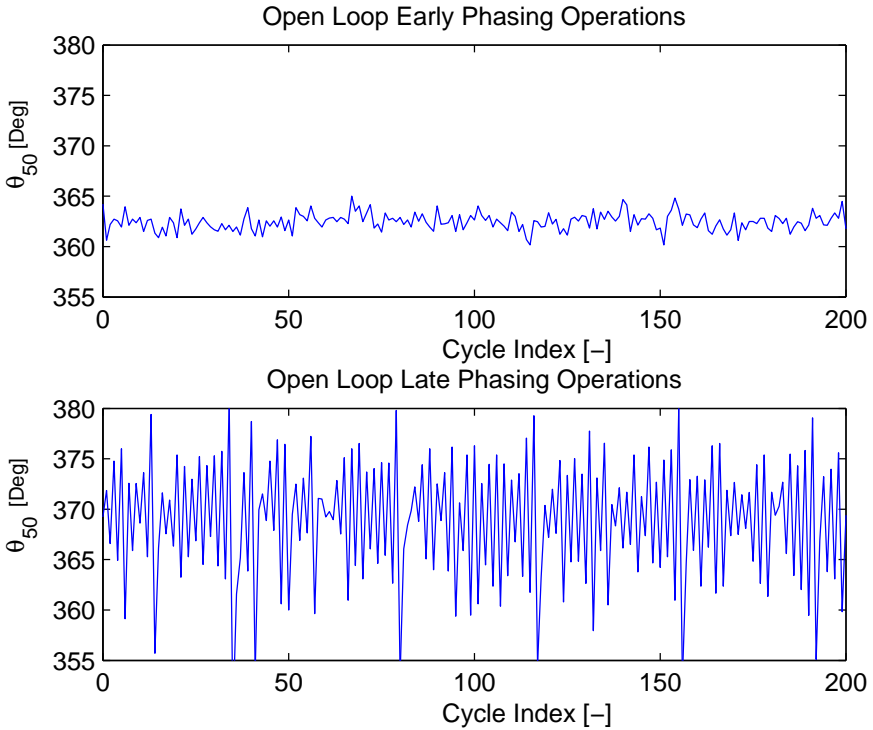
Figure 6.1   Early phasing and late phasing operation (reproduced from [Liao *et al.*, 2010b]).

cylinder and the charge temperature 60 degrees before combustion top dead center. As discussed further in Ch. 4, these states can be related to ignition timing through an Arrhenius integral [Ravi *et al.*, 2010]. Particularly, the charge temperature state has a dominant influence on combustion phasing. The crank angle where 50 percent of the energy in the injected fuel has been released, θ_{50}, was used as a proxy for ignition timing, and the control objective was to track a desired θ_{50} value. The control input V_{EVC} denotes the volume at the crank angle of exhaust valve closing, θ_{EVC}, and gives a measure of the amount of exhaust gases trapped in the cylinder.

Multiple Linearizations

Linearizations were obtained by numerically differentiating the functions in Eq. (6.1) around steady-state operating points. The linearizations were

of the form

$$x(k + 1) = A_i x(k) + B_i u(k) + d_i$$
$$y(k) = C_i x(k) + e_i$$
(6.2)

where

$$x(k) = \begin{pmatrix} [O_2](k) \\ T(k) \end{pmatrix}, \quad u(k) = V_{\text{EVC}}(k)$$
(6.3)

and A_i, B_i, C_i, d_i, and e_i constitute the system dynamics at linearization point i. The constants d_i and e_i were added since the models were normalized around baseline steady-state values, so that a given value of the state vector or control signal has a one-to-one correspondence to physical values, see [Liao *et al.*, 2010a] for more details.

In [Liao *et al.*, 2010a], it was observed that there are three qualitative types of temperature dynamics of exhaust recompression HCCI. For higher charge temperatures, corresponding to early phasing operation, the temperature is smoothly converging to the steady-state value. When the charge temperature is low, corresponding to late phasing operation, the temperature is oscillating around the steady-state temperature. The middle region, corresponding to moderate charge temperature, shows a considerably weaker cycle-to-cycle coupling of the temperature state. These three qualitative temperature dynamics manifest themselves in the linearizations of the nonlinear model about steady-state operating points, as seen in the respective A, B, and C matrices in Eqs. (6.4)-(6.6). Note that the linearizations shown in Eqs. (6.4)-(6.6) are associated with descending steady-state charge temperature.

Early phasing, higher charge temperature

$$A_1 = \begin{pmatrix} 0.579 & 0.512 \\ -0.005 & 0.1268 \end{pmatrix} \quad B_1 = \begin{pmatrix} -2.254 \\ 0.524 \end{pmatrix}$$

$$C_1 = \begin{pmatrix} -0.015 & -0.435 \end{pmatrix}$$
(6.4)

Middle region, moderate charge temperature

$$A_2 = \begin{pmatrix} 0.527 & 0.193 \\ -0.007 & -0.010 \end{pmatrix} \quad B_2 = \begin{pmatrix} -1.481 \\ 0.454 \end{pmatrix}$$

$$C_2 = \begin{pmatrix} -0.023 & -0.652 \end{pmatrix}$$
(6.5)

Table 6.1   Eigenvalues for the linearizations in Eqs. (6.4)-(6.6).

Linearization	Description	Eigenvalue 1	Eigenvalue 2
1	Early phasing	0.5733	0.1325
2	Middle region	0.5244	0.0016
3	Late phasing	0.4933	-0.3133

Late phasing, lower charge temperature

$$A_3 = \begin{pmatrix} 0.493 & -0.247 \\ -0.011 & -0.313 \end{pmatrix} \quad B_3 = \begin{pmatrix} -1.219 \\ 0.423 \end{pmatrix}$$

$$C_3 = \begin{pmatrix} -0.036 & -1.031 \end{pmatrix}$$

$$(6.6)$$

The eigenvalues of each linearization are presented in Table 6.1, where the change in sign of the eigenvalue corresponding to the temperature mode is apparent. The oscillating nature of the late phasing region is reflected in the eigenvalue located at -0.3133 while the corresponding eigenvalue for early phasing region is located at 0.1325. The well damped dynamics of the middle region correspond to the eigenvalue close to the origin.

Piecewise Affine Representation

To approximate the change in the nonlinear system behavior, a hybrid model description composed of several linearizations can be used, so that a particular linearization is active when the system state is in the corresponding region of the operating range. In the description below, the number of regions is denoted by n, as there may be advantages to include more regions in order to improve model fidelity, or reduce the number of regions in order to lower the complexity of the controllers. The experimental results were obtained using the three linearizations described in the previous section. Region i in the state space is defined by an upper and a lower temperature limit, denoted $T_{i,u}$ and $T_{i,l}$, respectively. To be consistent with the descending steady-state temperature of the linearization points in the previous section, it holds that $T_{i+1,u} = T_{i,l}$. Region i was active in cycle k when $T_{i,l} < T(k) \leq T_{i,u}$. The resulting system can be described by Eq. (6.2) where the linearization i in cycle k is chosen such that

$$x(k) \in \Omega_i, \quad \Omega_i = \{x : S_i x \leq T_i\} \tag{6.7}$$

The matrices S_i and T_i define the region where model i is active. The threshold on the temperature state, the second element of $x(k)$, can be expressed as

$$S_i = \begin{pmatrix} 0 & 1 \\ 0 & -1 \end{pmatrix}, \quad T_i = \begin{pmatrix} T_{i,u} \\ -T_{i,l} \end{pmatrix} \tag{6.8}$$

The model was implemented in the HYSDEL language [Jost and Torrisi, 2002], and the Hybrid Toolbox [Bemporad, 2004] was used to generate the model predictive controllers. The model was implemented by defining the states and outputs as sums of the dynamics of each region with a boolean weighting parameter, as suggested in [Bemporad, 2004].

HYSDEL Implementation

1. Define the boolean variables $c_1(k), \ldots, c_{n-1}(k)$ as

$$c_i(k) = x_2(k) \leq T_{i,u} \tag{6.9}$$

2. The boolean variables $\delta_1(k), \ldots, \delta_n(k)$, indicating if region i is active at cycle k, can then be defined by

$$\delta_1(k) = \neg c_1(k)$$
$$\delta_2(k) = c_1(k) \ \& \ \neg c_2(k)$$
$$\vdots \tag{6.10}$$
$$\delta_{n-1}(k) = c_{n-2}(k) \ \& \ \neg c_{n-1}(k)$$
$$\delta_n = c_{n-1}(k)$$

where '$\neg$' denotes 'not'.

3. As suggested in [Bemporad, 2004], define virtual states $z_1(k) \ldots z_n(k)$ and virtual outputs $w_1(k), \ldots, w_n(k)$ by

$$z_i(k) = \begin{cases} A_i x(k) + B_i u(k) + d_i & \text{if } \delta_i(k), \\ 0 & \text{otherwise} \end{cases}$$
$$\tag{6.11}$$
$$w_i(k) = \begin{cases} C_i x(k) + e_i & \text{if } \delta_i(k), \\ 0 & \text{otherwise} \end{cases}$$

4. Finally, the state update and output equations can be expressed as

$$x(k+1) = \sum_{i=1}^{n} z_i(k)$$
$$\tag{6.12}$$
$$y(k) = \sum_{i=1}^{n} w_i(k)$$

6.3 Control

A switched linear quadratic controller and a hybrid model predictive controller were implemented and compared in simulations and experiments. Both control strategies were combined with a switched state estimator based on output measurements. This section outlines the state estimator and the control design.

State Estimation

Measurements of the combustion phasing were used to estimate the temperature and oxygen concentration in the cylinder. Let $\hat{x}(k+j|k)$ denote the estimate of $x(k+j)$ given a measurement of the output $y(k)$. Given the current active region, i.e., the current value of i, the *measurement update* was performed according to

$$\hat{x}(k|k) = (I - M_i C_i)x(k|k-1) + M_i(y(k) - e_i) \qquad (6.13)$$

where M_i is the innovation gain for region i. The estimate $\hat{x}(k|k)$ was used to calculate the control signal. Using the computed control signal for the next cycle, the *time update* was performed by calculating the system response using Eqs. (6.2), (6.7), and (6.8) to determine an estimate of the active region at the next cycle and setting

$$\hat{x}(k+1|k) = A_i x(k|k) + B_i u(k) + d_i \qquad (6.14)$$

Switched Linear Quadratic Control

A linear quadratic controller of the form

$$u(k) = -Kx(k) \qquad (6.15)$$

was obtained, as described in Ch. 2, for each region by minimizing the following cost function

$$J_{\text{LQ}}(u) = \sum_{j=0}^{\infty} ||Q_y y(j)||_2 + ||Q_u u(j)||_2 \qquad (6.16)$$

Reference tracking was introduced by feedforward, so that the full control law took the form

$$u(k) = N_u y_r(k) + K(N_x y_r(k) - x(k)) \qquad (6.17)$$

The feedforward gains N_u and N_x were determined by checking which region that would be active at the requested reference value $y_r(k)$ while the feedback gain K was chosen as that corresponding to the current active model region.

Hybrid Model Predictive Control

The main motivation for MPC in this case is the ability to predict across model region changes in contrast to the more reactive nature of the LQ controller. The system response was predicted using the hybrid description of the dynamics in Eqs. (6.2), (6.7), and (6.8) [Bemporad *et al.*, 2000]. Since no constraints were considered, the optimal control problem to be solved at cycle k was

$$
\begin{aligned}
&\min J_{\mathrm{MPC}}(k) \\
&\text{subject to Eqs. } (6.2), (6.7), (6.8)
\end{aligned} \tag{6.18}
$$

where

$$
J_{\mathrm{MPC}}(k) = \sum_{j=k}^{k+H_p} ||Q_y \left(\hat{y}(j+1|k) - y_r(j+1)\right)||_2 + ||Q_u \hat{u}(j)||_2 \tag{6.19}
$$

The weights Q_y and Q_u were the same as those used when designing the LQ controller and H_p defined the length of the prediction horizon.

6.4 Experimental Implementation

This section describes the implementation of the model predictive controller and the experimental conditions.

Controller Implementation

The data acquisition and control system was implemented using xPC target [Mathworks, 2010]. The sample time was 0.1 ms in order to get a good reading of the pressure trace while the controller commands were executed once per engine cycle. As there is a certain overhead connected with data acquisition, signal processing, and control actuation, the actual computation time available to obtain the next control signal was shorter.

Explicit Model Predictive Control   To reduce the online computational demand, an explicit representation of the hybrid model predictive controller was computed, denoted EMPC in the following. The control action was then given by

$$
u(k) = F_i \begin{pmatrix} x(k) \\ r(k) \end{pmatrix} + g_i, \text{ for } \begin{pmatrix} x(k) \\ r(k) \end{pmatrix} \in \zeta_i \tag{6.20}
$$

where ζ_i defines controller partition i, and $\cup_i \zeta_i$ is the set of states and references for which a feasible solution to the original MPC problem exists,

see [Bemporad *et al.*, 2000; Bemporad, 2004]. Note that the controller partitions of Eq. (6.20) have the form

$$\zeta_i = \left\{ \begin{pmatrix} x \\ r \end{pmatrix} : H_i \begin{pmatrix} x \\ r \end{pmatrix} \leq R_i \right\} \tag{6.21}$$

and are distinct from the model regions of the switched linear model in Eqs. (6.2), (6.7), and (6.8).

To further reduce the computational requirements, the number of partitions can be decreased by reducing the prediction horizon H_p or by removing partitions based on size. Using the Hybrid Toolbox [Bemporad, 2004], this can be achieved by removing any partitions whose Chebychev radius is smaller than a given tolerance ρ_f. During tests, it was possible to run controllers with more than 60 partitions on the engine control computer with a 3.2 GHz Intel Pentium 4 CPU. The controller used for the experimental results in Sec. 6.5 consisted of 21 partitions, obtained with $H_p = 2$ and $\rho_f = 10^{-6}$.

Experimental Platform

The 2.2-liter 4-cylinder General Motors Ecotech gasoline engine described in Sec. 3.3 was used for the experiments. Only the exhaust valve was used as a control input. The intake valve was closed 30 crank angle degrees after bottom dead center, and all valve events had a duration of 140 crank angle degrees. Three of the cylinders were operated with switching state feedback controllers in all tests, while cylinder 4 was operated with either an EMPC or an LQ controller. All presented experimental results were obtained from this cylinder.

6.5 Results

This section presents numerical results obtained by simulating the nonlinear model in Eq. (6.1), followed by experimental results obtained on the real engine.

Numerical Results

To see the benefits of predicting across model regions, the nonlinear model in Eq. (6.1) was simulated with the switched LQ controller and the MPC. The result when making a step change in desired phasing from top dead center to 9 degrees after top dead center is shown in Fig. 6.2, and the corresponding control signals are shown in Fig. 6.3. The LQ controller produced a slight overshoot whereas the MPC showed a smoother convergence to the later set point. There were very minor differences between
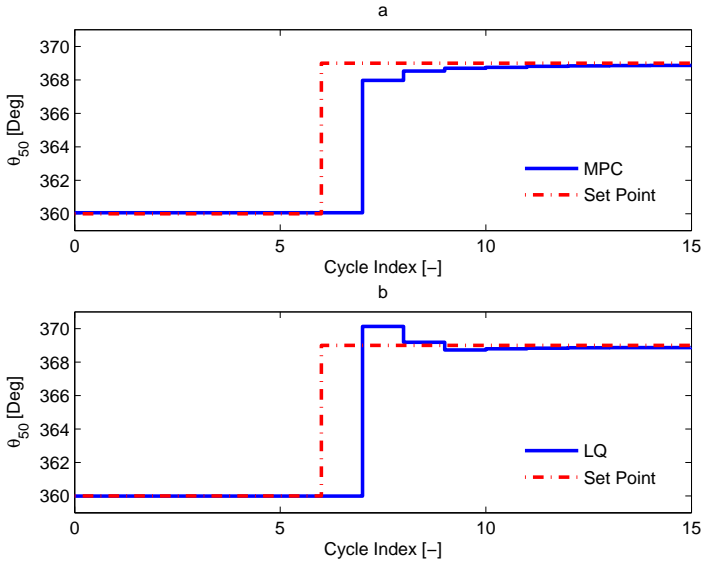
Figure 6.2 Simulated combustion phasing during a set point change using MPC (a) and LQ (b) controllers.

Figure 6.3 Simulated control signals for the MPC and LQ controllers corresponding to Fig. 6.2.

the two controllers during smaller set point changes. Note that the control signal at cycle k, $V_{\text{EVC}}(k)$, affects the combustion phasing of cycle $k + 1$, which creates a delay of one cycle in the response in Fig. 6.2 although the requested control signal changes in the cycle where the set point change occurs.
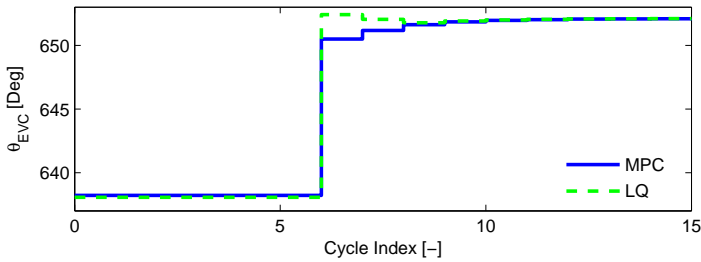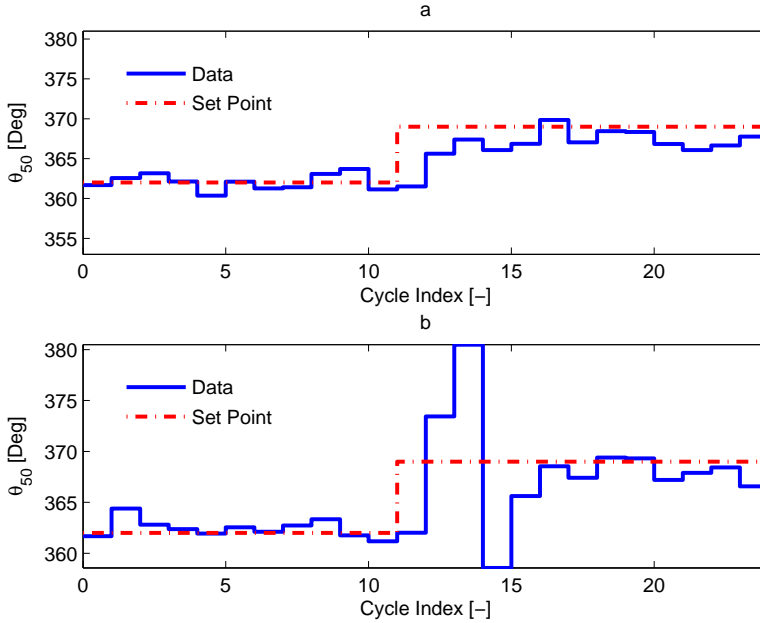
Figure 6.4 Experimental verification of combustion phasing during a set point change using EMPC (a) and LQ (b) controllers.

Experimental Results

Figures 6.4 and 6.5 show characteristic outputs and control signals of the LQ and EMPC in experiments. The desired θ_{50} was changed from 2 degrees ATDC to 9 degrees ATDC. The LQ controller produced a considerable overshoot during the step compared to the EMPC. In steady-state, the two controllers behaved very similarly. Compared to Fig. 6.2, the overshoot and subsequent variations with the LQ controller were worse in the experiments than the simulation results implied. The qualitative behavior in terms of the difference between the two control approaches was similar, but the results suggest that the nonlinear model in Eq. (6.1) underestimated the lack of damping around the later set point.

Figures 6.6 and 6.7 show the combustion phasing and control signal for the EMPC and LQ controllers during a sequence of step changes in the desired combustion phasing. The steady-state output variance was comparable between the two around all set points. Compared to the open-loop behavior in the lower plot in Fig. 6.1, both controllers improved steady-state performance considerably in terms of peak-to-peak variance. The
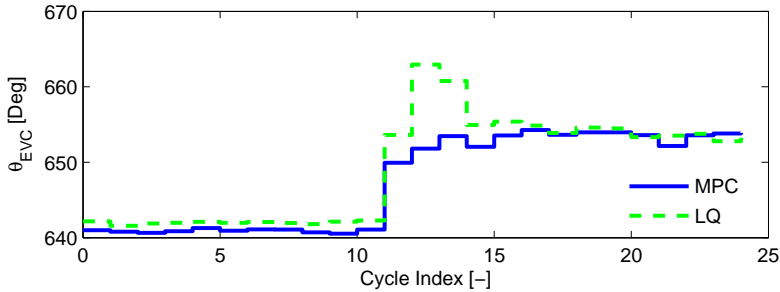
Figure 6.5 Experimental verification of control signals for the EMPC and LQ controllers corresponding to Fig. 6.4.

EMPC produced some oscillations in the control signal around the middle set points 364 and 367 which increased the output variance slightly compared to the LQ controller.

6.6 Discussion

The use of MPC improved the control performance when making large steps from an early phasing to a late phasing set point. The qualitative improvement was captured well in the simulation preceeding the experiments. There was, however, a pronounced difference between the experimental and simulated results in the amplitude and subsequent transient behavior when using the LQ controller. It should be noted that the controllers were tuned to achieve satisfactory steady-state behavior in each region. Further tuning might improve the performance of both controllers during the larger set point changes. Comparing the simulation results and the experimental results suggests that the nonlinear model underestimates the lack of damping in the late phasing region. A possible explanation for the overshoot in the LQ case is that only the feedforward part of the LQ implementation accounts for changing model regions while the feedback part uses the gains of the current region. The MPC, on the other hand, accounts for the future change in model region and produces a smaller initial change in the control signal followed by a smoother transient.

The two controller produced very similar results in steady-state and during smaller step changes in the reference signal. Since the same weight matrices were used in the design of both controllers, it seems reasonable
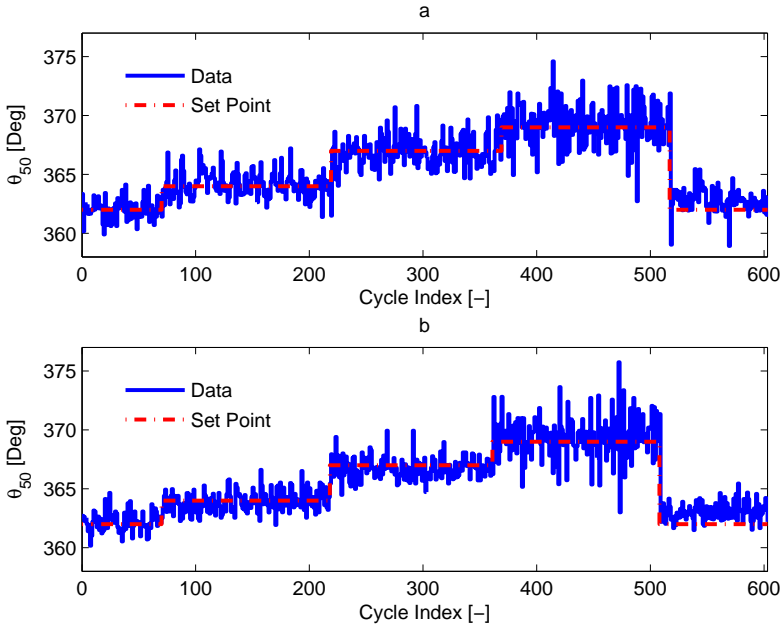
Figure 6.6   Combustion phasing during a series of set point changes using EMPC (a) and LQ (b) controllers.

that the steady-state behavior was similar. In Fig. 6.7 (a) some oscillations, chattering, occurs in the control signal around the operating points near the region thresholds. Figure 6.8 shows the corresponding temperature estimate along with the upper and lower thresholds for model region 2. During the oscillations, the temperature estimate is switching between model region 1 and 2 or between model region 3 and 2. A possible explanation for the behavior of the controller is that the model in region 2 suggests a substantially weaker cycle-to-cycle dependence of the charge temperature than the other regions, which should promote larger control signal changes. Since the control input has little effect in the middle region, the oscillations do not have a major impact on the control performance. They do, however, create some unnecessary control action.

A possible modification to the control structure to attenuate this behavior would be to include a hysteresis band around the temperature threshold between two neighboring model regions, so that the temperature estimate needs to be sufficiently far into a neighboring region before switching. This would not affect the performance across multiple regions
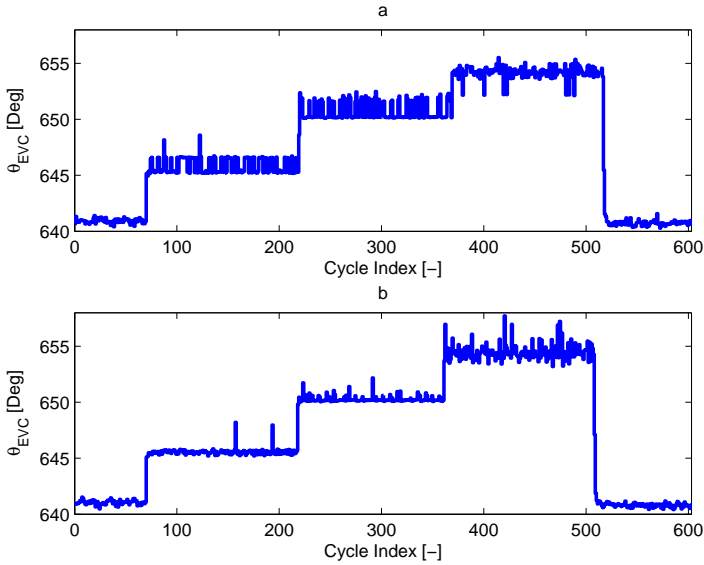
Figure 6.7 Control signal corresponding to Fig. 6.6 using EMPC (a) and LQ (b) controllers.
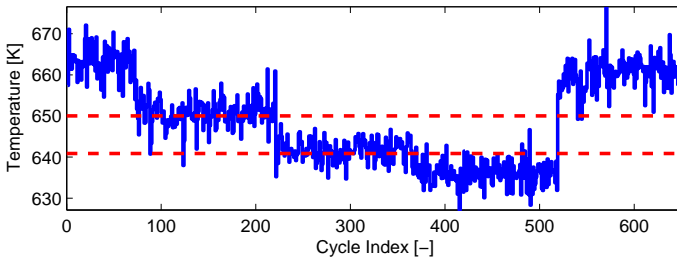
Figure 6.8 Temperature estimate and temperature thresholds (dashed) corresponding to the experimental results in Fig. 6.6.

presented in Figs. 6.4 and 6.5. A possible hysteresis scheme for when to stay in, or transition to, region 1 is shown in Table 6.2. It introduces constants $h_{1,2}$ and $h_{2,1}$ that modify the thresholds for passing from region 1 to region 2 and vice versa. When $h_{1,2} = h_{2,1} = 0$, the nominal thresholds are obtained. The condition for transitioning from region 3 to region 1 is left unchanged from the original model description. The transition rules

Table 6.2 Conditions for staying in, or transitioning to, region 1. The hysteresis band is specified by the constants $h_{1,2}$ and $h_{2,1}$.

Current region	Temperature Condition
1	$T(k) > T_{1,l} - h_{1,2}$
2	$T(k) > T_{1,l} + h_{2,1}$
3	$T(k) > T_{1,l}$

for regions 2 and 3 would follow the same principle. Figure 6.9 shows the active region estimate using the original PWA model formulation and that with hysteresis added. The hysteresis band was set to approximately 4 [K] around each threshold, which was sufficient to remove the oscillations in the region estimate. Another possible modification would be to increase the number of model regions so that the switched linear model approximates the original nonlinear model more closely.
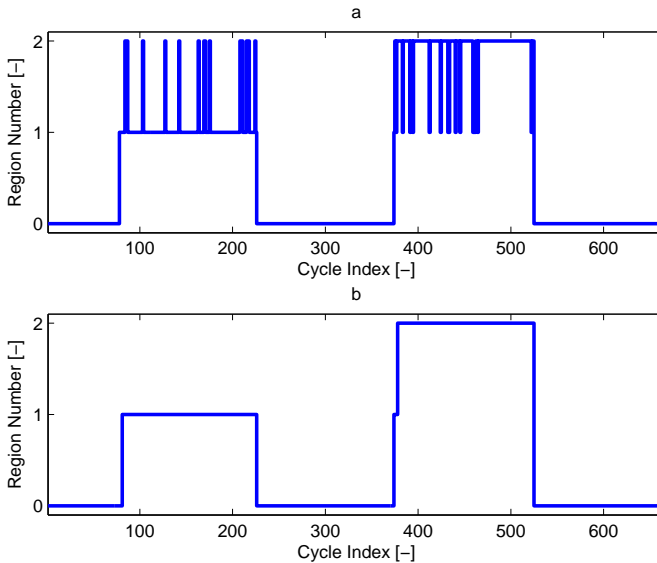
Figure 6.9 Region estimate using the original PWA formulation (a) and with hysteresis added (b) corresponding to Fig. 6.8.

6.7 Conclusion

Hybrid MPC was implemented to control the combustion phasing of exhaust recompression HCCI, and compared to a switched LQ controller. The controllers were based on a piecewise affine model constructed from linearizations of a physics-based nonlinear model. The qualitative behavior of the controllers could be observed both in simulation and in experiments. To reduce the computational requirements of experimental evaluation, the explicit form of the MPC was calculated. The ability to predict across model region changes resulted in a smoother transient with no overshoot when transitioning from an early phasing point to a late phasing point.

7

Modeling of PPC for Optimization

The model presented in this chapter aims to describe the main features of PPC combustion within the closed part of an engine cycle. It is given on DAE form and is a *single-zone* model, meaning that it does not consider spatial variations within the cylinder. The model includes heat losses to the cylinder walls as well as vaporization losses. The aim of the modeling is to be able to use it for optimization. The model complexity and simulation platform were chosen with this in mind. The single-zone approach reduces the complexity of the resulting model compared to multi-zone models, and the chosen platform allows optimization problems to be formulated based on the model equations.

7.1 Modeling

This section describes the model equations. The most relevant variables and parameters are summarized in Table 7.1.

Mechanical

The derivatives in this chapter are calculated with respect to time and the time $t = t_0$ corresponds to the start of simulation. In all simulations presented in this chapter, t_0 corresponded to bottom dead center before combustion and the simulation ended at bottom dead center after combustion. The crank angle is denoted θ, and can be described by

$$\dot{\theta} = 6N, \quad \theta(t_0) = \theta_0 \tag{7.1}$$

when θ is given in [deg] and N is the engine speed given in [rpm]. The initial value, θ_0, was set to 180 degrees before top dead center. The cylinder

Table 7.1 Model variables and parameters.

Name	Description	Unit
C_{Arr}	Arrhenius scaling factor	$(\mathrm{kg/m^3})^{1-a-b}\mathrm{s}^{-1}$
K	Arrhenius integral threshold	$\mathrm{kg/m^3}$
k_{Arr}	Arrhenius exponential factor	K
k_{pre}	Fuel mixing rate	s^{-1}
k_{vap}	Fuel evaporation rate	s^{-1}
m_{b}	Burned fuel	kg
m_{inj}	Injected fuel	kg
$m_{\mathrm{inj,tot}}$	Total amount of fuel to be injected	kg
m_{pre}	Prepared fuel	kg
m_{vap}	Evaporated fuel	kg
N	Engine rotational speed	Rot. per min.
p	Pressure	Pa
Q_{c}	Combustion heat release	J
Q_{ht}	Heat losses	J
Q_{tot}	Total thermal energy	J
Q_{vap}	Vaporization losses	J
T	Temperature	K
θ	Crank angle	deg or rad
θ_{SOC}	Crank angle at start of combustion	deg or rad
θ_{SOI}	Crank angle at start of fuel injection	deg or rad
V	Cylinder volume	$\mathrm{m^3}$

volume can be expressed on differential form as [Heywood, 1988]

$$\dot{V} = \dot{\theta}\frac{V_d}{2}\left(\sin\left(\theta\right) + \frac{\sin(\theta)\cos(\theta)}{\sqrt{R_v^2 - \sin^2(\theta)}} \right), \quad V(t_0) = V_0 \qquad (7.2)$$

with the initial value $V_0 = V(\theta_0)$, given by Eq. (1.1).

Pressure and Temperature Trace

The pressure in the cylinder, p, can be computed from the first law of

thermodynamics [Turns, 2006]

$$\dot{p} = \left(\dot{Q}_{\text{tot}} - \frac{\gamma}{\gamma - 1} p \dot{V} \right) \frac{\gamma - 1}{V}, \quad p(t_0) = p_0 \tag{7.3}$$

where Q_{tot} is the total thermal energy in the cylinder, sometimes referred to as *sensible internal energy* [Heywood, 1988], and γ is the ratio of specific heats. Without supercharging, the initial pressure, p_0, is the atmospheric pressure. The temperature, T, can then be computed using the ideal gas law [Turns, 2006]

$$T = \frac{pV}{nR} \tag{7.4}$$

where R is the universal gas constant and n is the number of moles in the cylinder.

It was assumed that some measure of the in-cylinder fraction of residuals was available, for instance the ratio $x_r = n_p/(n_r + n_p)$ or α, as defined in Eqs. (4.16) and (4.17), respectively. Based on the assumption that the present residuals in the current cycle correspond to the residuals produced in the same cycle, the number of moles of mixture per mole of fuel, x_{mix}, can be computed using Eqs. (4.18) and (4.19)

$$x_{\text{mix}} = 1 + \alpha \frac{y}{4} + \frac{(x + y/4)(1 + \alpha)(1 + 3.773)}{\phi} \tag{7.5}$$

Using the molar mass of the fuel, M_{f}, the number of moles of injected fuel can be calculated from the total injected fuel mass of the cycle, $m_{\text{inj,tot}}$. The total number of moles is then given by

$$n^* = \frac{m_{\text{inj,tot}}}{M_{\text{f}}} x_{\text{mix}} \tag{7.6}$$

A possible drawback with this approach is that the exact amount of injected fuel is difficult to measure with high precision. A standard way of determining the fuel consumption in steady-state operation is to use a fuel scale, which produces a reasonably accurate estimate of the total fuel consumption over several hundred engine cycles. However, this measure is difficult to use in transient and there is a loss of accuracy when converting this measure to units of mass injected per cycle, particularly at higher engine speeds.

An alternative way of estimating the number of moles in the cylinder is to assume that the cylinder at inlet valve closing is filled with a mixture with the composition given by Eq. (4.18) at pressure p_0 with approximately

the same density as air, i.e., that the fuel mass is very small compared to the air mass. Given the molar mass M_{mix} of the mixture

$$M_{\text{mix}} = \frac{\sum_i n_i M_i}{\sum_i n_i} \tag{7.7}$$

where the summation index, i, is taken over the molecules in the cylinder, and n_i and M_i denotes to the number of molecules and molar mass of molecule i in Eq. (4.18), respectively, the number of moles in the cylinder can be estimated as

$$n = \frac{\rho_{\text{air}} V(\theta_{\text{IVC}})}{M_{\text{mix}}} \tag{7.8}$$

where ρ_{air} is the density of air at pressure p_0.

Since diesel fuel was used in the experiments, an approximate composition had to be used. Diesel fuel can be modeled with a hydrogen to carbon ratio between 1.7 and 1.8 [Heywood, 1988], and one possible choice for modeling purposes would be $C_{10.8}H_{18.7}$ [Turns, 2006].

Prediction of the Start of Combustion

The point of auto-ignition was modeled using an Arrhenius type condition similar to that described in Ch. 4

$$\frac{1}{K} \int_{\theta_{\text{SOI}}}^{\theta_{\text{SOC}}} r_{\text{Arr}} dt = 1 \tag{7.9}$$

where K is a constant, and θ_{SOI} and θ_{SOC} are the crank angles at start of injection and start of combustion, respectively. The Arrhenius rate, r_{Arr}, was modeled as

$$r_{\text{Arr}} = C_{\text{Arr}} [C_x H_y]^a [O_2]^b e^{-\frac{k_{\text{Arr}}}{T}} \tag{7.10}$$

where $[C_x H_y]$ and $[O_2]$ denote the concentrations of fuel and air, respectively, C_{Arr} is a constant, a and b express the sensitivities to the oxygen and fuel concentrations, respectively, and

$$k_{\text{Arr}} = \frac{E_a}{R} \tag{7.11}$$

where E_a is the activation energy for the fuel. Similar formulations were used in [Gogoi and Baruah, 2010; Assanis *et al.*, 2003] among others. The concentrations can be estimated as

$$[C_x H_y] = \frac{m_f}{V} \tag{7.12}$$

$$[O_2] = (\alpha(1 - \phi) + 1) \left(x + \frac{y}{4} \right) \frac{1}{\phi} [C_x H_y] \tag{7.13}$$

where Eq. (7.12) estimates the concentration in $[kg/m^3]$ via the amount of unburned fuel in the cylinder, m_f, and Eq. (7.13) is obtained from Eq. (4.18).

Fuel Mass and Burn Rate

Fuel was divided into four categories; injected, evaporated, prepared, and burned fuel, similar to the approach taken in [Tauzia *et al.*, 2006]. The amount of currently injected fuel, m_{inj}, was assumed to be a model input and the remaining fuel masses were denoted m_{vap}, m_{pre}, and m_b, respectively.

The fuel evaporation and mixing process rates were modeled as constant. It was assumed that evaporation proceeds considerably faster than mixing, so that the processes can be modeled in series. The evaporation was described by

$$\dot{m}_{vap} = k_{vap} \left(m_{inj} - m_{vap} \right), \quad m_{vap}(t_0) = 0 \tag{7.14}$$

where k_{vap} is a constant vaporization rate. After evaporation, prepared (evaporated and mixed) fuel was modeled with a constant preparation rate k_{pre} as

$$\dot{m}_{pre} = k_{pre} \left(m_{vap} - m_{pre} \right), \quad m_{pre}(t_0) = 0 \tag{7.15}$$

The subsequent combustion rate of the prepared fuel was modeled as limited by the Arrhenius rate and a quadratic term in the combustion duration

$$\dot{m}_b = r_{Arr} \left(m_{pre} - m_b \right) \left(\theta - \theta_{SOC} \right)^2, \quad m_b(t_0) = 0 \tag{7.16}$$

A quadratic dependency on the combustion duration was previously used in [Chmela *et al.*, 2007; Gogoi and Baruah, 2010] among others.

Note that by these definitions, the amount of prepared but not yet burned fuel is given by $m_{pre} - m_b$ and the unburned fuel in the cylinder in Eq. (7.12), m_f, is given by

$$m_f = m_{inj} - m_b \tag{7.17}$$

Thermal Energy

The total change in thermal energy in the cylinder was modeled as composed of thee terms, given by

$$\dot{Q}_{tot} = \dot{Q}_c - \dot{Q}_{ht} - \dot{Q}_{vap}, \quad Q_{tot}(t_0) = 0 \tag{7.18}$$

where $\dot{Q}_c$ corresponds to the heat release from combustion, $\dot{Q}_{ht}$ to heat transfer to and from the cylinder wall, and $\dot{Q}_{vap}$ corresponds to vaporization of the fuel.

Combustion Heat Release

The heat release from combustion was calculated from the amount of burned fuel and the lower heating value of the fuel, ξ_{LHV} [J/kg]

$$\dot{Q}_c = \xi_{\mathrm{LHV}}\dot{m}_b, \quad Q_c(t_0) = 0 \tag{7.19}$$

Heat Losses to the Cylinder Walls

Similar to the model in Ch. 4, the heat losses to the cylinder walls were modeled as convection with a convection coefficient h_c

$$\dot{Q}_{\mathrm{ht}} = h_c A_c (T - T_w), \quad Q_{\mathrm{ht}}(t_0) = 0 \tag{7.20}$$

where A_c is the cylinder surface area and T_w is the wall surface temperature. Since PPC is characterized by a substantial amount of the fuel burning in a premixed manner, particularly at low load, the Hohenberg model of the convection coefficient was chosen [Hohenberg, 1979], which was found advantageous for HCCI modeling in [Soyhan *et al.*, 2009]

$$h_c = \alpha_s V^{-0.06} p^{0.8} T^{-0.4} (S_p + b)^{0.8} \tag{7.21}$$

where α_s and b are constants, and S_p is the mean piston speed [Hohenberg, 1979].

The conduction through the cylinder wall, $\dot{Q}_{\mathrm{con}}$, was modeled as

$$\dot{Q}_{\mathrm{con}} = \frac{(T_w - T_c)k_c A_c}{L_c}, \quad Q_{\mathrm{con}}(t_0) = 0 \tag{7.22}$$

where T_c is the coolant temperature, k_c is the conduction coefficient, and L_c is the wall thickness. Assuming that the steady-state temperature inside the wall is the mean of the surface temperature and the coolant temperature, a simple model of the wall surface temperature is given by

$$\dot{T}_w = 2\frac{\dot{Q}_{\mathrm{ht}} - \dot{Q}_{\mathrm{con}}}{m_c C_p}, \quad T_w(0) = T_{w,0} \tag{7.23}$$

where C_p is the specific heat of the cylinder wall and m_c is the wall mass. Similar models were used for modeling of HCCI heat transfer in [Roelle *et al.*, 2006; Blom *et al.*, 2008].

Fuel Vaporization

The vaporization losses were modeled using the *heat of vaporization* of the fuel, ξ_{vap} [J/kg], i.e., the energy required to vaporize 1 [kg] of the fuel

$$\dot{Q}_{\mathrm{vap}} = \xi_{\mathrm{vap}}\dot{m}_{\mathrm{vap}}, \quad Q_{\mathrm{vap}}(t_0) = 0 \tag{7.24}$$

Model Summary

The resulting model is on DAE form

$$F(\dot{x}(t), x(t), w(t), u(t), \mathbf{p}) = 0 \qquad (7.25)$$

where x, w, and u correspond to the continuous states (such as pressure, prepared and burned fuel), the algebraic states (such as temperature and injected fuel), and the control signals, respectively. The vector of free model parameters is denoted $\mathbf{p}$.

7.2 Implementation

The model was implemented in the Modelica language [The Modelica Association, 2009], an object-oriented, equation-based modeling language aimed at modeling of complex physical systems.

To enable optimization based on the model, the open source framework JModelica.org was used [Åkesson *et al.*, 2010]. JModelica.org extends Modelica with support for dynamic optimization and solves the resulting optimization problem using a collocation method [Biegler *et al.*, 2002], as described in Ch. 2. The possibility to vary the individual element lengths was utilized to shorten the segments during the combustion event while using fewer and longer segments during the subsequent expansion, and during the compression before fuel injection.

The derivatives were calculated using CasADi [Andersson *et al.*, 2010] and the numerical optimization was done using IPOPT [Wächter and Biegler, 2006].

Implementation of Discrete Events

Simulation, and subsequent optimization, of discrete events can be problematic. For instance, a possible DAE implementation to obtain the crank angle of start of combustion according to Eq. (7.9) using discrete events is given by

$$\dot{r}_{\text{int}} = \begin{cases} r_{\text{Arr}}/K & \text{when } \theta \geq \theta_{\text{SOI}}, \\ 0 & \text{otherwise} \end{cases} \qquad (7.26)$$

with the initial condition $r_{\text{int}}(t_0) = 0$, and

$$\dot{\theta}_{\text{SOC}} = \begin{cases} \dot{\theta} & \text{when } r_{\text{int}} < 1, \\ 0 & \text{otherwise} \end{cases} \qquad (7.27)$$
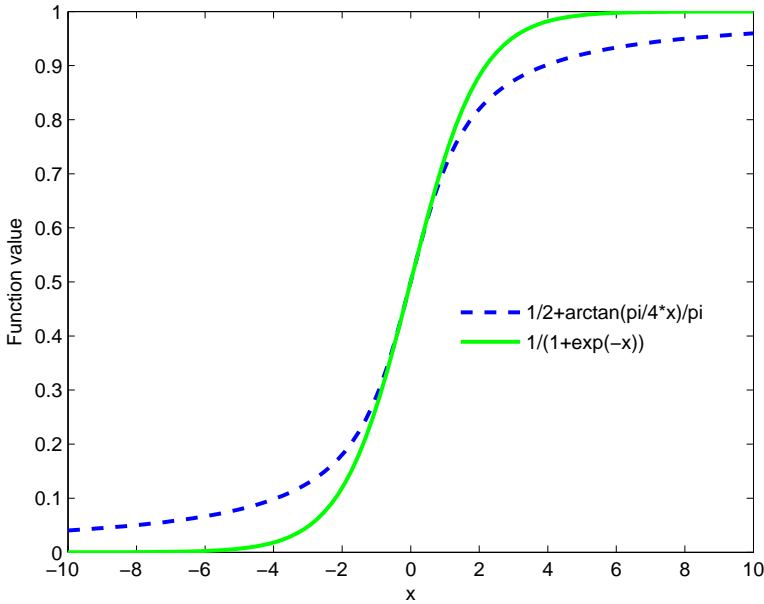
Figure 7.1   The functions, $f_{\mathrm{atan}}(x)$ and $f_{\mathrm{exp}}(x)$, in Eq. (7.28) vs. x. The parameters C_{atan} and C_{exp} were chosen to yield the same maximum derivative.

with the initial condition $\theta_{\mathrm{SOC}}(t_0) = \theta_0$. In Eq. (7.26), the integration starts at the point when fuel injection starts, and in Eq. (7.27), the derivative is set to 0 when r_{int} is greater than, or equal to, 1. A possible approximation would be to replace the discrete events with a smooth function that approximates the step functions in Eqs. (7.26) and (7.27). Possible choices include

$$f_{\mathrm{atan}}(x) = \frac{1}{2} + \frac{\arctan(C_{\mathrm{atan}}x)}{\pi} \qquad (7.28a)$$

$$f_{\mathrm{exp}}(x) = \frac{1}{1 + \exp(-C_{\mathrm{exp}}x)} \qquad (7.28b)$$

where C_{atan} and C_{exp} are parameters that influence the maximum derivative of the functions. Figure 7.1 shows the functions in Eq. (7.28) with C_{atan} and C_{exp} chosen in order to yield the same maximum derivative. It is evident from Fig. 7.1 that $f_{\mathrm{exp}}(x)$ produces less error compared to a step function than $f_{\mathrm{atan}}(x)$.

Using, for example, $f_{\exp}$, to approximate Eqs. (7.26)–(7.27) yields

$$\dot{r}_{\text{int}} = f_{\exp}(\theta - \theta_{\text{SOI}})\frac{r_{\text{Arr}}}{K}, \quad r_{\text{int}}(t_0) = 0 \tag{7.29}$$

$$\dot{\theta}_{\text{SOC}} = f_{\exp}(1 - r_{\text{int}})\dot{\theta}, \quad \theta_{\text{SOC}}(t_0) = \theta_0 \tag{7.30}$$

Similar expressions can be used for, e.g., the fuel injection. Choosing which approximation to use, as well as determining suitable values for the parameters, depends on how severe the numerical issues associated with the particular equation is, as well as how crucial the accuracy of the equation is. For instance, a small error in the exact shape of the injection profile is not likely to affect the results substantially.

7.3 Model Scaling

For numerical purposes, it is often desirable to keep all variables and derivatives in a similar magnitude range. In engine models, however, the magnitudes of the variables and derivatives are typically very disparate when using SI units. For example, the pressure in the cylinder can be on the order of 10^6 [Pa] while the injected fuel mass is on the order of 10^{-6} [kg]. Additionally, the derivatives of the model variables show similar disparities. This can be improved in some cases by choosing non SI units. However, a more general approach is to use nominal attribute scaling and scaling of time, as described in the following two sections.

Variable Scaling

In the Modelica language, each model variable can be given a *nominal attribute* which determines the scaling for that variable and its derivative where applicable [Åkesson *et al.*, 2010]. One possibility would be to attempt to strike a balance between the excessively large derivatives and variable values when setting the nominal attributes. This can, however, be difficult to achieve for certain variables that combine a small variable value with larger derivatives, such as the fuel masses.

Scaling of Time

A straightforward way of reducing the magnitude of the derivatives is to scale the model time. If the model time is scaled so that the simulation time is extended by a certain factor, the magnitudes of all derivatives will be reduced by the same factor. The possible drawbacks with this approach include the risk of introducing numerical noise on those derivatives that are already small, and that the collocation segments are stretched out which might lower the accuracy.
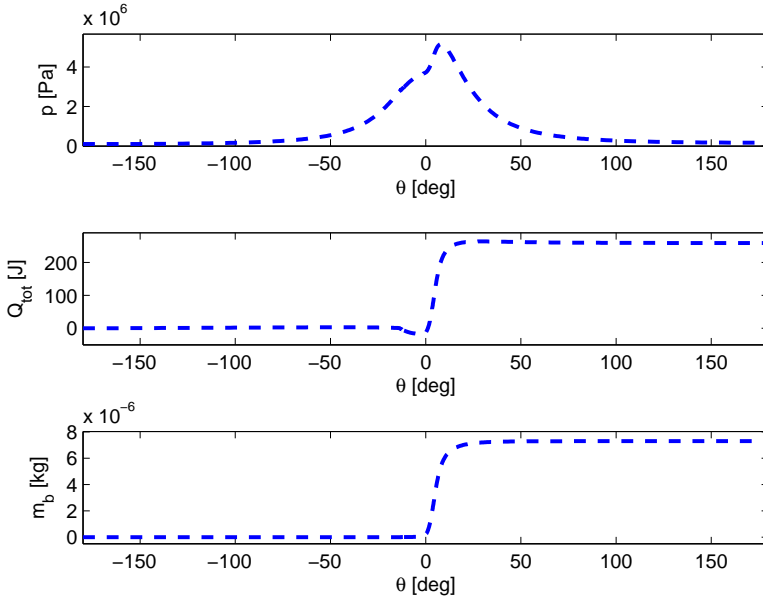
Figure 7.2 p, Q_{tot}, and m_{b} vs. crank angle. The variables are shown without any scaling.

Model Scaling Results

To illustrate the effects of parameter scaling and time scaling, the simulated pressure, total heat release, and burned fuel amount are presented with different scaling. It should be noted that $\dot{p}$ here refers to the value of the time derivative of the model variable p. Pressure derivatives, usually denoted dp, are often presented as pressure increments in bar per crank angle, which produces very different numbers. In the presented case, the maximum dp was around 4 bar per crank angle.

Figures 7.2 and 7.3 show the unscaled variables and derivatives when the model is implemented using SI units. The pressure peaks around 5 [MPa], the total heat release around 250 [J], and the burned fuel mass at 7 [mg]. The corresponding derivatives reach approximately 2 [GPa/s], 3 [kJ/s], and 8 [g/s] respectively. When introducing nominal attribute scaling and time scaling, the shapes of the profiles stay the same when plotted against θ, but their magnitudes are changed.

Table 7.2 shows the peak value and derivative peak value for the three variables using no scaling, nominal attribute scaling, and nominal at-

Table 7.2 Effects of scaling with nominal attribute and time scaling on peak variable and peak derivative values of p [Pa], Q_{tot} [J], and m_b [kg]. Case A: Without scaling. Case B: Nominal attribute scaling. Case C: Nominal attribute and time scaling.

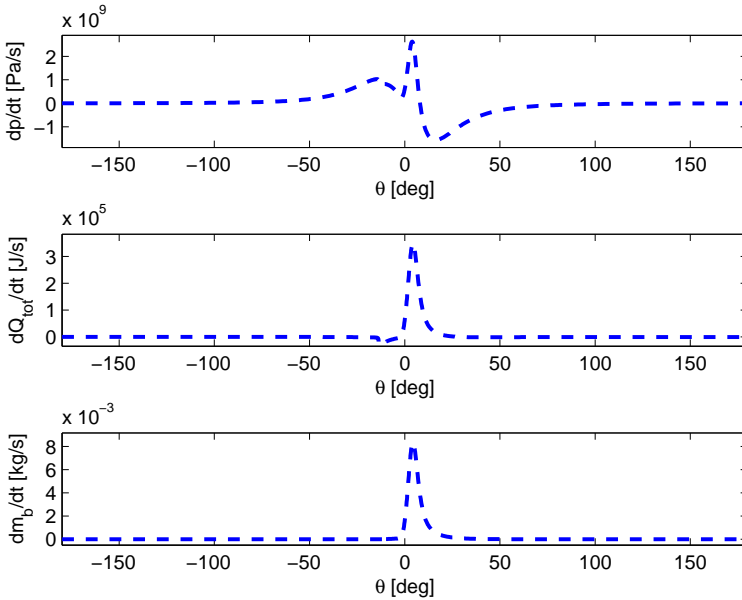| Case	p	Q_{tot}	m_b	$\dot{p}$	$\dot{Q}_{tot}$	$\dot{m}_b$
A	$5.15 \cdot 10^6$	264.07	$7.30 \cdot 10^{-6}$	$2.63 \cdot 10^9$	$3.48 \cdot 10^5$	$8.34 \cdot 10^{-3}$
B	1.02	0.88	0.73	$5.05 \cdot 10^2$	$1.13 \cdot 10^3$	$8.16 \cdot 10^2$
C	1.02	0.88	0.73	0.51	1.13	0.82

Figure 7.3 $\dot{p}$, $\dot{Q}_{tot}$, and $\dot{m}_b$ vs. crank angle. The variables are shown without any scaling.

tribute scaling combined with time scaling. In the example, time was scaled so that the simulation was extended by a factor 1000 and the nominal attributes were set to bring the variable values close to the range $[0, 1]$.

7.4 Experimental Setup

Experimental data were obtained from the Volvo D5 light duty engine described in Sec. 3.4. The experiments were performed at an engine speed of 1500 [rpm] and diesel fuel was used. The exhaust valve was closed 30 degrees before, and the inlet valve was opened 30 degrees after, top dead center. The start of fuel injection was varied between 16.7 degrees and 12.7 degrees before top dead center. Data sets of 1000 cycles were collected and the average pressure was used for model validation. Using the average pressure trace could potentially introduce errors since it is likely that there are variations both in the amount of injected fuel and the injection timing between cycles. The motivation for using average values is that the model is aimed at describing the average cycle given the inputs.

7.5 Calibration Procedure

This section describes how automatic calibration of the model parameters was performed and discusses which parameters to include in the optimization. Calibration of physically based models can be time-consuming and must sometimes be repeated when the engine setup is modified or new control inputs are considered. By means of optimization, parts of the calibration can be done automatically. An earlier publication concerning automatic calibration is [Friedrich *et al.*, 2006], where the calibration was performed against the calculated heat release rate. The parameters influencing the early heat release were calibrated first and then held constant while the remaining parameters and sub-models were calibrated. The approach presented in this section is based on the pressure trace and aims to calibrate all free parameters simultaneously.

Optimization Problem

The cost function penalized the squared error between the model pressure and a measured pressure trace, p^m, yielding an optimization problem on the form

$$
\begin{aligned}
\min_{\mathbf{p}} \quad & \int_{t_0}^{t_f} \left(p(t) - p^m(t) \right)^2 dt \\
\text{s.t. } & F(\dot{x}(t), x(t), w(t), u(t), \mathbf{p}) = 0 \\
& x_{\min} \leq x \leq x_{\max} \\
& w_{\min} \leq w \leq w_{\max} \\
& \mathbf{p}_{\min} \leq \mathbf{p} \leq \mathbf{p}_{\max} \\
& x(t_0) = x_0
\end{aligned}
\tag{7.31}
$$

where $F(\dot{x}(t), x(t), w(t), u(t), \mathbf{p}) = 0$ constitute the DAE model description, x_0 is the initial state, and x_{min}, x_{max}, w_{min}, w_{max}, $\mathbf{p}_{min}$, and $\mathbf{p}_{max}$ specify lower and upper bounds on the states, algebraic variables, and calibration parameters, respectively.

As mentioned in Sec. 7.4, the average of 1000 steady-state engine cycles was used in the optimization, so that p^m was a vector of averaged pressure samples rather than continuous data. Approximately one pressure sample per crank angle were used in the optimization. The integral in Eq. (7.31) was approximated as described in Ch. 2

$$\int_{t_0}^{t_f} (p(t) - p^m(t))^2 \, dt \approx \sum_{i=1}^{N_e} \left(h_i \sum_{j=1}^{N_c} \omega_k \left(p_{i,j} - p^m(t(\tau_j)) \right)^2 \right) \tag{7.32}$$

where $p_{i,j}$ denotes the pressure at collocation point j in segment i, and $p^m(t(\tau_j))$ was obtained by linearly interpolating the measured pressure samples.

Estimate of Standard Deviation

Estimating standard deviations or confidence regions for the obtained parameters is not straightforward. As an estimate, approximate regions could be calculated in the same manner as is usually done for the linear least-squares case [Johansson, 1993]. This can be accomplished by defining an error vector, ϵ, as

$$\epsilon = \begin{pmatrix} y(t_0) - \hat{y}(t_0) \\ y(t_1) - \hat{y}(t_1) \\ \vdots \\ y(t_{N_m}) - \hat{y}(t_{N_m}) \end{pmatrix} \tag{7.33}$$

and a Jacobian, J_j, of the sensitivities

$$J_j = \begin{pmatrix} \dfrac{\partial y}{\partial \mathbf{p}_1}(t_0) & \dfrac{\partial y}{\partial \mathbf{p}_2}(t_0) & \cdots & \dfrac{\partial y}{\partial \mathbf{p}_{N_p}}(t_0) \\ \dfrac{\partial y}{\partial \mathbf{p}_1}(t_1) & \dfrac{\partial y}{\partial \mathbf{p}_2}(t_1) & \cdots & \dfrac{\partial y}{\partial \mathbf{p}_{N_p}}(t_1) \\ \vdots & \vdots & & \vdots \\ \dfrac{\partial y}{\partial \mathbf{p}_1}(t_{N_m}) & \dfrac{\partial y}{\partial \mathbf{p}_2}(t_{N_m}) & \cdots & \dfrac{\partial y}{\partial \mathbf{p}_{N_p}}(t_{N_m}) \end{pmatrix} \tag{7.34}$$

where N_m is the number of measurement points, t_0, t_1, ..., t_{N_m} denotes the measurement times, $\mathbf{p}_i$ denotes parameter i out of a total of N_p parameters, and the model output $\hat{y}(t_i)$ and partial derivatives are obtained by linear interpolation of the simulated data.

An estimate of the covariance matrix of the parameter estimates is then given by

$$\hat{P} = \frac{\epsilon^T \epsilon}{N_m - N_p} \left(J_j^T J_j \right)^{-1} \tag{7.35}$$

The standard deviation for parameter i, σ_i, can then be estimated by the square root of diagonal element i of $\hat{P}$

$$\hat{\sigma}_i = \sqrt{\hat{P}_{[i,i]}} \tag{7.36}$$

However, since average pressure traces were used for the calibration, any noise characteristics will be lost, meaning that $\epsilon^T \epsilon$ will be an unreliable estimate of the measurement noise. The relative magnitudes between the parameters, however, mainly depend on the sensitivities in the Jacobian.

Choice of Calibration Parameters

The model contains several parameters that could be included in the vector of free parameters. However, there is some over-parametrization in the model, particularly when only one set of calibration data is used at a time. To limit the number of free parameters in the optimization, parts of the model was implemented using tabulated parameter values.

The values of the exponents a and b in Eq. (7.10) were set to those suggested for the fuel in [Turns, 2006], leaving C_{Arr} and k_{Arr} to be calibrated. While both parameters influence the instantaneous value of r_{Arr}, k_{Arr} also affects the shape of the profile. A larger value of k_{Arr} will result in a smaller value of the integral in Eq. (7.9), and a lower burn rate in Eq. (7.16).

The third free parameter related to the auto-ignition model was K. Since it is difficult to tune all parameters related to the auto-ignition using only one set of data, K was set to the mean of the calibrated values corresponding to two of the data sets used.

The parameters in the Hohenberg expression in Eq. (7.21) were not varied.

As previously discussed, the measurement of the injected fuel amount is a possible source of errors and it was therefore treated as a calibration parameter.

The vaporization rate, k_{vap} in Eq. (7.14), and the preparation rate, k_{pre} in Eq. (7.15), were left as free parameters. The vaporization rate mainly describes the decrease in thermal energy preceding combustion, while the preparation rate has a pronounced effect on the heat release by limiting the combustion rate.

In summary, the vector of free parameters, $\mathbf{p}$, in the calibration was

$$\mathbf{p} = \begin{pmatrix} C_{\text{Arr}} & K & k_{\text{Arr}} & k_{\text{pre}} & k_{\text{vap}} & m_{\text{inj,tot}} \end{pmatrix} \tag{7.37}$$
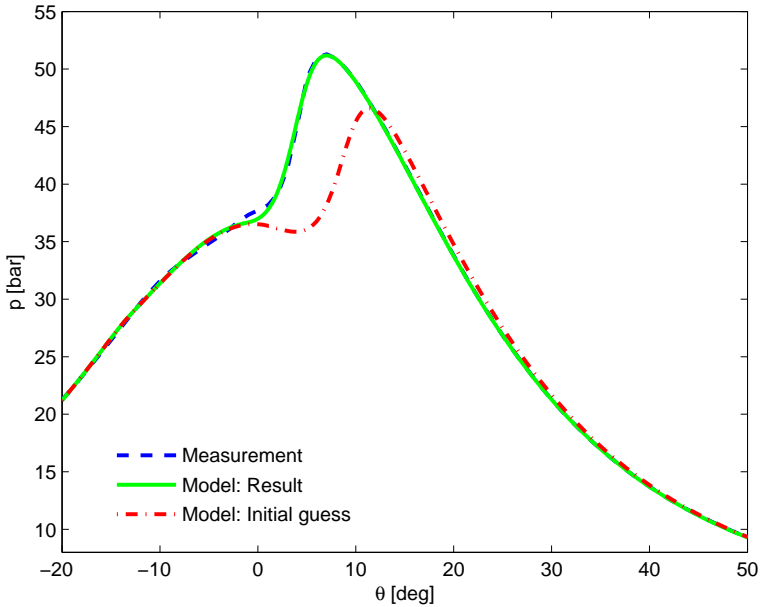
Figure 7.4 Pressure vs. crank angle. Data and model ouput as indicated. The model output is shown using both initial parameter values and calibrated values.

7.6 Automatic Calibration Results

Figure 7.4 shows a measured pressure trace with the pressure predicted by the calibrated model superimposed. The modeled pressure trace using the initial parameter values is also shown. The overall cost was reduced by a factor 100 from approximately $3.83 \cdot 10^{-6}$ to $1.78 \cdot 10^{-8}$. The error in the peak pressure in Fig. 7.4 was less than 0.5 [bar] with the calibrated parameters. There is a slight mismatch in the pressure profile just before combustion starts of approximately 0.8 [bar]. Table 7.3 shows the parameter values of the initial guess and the calibrated values. The standard deviation for the calibrated parameters, obtained according to Sec. 7.5, were approximately $1.5 \cdot 10^9$ for C_{Arr}, 0.02 for K, 314 for k_{Arr}, 13 for k_{pre}, 99 for k_{vap}, and $2.54 \cdot 10^{-8}$ for $m_{\mathrm{inj,tot}}$, respectively. This equals approximately 30, 22, 11, 2, 5, and 0.3 percent of the corresponding parameter values.

Figure 7.5 shows the total thermal energy calculated from the measured pressure, with the model output superimposed. The thermal energy calculated from the pressure trace used all the pressure samples in the

Table 7.3 Initial and calibrated values of C_{Arr} [(kg/m^3)$^{1-a-b}$s^{-1}], K [kg/m^3], k_{Arr} [K], k_{pre} [s^{-1}], k_{vap} [s^{-1}], and $m_{\text{inj,tot}}$ [kg] corresponding to Fig. 7.4.

Parameter	Initial Guess	Calibrated Value
C_{Arr}	$5.00 \cdot 10^9$	$5.08 \cdot 10^9$
K	0.04	0.11
k_{Arr}	3500	2763
k_{pre}	800	659
k_{vap}	2000	1896
$m_{\text{inj,tot}}$	$8.22 \cdot 10^{-6}$	$8.33 \cdot 10^{-6}$

data, which corresponded to five samples per crank angle, and was calculated between 30 degrees before and 50 degrees after top dead center. The modeled thermal energy is increasing slightly during the compression due to heat transfer from the cylinder walls to the gas. This results in an offset of approximately 10 [J] in Q_{tot} during the decrease before combustion and the final value after combustion. The slight decrease in Q_{tot} during the expansion is due to heat losses.

Figures 7.6 and 7.7 show the modeled thermal energy components and the fuel mass categories, respectively. The decrease in thermal energy due to vaporization occurs rather rapidly following fuel injection while the main effects of heat transfer occur during, and after, combustion. The mixing controlled part of combustion can be seen in Fig. 7.7 where m_{b} is limited by m_{pre}.

Figure 7.8 shows the pressure from measurements and model output for four different values of θ_{SOI} (15.7, 13.7, 16.7, and 12.7 degrees before top dead center). The model parameters were the same for all cases with only K modified slightly from the values in Table 7.3. The agreement is fairly good in all cases with slightly worse agreement before start of combustion for the two last cases.

7.7 Discussion

The presented model predicted the experimental results with an error of less than one [bar] in the peak pressure and a maximum error of less than two [bar] for the four cases shown in Fig. 7.8, which compares well with earlier models of similar complexity [Tauzia *et al.*, 2006].
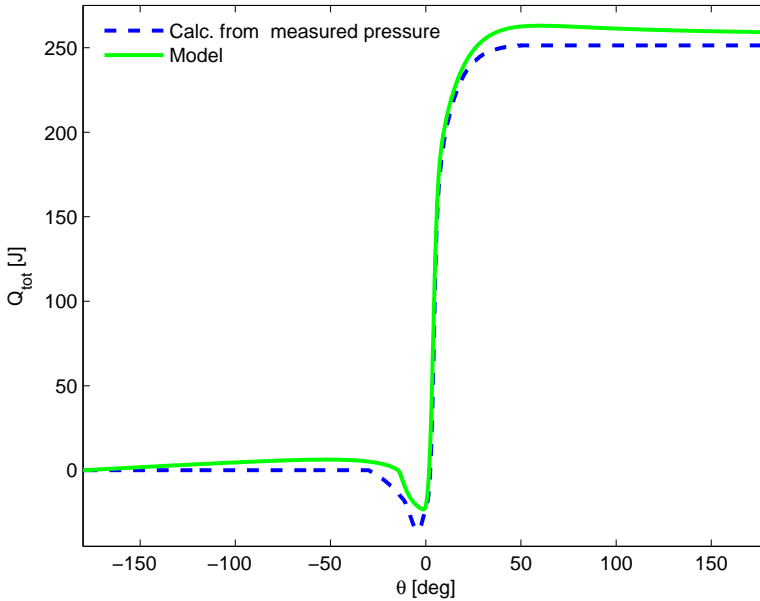
Figure 7.5 Total change in thermal energy Q_{tot} vs. crank angle corresponding to the pressure trace in Fig. 7.4. Estimate calculated from experimental data and model output as indicated.

An optimization problem was formulated for automatic calibration of a few of the model parameters. Scaling of the model variables and derivatives using both nominal attributes and time scaling was employed in order to obtain an optimization problem that could be solved successfully. Without scaling, the model equations could not always be fulfilled with the number of collocation points used, N_e was 200 and N_c was 3. A desirable alternative to using the average pressure trace in the calibration would be to run the optimization against several data sets simultaneously, and thus do the averaging as part of the optimization instead. This was, however, currently not supported in the software. A related functionality would be to be able to include several operating points corresponding to, for example, different injection timings, loads, and engine speeds in the optimization. This would most likely help improve the results in Fig. 7.8, since additional parameters related to the prediction of auto-ignition, such as k_{Arr}, could be optimized to yield the best average agreement with experimental data.
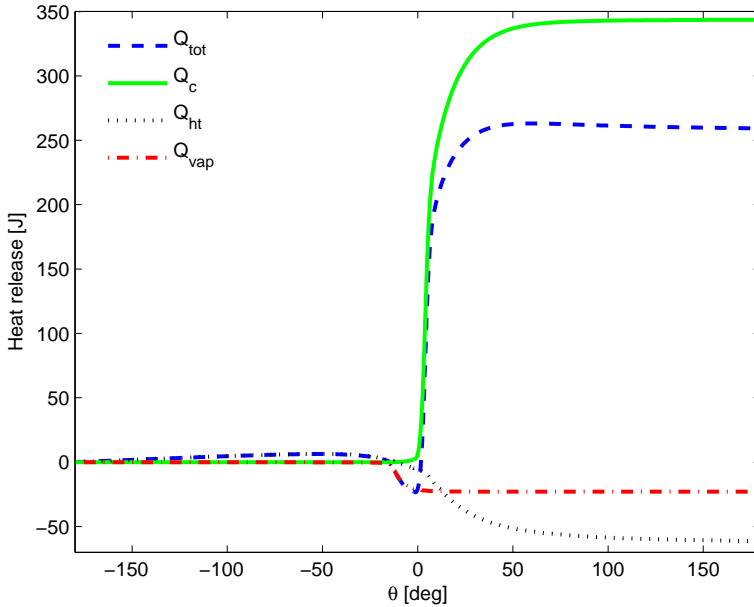
Figure 7.6 Simulated total thermal energy and combustion heat release, heat loss, and vaporization energy components corresponding to the pressure trace in Fig. 7.4.

Modeling of Fuel Evaporation and Mixing

The main improvement, in terms of model fit from the separation of fuel vaporization and mixing, was that the dip in heat release (visible in Fig. 7.5), following fuel injection, could be described while still retaining the mixing controlled part of the combustion. Figure 7.7 shows the four fuel categories corresponding to Fig. 7.4. It is evident that m_{pre} limits m_b. The mixing controlled part of the combustion can also be seen in Q_c in Fig. 7.6 where the combustion slows down towards the end. A simpler model could be formulated where the evaporation and mixing processes are described by a single, constant, rate. It would, however, make it more challenging to capture both of these phenomena.

Burn Rate Modeling

The rate at which fuel burns, following the preparation through evaporation and mixing described in the previous section, was modeled as mainly limited by the Arrhenius rate, which corresponds to chemical kinetics.
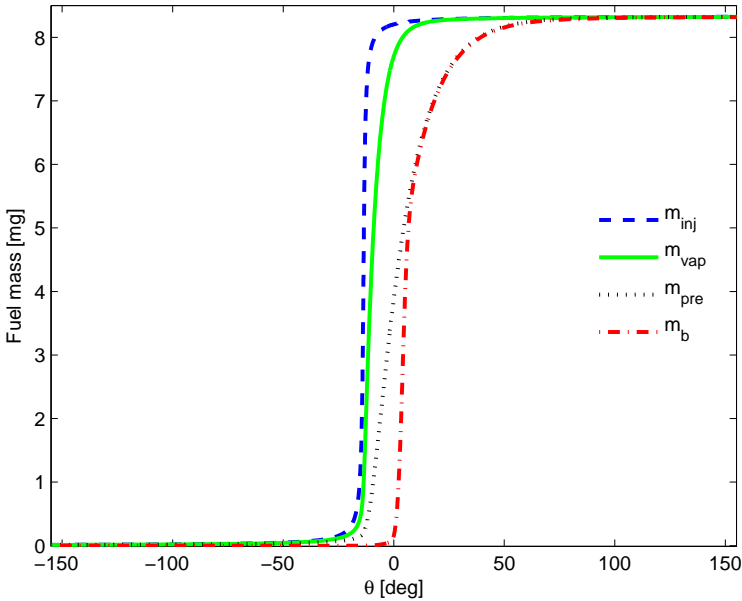
Figure 7.7 Simulated fuel masses vs. crank angle. Injected, evaporated, prepared, and burned fuel as indicated. The profiles correspond to the pressure trace in Fig. 7.4.

Previous work in Diesel modeling presented in [Chmela *et al.*, 2007] used a combination of the Arrhenius rate and the Magnussen rate [Magnussen and Hjertager, 1977], which describes the effects of turbulence. The motivation for omitting the turbulence dependence in the current model was that PPC operation features a larger portion of pre-mixed combustion than traditional Diesel combustion, particularly at lower loads, which should increase the importance of chemistry. To increase the amount of fuel that burns in a mixing controlled fashion, the burn rate in Eq. (7.16) can be increased or the mixing rate in Eq. (7.15) can be decreased. The quadratic term in combustion duration has been used in several previous models [Chmela *et al.*, 2007; Gogoi and Baruah, 2010]. It corresponds to a Wiebe function [Wiebe, 1970]

$$x_b = 1 - \exp\left(-a_W \left(\frac{\theta - \theta_{\text{SOC}}}{\Delta\theta} \right)^{m_W+1} \right) \tag{7.38}$$
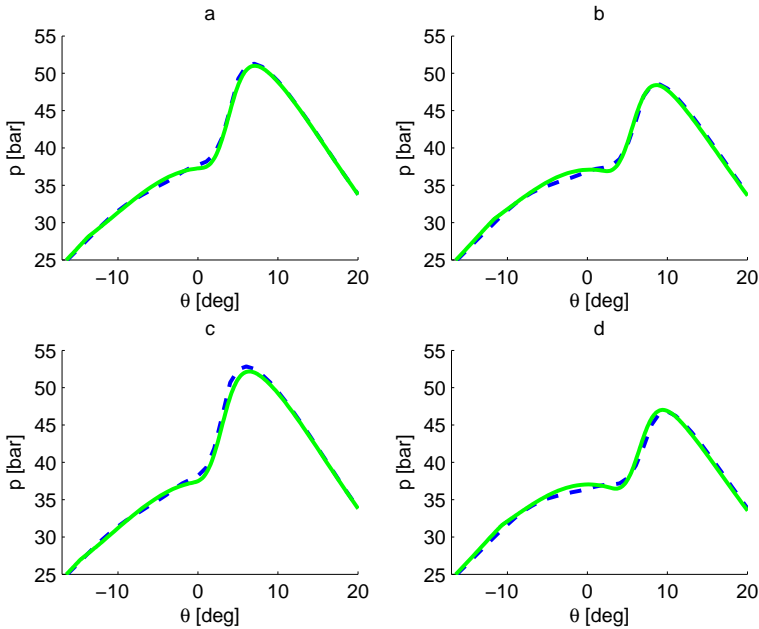
Figure 7.8 Pressure vs. crank angle for θ_{SOI} -15.7 (a), -13.7 (b), -16.7 (c), and -12.7 (d). Data (dashed lines) and model output (solid lines).

that can be used to describe the mass fraction burned, x_b, parametrized by the model parameters a_W and m_W, and the total combustion duration $\Delta\theta$, with $m_W = 2$ [Gogoi and Baruah, 2010].

Heat Transfer

Heat transfer had a considerable effect on the resulting heat release as seen in Fig. 7.6. During the model development, it was difficult to describe the nonlinear influence of heat transfer while assuming a constant wall temperature. The heat transfer characteristics can then only be described by the convection coefficient's dependence on charge pressure and temperature. In the simulations, the cylinder wall temperature varied by a few degrees during the closed part of the cycle.

Parameter Sensitivities

JModelica.org allows the sensitivities of the model parameters to be calculated automatically. Figure 7.9 shows the partial derivatives of p with respect to C_{Arr}, K, k_{Arr}, k_{pre}, k_{vap} and $m_{\text{inj,tot}}$ corresponding to the pressure
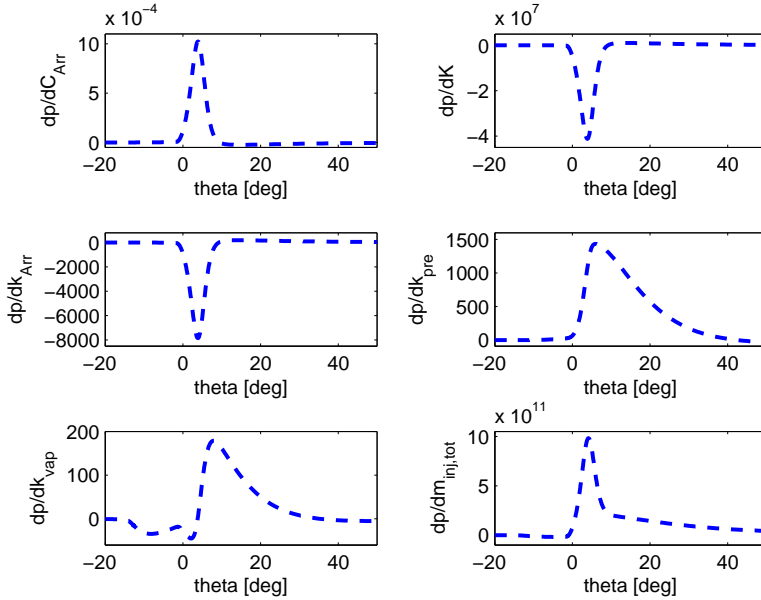
Figure 7.9 Partial derivatives of p with respect to C_{Arr}, K, k_{Arr}, and k_{pre}, k_{vap}, and $m_{\mathrm{inj,tot}}$. The derivatives are shown for the case corresponding to Fig. 7.4.

trace shown in Fig. 7.4. It can be seen that C_{Arr}, K, and k_{Arr} mainly influence the pressure trace during the early stage of combustion, while the remaining parameters also influence the pressure during the expansion. A larger value of C_{Arr} will make the combustion start earlier and increase the burn rate, yielding an increase in the pressure. Larger values of K and k_{Arr} will instead delay combustion, and, in the case of k_{Arr}, result in a lower a burn rate. The partial derivative with respect to k_{pre} decays slowly since the preparation rate influences the mixing controlled part of combustion. The partial derivative with respect to k_{vap} is negative between θ_{SOI} and start of combustion, since a higher vaporization rate yields a faster decrease in thermal energy due to vaporization. The partial derivative with respect to $m_{\mathrm{inj,tot}}$ does not return to zero, as an increase in the amount of fuel corresponds to a higher pressure during the expansion.

Optimization of Steady-State PPC Operation

A possible utilization of the model framework presented in this chapter is to use it for optimization of steady-state PPC operation. To characterize

the combustion, several key values can be defined. In previous chapters, θ_{50} was used as a proxy for combustion timing. The total energy released from combustion could also be included, as well as additional intermediate key values that indicate the rate of combustion, for instance θ_{10} and θ_{90} as defined in Eq. (1.5). Several of the possible control signals for PPC can be expressed as parameters for a particular cycle. The injection of fuel can be characterized by the start of injection and injection duration both for a single injection and for multiple injections, the valve timings and the amount of residuals are inherently given on a cycle-to-cycle basis.

An optimization problem on a form similar to the parameter estimation problems considered in Sec. 7.5 can be formulated to achieve a reference θ_{50}, θ_{50}^r, and a reference total heat release, $Q_{c,\text{tot}}^r$, with the injection timing and total fuel amount as optimization variables, as

$$
\begin{aligned}
\min_{\mathbf{p}} \ \ & \left(Q_{c,\text{tot}}^r - Q_c(\theta_{100})\right)^2 + \left(\frac{1}{2}Q_{c,\text{tot}}^r - Q_c(\theta_{50}^r)\right)^2 \\
\text{s.t. } & F(\dot{x}(t), x(t), w(t), u(t), \mathbf{p}) = 0 \\
& x_{\min} \le x \le x_{\max} \\
& w_{\min} \le w \le w_{\max} \\
& \mathbf{p}_{\min} \le \mathbf{p} \le \mathbf{p}_{\max} \\
& x(t_0) = x_0
\end{aligned}
\tag{7.39}
$$

where $\mathbf{p}$ contains the control signals θ_{SOI} and $m_{\text{inj,tot}}$. A similar optimization problem can be formulated to achieve a desired combustion duration, specified using θ_{10}^r and θ_{90}^r, with θ_{SOI} and α as control signals

$$
\begin{aligned}
\min_{\mathbf{p}} \ \ & \left(\frac{1}{10}Q_{c,\text{tot}}^r - Q_c(\theta_{10}^r)\right)^2 + \left(\frac{9}{10}Q_{c,\text{tot}}^r - Q_c(\theta_{90}^r)\right)^2 \\
\text{s.t. } & F(\dot{x}(t), x(t), w(t), u(t), \mathbf{p}) = 0 \\
& x_{\min} \le x \le x_{\max} \\
& w_{\min} \le w \le w_{\max} \\
& \mathbf{p}_{\min} \le \mathbf{p} \le \mathbf{p}_{\max} \\
& x(t_0) = x_0
\end{aligned}
\tag{7.40}
$$

where $\mathbf{p}$ contains the control signals θ_{SOI} and α.

A major difference between the optimization problem in Eqs. (7.39) and (7.40) and the parameter estimation problem in Eq. (7.31) is that the reference only consists of a few values rather than an entire trajectory. Thus, the interpolation described in Sec. 2.3 is not suitable. Instead, the cost function can be constructed by penalizing the collocation points closest

to the reference points. Since θ is modeled as a linear function of time, and the simulation covers exactly one engine revolution starting at bottom dead center before combustion, the time, t_{θ_i}, corresponding to a specific crank angle θ_i can be calculated explicitly. To reduce the approximation error, the element lengths can then be chosen so that an element junction point occurs close to each t_{θ_i}.

The optimization problems in Eqs. (7.39) and (7.40) could be successfully solved and evaluated in simulation. However, experimental validation of the optimization results would be desired.

7.8 Conclusion

A single-zone model of PPC combustion was implemented and validated against Diesel PPC data. The model included heat losses to the cylinder walls as well as vaporization losses. The burn rate was limited by the Arrhenius rate and the fuel preparation rate towards the end of combustion. The aim of the modeling was to enable numerical optimization. The single-zone model structure has a lower complexity than multi-zone models, and the model was implemented in JModelica.org, which allowed optimization problems to be formulated based on the model equations. As an initial use of this possibility, automatic calibration of the model parameters was demonstrated.

8

Conclusion

The topic of this thesis is physical modeling and model-based control of HCCI and PPC engines. Since there is substantial mixing of fuel and air, and combustion is initiated by auto-ignition in both combustion modes, the presented models have several similar traits. However, the HCCI model was formulated on a cycle-to-cycle basis while the PPC model was formulated in continuous time, which results in models of differing complexity and different uses. The following sections summarize the contributions within each area.

8.1 Summary

The following summary is organized by the combustion mode studied.

HCCI

A cycle-to-cycle model of HCCI that captured the main dynamics of the thermal interaction between the gas and the cylinder walls was presented in Ch. 4. The continuous heat transfer between the cylinder wall and the gas charge was approximated by three heat transfer events during each cycle, while the compression and expansion were modeled as isentropic processes. This allowed the model to capture the time constant of the wall temperature while keeping the complexity of the resulting model at a tractable level. The cylinder wall temperature dynamics provide a reasonable explanation for the slower cycle-to-cycle dynamics in HCCI when only small amounts of residuals are trapped in the cylinder. The model was of second order and could be formulated so that the states were the measured outputs IMEP and θ_{50}. The heat transfer parameters were calibrated using numerical optimization and the calibrated model captured the characteristics of the studied outputs well.

   The resulting model was used to design model predictive controllers

that were evaluated experimentally. The objective was to control the combustion phasing and the control variables were the inlet valve closing timing and the temperature of the intake air. The control design and analysis of the experimental results were presented in Ch. 5. The controller achieved satisfactory reference tracking and efficiently suppressed the test disturbances.

A second control study, presented in Ch. 6, investigated the differences in performance between using a switched state feedback controller and a hybrid model predictive controller for controlling exhaust recompression HCCI. The dynamics of exhaust recompression HCCI vary dramatically with the operating point which motivates the use of more than one linear controller. The model predictive controller produced smoother transients in both simulations and experiments.

PPC

In Ch. 7, the development and implementation of a continuous-time PPC model were presented. The model structure and implementation platform were chosen with the aim of allowing for numerical optimization. The model was a single-zone model including simple models of heat losses and vaporization losses, and the resulting model was implemented in the JModelica.org platform. Particular care was taken to reduce the numerical problems associated with variable scaling simulation of discrete events such as the start of combustion.

The resulting framework allowed the parameter calibration to be formulated as an optimization problem penalizing deviations between a measured pressure trace and that of the model. The calibrated model predicted the effects of variations in the injection timing with satisfactory accuracy.

8.2 Suggestions for Future Work

The presented HCCI control seem promising in terms of tracking of the combustion phasing. However, additional outputs and inputs need to be considered to enable the use of an HCCI engine in a vehicle. For instance, the work output needs to be controlled in order to respond to driver demands. Additionally, the hybrid control results presented in Ch. 6 exhibited some undesirable control signal activity. The presented hysteresis scheme reduced the model region changes in simulation, but has not yet been validated experimentally.

The presented PPC model only considers the closed part of the cycle. An advantage of continuous-time models is that they allow for a natural formulation of flow phenomena such as those associated with the intake and

exhaust ports, and this feature could be exploited. Additional validation of the model at different engine speeds, loads, and injections strategies would be desirable. Experimental evaluation of the optimization problems discussed in Sec. 7.7 would also be of interest.

9

Bibliography

Åkesson, J. (2006): *MPCtools 1.0—Reference Manual*. Tech. Rep. TFRT--7613--SE, Department of Automatic Control, Lund University, Sweden.

Åkesson, J. (2007): *Languages and Tools for Optimization of Large-Scale Systems*. PhD thesis TFRT--1081--SE, Department of Automatic Control, Lund University, Sweden.

Åkesson, J. (2008): "Optimica—an extension of modelica supporting dynamic optimization." In *6th International Modelica Conference 2008*. Modelica Association. Bielefeld, Germany.

Åkesson, J., K.-E. Årzén, M. Gäfvert, T. Bergdahl, and H. Tummescheit (2010): "Modeling and optimization with Optimica and JModelica.org—languages and tools for solving large-scale dynamic optimization problem." *Computers and Chemical Engineering*, **34:11**, pp. 1737–1749. Doi:10.1016/j.compchemeng.2009.11.011.

Åkesson, J. and P. Hagander (2003): "Integral action—A disturbance observer approach." In *Proceedings of European Control Conference*. Cambridge, UK.

Allison, B. J. and A. J. Isaksson (1998): "Design and performance of midranging controllers." *Journal of Process Control*, **8:5-6**, pp. 469–474.

Anderson, B. D. and J. B. Moore (1990): *Linear Optimal Control*. Prentice Hall, Eaglewood Cliffs, NJ.

Andersson, J., B. Houska, and M. Diehl (2010): "Towards a computer algebra system with automatic differentiation for use with object-oriented modelling languages." In *3rd International Workshop on Equation-Based Object-Oriented Modeling Languages and Tools*. Oslo, Norway.

Aoyama, T., Y. Hattori, J. Mizuta, and Y. Sato (1996): "An experimental study on premixed-charge compression ignition gasoline engine." *SAE Technical Papers*, **No 960081**.

Assanis, D. N., Z. S. Filipi, S. B. Fiveland, and M. Syrimis (2003): "A predictive ignition delay correlation under steady-state and transient operation of a direct injection diesel engine." *Journal of Engineering for Gas Turbines and Power*, **125:2**, pp. 450–457.

Åström, K. J. and T. Hägglund (2005): *Advanced PID Control*. ISA - The Instrumentation, Systems, and Automation Society, Research Triangle Park, NC 27709.

Bemporad, A. (2004): "Hybrid Toolbox - User's Guide." `http://www.dii.unisi.it/hybrid/toolbox`

Bemporad, A., F. Borrelli, and M. Morari (2000): "Optimal controllers for hybrid systems: Stability and piecewise linear explicit form." In *39th IEEE Conference on Decision and Control*, pp. 1810–1815. Sydney, Australia.

Bemporad, A., M. Morari, and N. L. Ricker (2004): *Model Predictive Control Toolbox. User's Guide*. The MathWorks Inc. MA, USA.

Bengtsson, J. (2004): *Closed-Loop Control of HCCI Engine Dynamics*. PhD thesis TFRT--1070--SE, Department of Automatic Control, Lund Institute of Technology, Lund University, Sweden.

Bengtsson, J., M. Gäfvert, and P. Strandh (2004): "Modeling of HCCI engine combustion for control analysis." In *IEEE Conference in Decision and Control (CDC 2004)*, pp. 1682–1687. Bahamas.

Bengtsson, J., P. Strandh, R. Johansson, P. Tunestål, and B. Johansson (2006): "Model predictive control of homogeneous charge compression ignition (HCCI) engine dynamics." In *2006 IEEE International Conference on Control Applications*. Munich, Germany. pp. 1675-1680.

Bengtsson, J., P. Strandh, R. Johansson, P. Tunestål, and B. Johansson (2007): "Hybrid modelling of homogeneous charge compression ignition (HCCI) engine dynamic—A survey." *International Journal of Control*, **80:11**, pp. 1814–1848.

Biegler, L., A. Cervantes, and A. Wächter (2002): "Advances in simultaneous strategies for dynamic optimization." *Chemical Engineering Science*, **57**, pp. 575–593.

Biegler, L. T. (2010): *Nonlinear Programming: Concepts, Algorithms, and Applications to Chemical Processes*. Society for Industrial Mathematics. PA, USA.

Blom, D., M. Karlsson, K. Ekholm, P. Tunestål, and R. Johansson (2008): "HCCI engine modeling and control using conservation principles." *SAE Technical Papers*, **No 2008-01-0789**.

Borgqvist, P., P. Tunestål, and B. Johansson (2011): "Investigation and comparison of residual gas enhanced HCCI using trapping (NVO HCCI) or rebreathing of residual gases." *JSAE Technical Papers*, **No 20119058**.

Canova, M., R. Garcin, S. Midlam-Mohler, Y. Guezennec, and G. Rizzoni (2005): "A control-oriented model of combustion process in a HCCI diesel engine." In *Proc. 2005 American Control Conference (ACC 2005)*, pp. 4446–4451. Portland, OR, USA.

Chang, J., O. Güralp, Z. Filipi, D. Assanis, T.-W. Kuo, P. Najt, and R. Rask (2004): "New heat transfer correlation for an HCCI engine derived from measurements of instantaneous surface heat flux." *SAE Technical Papers*, **No 2004-01-2996**.

Chang, K., G. A. Lavoie, A. Babajimopoulos, Z. S. Filipi, and D. N. Assanis (2007): "Control of a multi-cylinder HCCI engine during transient operation by modulating residual gas fraction to compensate for wall temperature effects." *SAE Technical Papers*, **No 2007-01-0204**.

Chauvin, J., O. Grondin, E. Nguyen, and F. Guillemin (2008): "Real-time combustion parameters estimation for HCCI-diesel engine based on knock sensor measurement." In *Proc. 17th IFAC World Congress*, pp. 8501–8507. Seoul, Korea.

Chiang, C. and A. Stefanopoulou (2004): "Steady-state multiplicity and stability of thermal equilibria in homogeneous charge compression ignition (HCCI) engines." In *Proc. 2004 Conference on Decision and Control (CDC 2004)*, pp. 1676–1681. Atlantis, Paradise Island, Bahamas.

Chiang, C. and A. Stefanopoulou (2009): "Sensitivity analysis of combustion timing and duration of homogeneous charge compression ignition gasoline engines." *Journal of Dynamic Systems Measurement & Control*, **131:1**, pp. 014506–1–014506–5.

Chiang, C.-J. and A. G. Stefanopoulou (2007): "Stability analysis in homogeneous charge compression ignition (HCCI) engines with high dilution." *IEEE Transactions on Control Systems Technology*, **15:2**, pp. 209–219.

Chiang, C.-J., A. G. Stefanopoulou, and M. Jankovic (2007): "Nonlinear observer-based control of load transitions in homogeneous charge

compression ignition engines." *IEEE Transactions on Control Systems Technology*, **15:3**, pp. 438–448.

Chmela, F. G., G. H. Pirker, and A. Wimmer (2007): "Zero-dimensional rohr simulation for DI diesel engines - a generic approach." *Energy Conversion and Management*, **48:11**, pp. 2942 – 2950.

Christensen, M., A. Hultqvist, and B. Johansson (1999): "Demonstrating the multi fuel capability of a homogeneous charge compression ignition engine with variable compression ratio." *SAE Technical Papers*, **No 1999-01-3679**.

Christensen, M. and B. Johansson (2000): "Supercharged homogeneous charge compression ignition (HCCI) with exhaust gas recirculation and pilot fuel." *SAE Technical Papers*, **No 2000-01-1835**.

Dec, J. E. (1997): "A conceptual model of DI diesel combustion based on laser-sheet imaging." *SAE Technical Papers*, **No 970873**.

Dempsey, A. B. and R. D. Reitz (2011): "Computational optimization of a heavy-duty compression ignition engine fueled with conventional gasoline." *SAE Technical Papers*, **No 2011-01-0356**.

Fourer, R., D. M. Gay, and B. W. Kernighan (2002): *AMPL: A Modeling Language for Mathematical Programming*. Duxbury Press.

Friedrich, I., H. Pucher, and T. Offer (2006): "Automatic model calibration for engine-process simulation with heat-release prediction." *SAE Technical Papers*, **No 2006-01-0655**.

Gambarotta, A. and G. Lucchetti (2011): "Control-oriented crank-angle based modeling of automotive engines." *SAE Technical Papers*, **No 2011-24-0144**.

Gatowski, J. A., E. N. Balles, K. M. Chun, F. E. Nelson, J. A. Ekchian, and J. B. Heywood (1984): "Heat release analysis of engine pressure data." *SAE Technical Papers*, **No 841359**.

Giorgetti, N., G. Ripaccioli, A. Bemporad, I. Kolmanovsky, and D. Hrovat (2006): "Hybrid model predictive control of direct injection stratified charge engines." *Mechatronics, IEEE/ASME Transactions on*, **11:5**, pp. 499–506.

Gogoi, T. and D. Baruah (2010): "A cycle simulation model for predicting the performance of a diesel engine fuelled by diesel and biodiesel blends." *Energy*, **35:3**, pp. 1317 – 1323.

Guzzella, L. and C. H. Onder (2004): *Introduction to Modeling and Control of Internal Combustion Engine Systems*. Springer-Verlag, Berlin Heidelberg.

Haraldsson, G. (2005): *Closed-Loop Combustion Control of a Multi Cylinder HCCI Engine using Variable Compression Ratio and Fast Thermal Management*. PhD thesis TMHP--05/1028--SE, Department of Heat and Power Engineering, Lund Institute of Technology, Lund University, Sweden.

Hendricks, E. (1986): "A compact, comprehensive model of large turbocharged two-stroke diesel engines." *SAE Technical Papers*, **No 861190**.

Heywood, J. B. (1988): *Internal Combustion Engine Fundamentals*. McGraw-Hill International Editions, New York.

Hillion, M., J. Chauvin, and N. Petit (2008): "Controlling the start of combustion on an HCCI diesel engine." In *Proc. 2008 American Control Conference*, pp. 2084–2091. Seattle, Washington, USA.

Hohenberg, G. F. (1979): "Advanced approaches for heat transfer calculations." *SAE Technical Papers*, **No 79-08-25**.

Ishibashi, Y. and M. Asai (1979): "Improving the exhaust emissions of two-stroke engines by applying the activated radical combustion." *SAE Technical Papers*, **No 790501**.

Jääskeläinen, H. (2008): *Low Temperature Combustion*, 2010.12a edition. DieselNet Technology Guide.

Johansson, R. (1993): *System Modeling and Identification*. Prentice Hall, Englewood Cliffs, New Jersey.

Jost, D. and F. Torrisi (2002): "HYSDEL - Programmer Manual." Technical Report. http://control.ee.ethz.ch/index.cgi?page= \publications;action=details;id=799.

Kang, J.-M., C.-F. Chang, J.-S. Chen, and M.-F. Chang (2009): "Concept and implementation of a robust HCCI controller." *SAE Technical Papers*, **No 2009-01-1131**.

Karlsson, M. (2008): "Control structures for low-emission combustion in multi-cylinder engines." Licentiate Thesis TFRT--3243--SE. Department of Automatic Control, Lund University, Sweden.

Karlsson, M., K. Ekholm, P. Strandh, R. Johansson, P. Tunestål, and B. Johansson (2007): "Closed-loop control of combustion phasing in an HCCI engine using VVA and variable EGR." In *Fifth IFAC Symposion on Advances in Automotive Control*. Monterey, USA.

Kiencke, U. and L. Nielsen (2005): *Automotive Control Systems, For Engine, Driveline, and Vehicle*, 2nd edition. Springer Verlag, Berlin Heidelberg.

Lewander, M. (2011): *Characterization and Control of Multi-Cylinder Partially Premixed Combustion.* PhD thesis TMHP--11/1083--SE, Department of Energy Sciences, Lund University, Sweden.

Liao, H.-H., N. Ravi, A. F. Jungkunz, J.-M. Kang, and J. C. Gerdes (2010a): "Representing change in HCCI dynamics with a switching linear model." In *2010 American Control Conference (ACC2010)*. Baltimore, Maryland, USA.

Liao, H.-H., N. Ravi, A. F. Jungkunz, A. Widd, and J. C. Gerdes (2010b): "Controlling combustion phasing of recompression HCCI with a switching controller." In *Proc. Fifth IFAC Symposium on Advances in Automotive Control.* Munich, Germany.

Liao, H.-H., M. J. Roelle, C.-F. Chen, S. Park, and J. C. Gerdes (2011): "Implementation and analysis of a repetitive controller for and electro-hydraulic engine valve system." *IEEE Transactions on Control Systems Technology*, **19:5**, pp. 1102–1113.

Maciejowski, J. (2002): *Predictive Control with Constraints.* Prentice Hall, Essex, England.

Magnussen, B. and B. Hjertager (1977): "On mathematical modeling of turbulent combustion with special emphasis on soot formation and combustion." *Symposium (International) on Combustion*, **16:1**, pp. 719 – 729.

Magnusson, F. (2012): "Collocation methods in JModelica.org." Master's Thesis TFRT--5881--SE.

Majewski, W. A. (2005): *Selective Catalytic Reduction*, 2005.05g edition. DieselNet Technology Guide.

Manente, V., B. Johansson, P. Tunestål, and W. Cannella (2010a): "Influence of inlet pressure, EGR, combustion phasing, speed and pilot ratio on high load gasoline partially premixed combustion." *SAE Technical Papers*, **No 2010-01-1471**.

Manente, V., C.-G. Zander, B. Johansson, P. Tunestål, and W. Cannella (2010b): "An advanced internal combustion engine concept for low emissions and high efficiency from idle to max load using gasoline partially premixed combustion." *SAE Technical Papers*, **No 2010-01-2198**.

Mathworks (2006): *Real-Time Workshop. User's Guide.* The MathWorks Inc.

Mathworks (2008): *Symbolic Math Toolbox 5. User's Guide.* The Mathworks Inc.

Mathworks (2010): *xPC Target 4. User's Guide*. The Mathworks Inc.

Najt, P. M. and D. E. Foster (1983): "Compression-ignited homogeneous charge combustion." *SAE Technical Papers*, **No 830264**.

Olsson, J., P. Tunestål, G. Haraldsson, and B. Johansson (2001): "A turbo charged dual fuel HCCI engine." *SAE Technical Papers*, **No 2001-01-1896**.

Onishi, S., S. H. Jo, K. Shoda, P. D. Jo, and S. Kato (1979): "Active thermo-atmosphere combustion (ATAC) - a new combustion process for internal combustion engines." *SAE Technical Papers*, **No 790501**.

Python Software Foundation (2012): "Python programming language - official website." http://www.python.org/.

Rakopoulos, C. D., D. C. Rakopoulos, G. C. Mavropoulos, and E. G. Giakoumis (2004): "Experimental and theoretical study of the short term response temperature transients in the cylinder walls of a diesel engine at various operating conditions." *Applied Thermal Engineering*, **No 24**, pp. 679–702.

Rausen, D. J. and A. G. Stefanopoulou (2005): "A mean-value model for control of homogeneous charge compression ignition (HCCI) engines." *Journal of Dynamical Systems, Measurement, and Control*, **No 127**, pp. 355–362.

Ravi, N., M. J. Roelle, H.-H. Liao, A. F. Jungkunz, C.-F. Chang, S. Park, and J. C. Gerdes (2010): "Model-based control of HCCI engines using exhaust recompression." *IEEE Transactions on Control Systems Technology*, **18:6**, pp. 1289–1302.

Roelle, M. J., N. Ravi, A. F. Jungkunz, and J. C. Gerdes (2006): "A dynamic model of recompression HCCI combustion including cylinder wall temperature." In *Proc. IMECE2006*. Chicago, Illinois, USA.

Särner, G., M. Richter, M. Aldén, A. Vressner, and B. Johansson (2005): "Cycle resolved wall temperature measurements using laser-induced phosphorescence in an HCCI engine." *SAE Technical Papers*, **No 2005-01-3870**.

Shahbakhti, M. and R. Koch (2007): "Control oriented modeling of combustion phasing for an HCCI engine." In *Proc. 2007 American Control Conference (ACC2007)*, pp. 3694–3699. New York City, USA.

Shaver, G. M., J. C. Gerdes, and M. J. Roelle (2009): "Physics-based modeling and control of residual-affected HCCI engines." *Journal of Dynamic Systems, Measurement, and Control*, **131:2**, p. 021002.

Shaver, G. M., J. C. Gerdes, M. J. Roelle, P. A. Caton, and C. F. Edwards (2005): "Dynamic modeling of residual-affected homogenous charge compression ignition engines with variable valve actuation." *Journal of Dynamic Systems, Measurement, and Control*, **127:3**, pp. 374–381.

Shaver, G. M., M. Roelle, and J. C. Gerdes (2006a): "Modeling cycle-to-cycle dynamics and mode transition in HCCI engines with variable valve actuation." *Control Engineering Practice*, **No 14**, pp. 213–222.

Shaver, G. M., M. Roelle, and J. C. Gerdes (2006b): "A two-input two-output control model of HCCI engines." In *Proc. 2006 American Control Conference (ACC2006)*, pp. 472–477. Minneapolis, Minnesota, USA.

Soyhan, H., H. Yasar, H. Walmsley, B. Head, G. Kalghatgi, and C. Sorusbay (2009): "Evaluation of heat transfer correlations for HCCI engine modeling." *Applied Thermal Engineering*, **No 29**, pp. 541–549.

Strandh, P. (2006): *HCCI Operation - Closed Loop Combustion Control Using VVA or Dual Fuel*. PhD thesis TMHP- -06/1039- -SE, Department of Energy Sciences, Lund University, Sweden.

Strandh, P., J. Bengtsson, M. Christensen, R. Johansson, A. Vressner, P. Tunestål, and B. Johansson (2003): "Ion current sensing for HCCI combustion feedback." *SAE Technical Papers*, **No 2003-01-3216**.

Strandh, P., J. Bengtsson, R. Johansson, P. Tunestål, and B. Johansson (2004): "Cycle-to-cycle control of a dual-fuel HCCI engine." *SAE Paper 2004-01-0941*, **SP-1819**, March. SAE International, Homogeneous Charge Compression Ignition (HCCI) Combustion 2004, ISBN: 0-7680-1355-0.

Tauzia, X., A. Maiboom, P. Chesse, and N. Thouvenel (2006): "A new phenomenological heat release model for thermodynamical simulation of modern turbocharged heavy duty diesel engines." *Applied Thermal Engineering*, **26:16**, pp. 1851 – 1857.

The Modelica Association (2009): "The Modelica Association Home Page." `http://www.modelica.org`.

Tunestål, P. (2009): "Self-tuning gross heat release computation for internal combustion engines." *Control Engineering Practice*, **17:4**, pp. 518 – 524.

Turns, S. R. (2006): *An Introduction to Combustion: Concepts and Applications - 2nd ed.* McGraw-Hill Higher Education.

Wächter, A. and L. T. Biegler (2006): "On the implementation of an interior-point filter line-search algorithm for large-scale nonlinear programming." *Mathematical Programming*, **No 1**, pp. 25–58.

Wang, Z., S.-J. Shuai, J.-X. Wang, G.-H. Tian, and X.-L. An (2006): "Modeling of HCCI combustion: From 0D to 3D." *SAE Technical Papers*, **No 2006-01-1364**.

Wiebe, I. I. (1970): *Brennverlauf und Kreisprozessrechnung*. VEB Verlag Technik, Berlin.

Wilhelmsson, C., A. Vressner, P. Tunestål, B. Johansson, G. Särner, and M. Aldén (2005): "Combustion chamber wall temperature measurement and modeling during transient HCCI operation." *SAE Technical Papers*, **No 2005-01-3731**.

Woschni, G. (1967): "A universally applicable equation for instantaneous heat transfer coefficient in the internal combustion egnine." *SAE Technical Papers*, **No 670931**.

Zhao, F. and T. Asmus (2003): "HCCI control and operating range extension." In Zhao *et al.*, Eds., *Homogeneous Charge Compression Ignition (HCCI) Engines—Key Research and Development Issues*. Society of Automotive Engineers Inc.

Nomenclature

Symbols

Symbol	Description	Unit
A_c	Cylinder wall area	m^2
α	Molar ratio of exhaust gases	-
C_{Arr}	Arrhenius scaling factor	$(\text{kg/m}^3)^{1-a-b}\text{s}^{-1}$
c_v	Specific heat capacity (const. volume)	J/(kg·K)
c_p	Specific heat capacity (const. pressure)	J/(kg·K)
C_p	Cylinder wall specific heat capacity	J/(kg·K)
E_a	Arrhenius activation energy	J/kg
ϕ	Equivalence ratio	-
γ	Ratio of specific heats	-
h_c	Convective heat transfer coeff.	$\text{W/(m}^2\text{·K)}$
K	Arrhenius integral threshold	kg/m^3
k_{Arr}	Arrhenius exponential factor	K
k_c	Conductive heat transfer coeff.	$\text{W/(m}^2\text{·K)}$
k_{pre}	Fuel mixing rate	s^{-1}
k_{vap}	Fuel evaporation rate	s^{-1}
L_c	Cylinder wall thickness	m
M_{X}	Molar mass of species X	kg/mol
m	Gas mass	kg
m_{b}	Burned fuel	kg

Nomenclature

m_c	Cylinder wall mass	kg
m_{inj}	Injected fuel	kg
$m_{\text{inj,tot}}$	Total amount of fuel to be injected	kg
m_{pre}	Prepared fuel	kg
m_{vap}	Evaporated fuel	kg
m_X	Mass of species X	kg
N	Engine speed	Rot. per min.
n_X	Amount of species X	mol
ξ_{LHV}	Lower heating value of fuel	J/kg
ξ_{vap}	Heat of vaporization of fuel	J/kg
p	Pressure	Pa
R	Gas constant	J/(kg·K)
Q_c	Combustion heat release	J
Q_{ht}	Heat losses	J
Q_{tot}	Total thermal energy	J
Q_{vap}	Vaporization losses	J
T	Gas temperature	K
T_c	Coolant temperature	K
T_{in}	Inlet temperature	K
T_{iw}	Cylinder wall inner temperature	K
T_w	Cylinder wall surface temperature	K
θ	Crank angle	rad or deg
θ_{50}	Crank angle of 50 percent burned	rad or deg
θ_{EVC}	Crank angle of exhaust valve closing	rad or deg
θ_{IVC}	Crank angle of inlet valve closing	rad or deg
θ_{SOC}	Crank angle at start of combustion	rad or deg
θ_{SOI}	Crank angle at start of fuel injection	rad or deg
θ_{TDC}	Crank angle at top dead center	rad or deg
V	Cylinder volume	m^3
V_c	Clearance volume	m^3
V_d	Displacement volume	m^3

Acronyms

Acronym	Description
ABDC	After Bottom Dead Center
ATDC	After Top Dead Center
BBDC	Before Bottom Dead Center
BTDC	Before Top Dead Center
CA	Crank Angle
CI	Compression Ignition
DAE	Differential Algebraic Equation
EGR	Exhaust Gas Recirculation
EVC	Exhaust valve closing
FTM	Fast Thermal Management
HCCI	Homogeneous Charge Compression Ignition
IMEP	Indicated Mean Effective Pressure
IVC	Inlet Valve Closing
LQ	Linear Quadratic
MIMO	Multiple-Input, Multiple-Output
MPC	Model Predictive Control
NLP	Nonlinear Program
ODE	Ordinary Differential Equation
PID	Proportional-Integral-Derivative
PPC	Partially Premixed Combustion
SI	Spark Ignition
TDC	Top Dead Center
VVA	Variable Valve Actuation